Multi-Photon Blockade in Cavity QED

Sophie S. Shamailov

Supervisor: Professor Howard J. Carmichael

Bachelor of Science
in
Physics

The University of Auckland
2009

Abstract

The driven Jaynes-Cummings model is studied in the strong-coupling, strong-drive regime by way of numerical simulations. The investigation is motivated by recent advances from Circuit QED which show conclusively that the model and parameter regimes considered are realistic experimentally. The focus is on the multi-photon transitions to higher excitation dressed-states, as observed in [13]. Photon statistics of the light leaking out of the cavity are examined when the laser is tuned to such a multi-photon resonance. We find that (*un*like a two-state system) with increasing drive strength, bunched, super-poissonian light is transformed into antibunched and sub-poissonian. These results are interpreted and a simple model is constructed to explain our observations analytically. Moreover, the incoherent spectrum is computed, leading to observation of a saturation effect and multiple dynamic Stark splittings, resulting in a Mollow triplet. This is interpreted analogously to Resonance Fluorescence in the context of Floquet theory and the simplest example is treated analytically. In summary, we observe *Multi-Photon Blockade*.

Acknowledgments

Well, first of all, I want to say a huge thank-you to Howard, Matthew and Scott who warmly invited me to join our little Quantum Optics Mafia. You were always very inspiring teachers, always made Physics just that little bit more exciting, more *fun*. Your (seriously scary!) insight and ability to explain what is going on in terms of simple Physics is beyond amazing. Thanks for being so casual and friendly, not to mention putting up with me for so long!

Thanks for the extremely fun weekly meetings and nearly daily bugging sessions! You are always there, always ready to help, happy to answer the millions of questions. Thanks for not giving up on me when I said things like "ahhhh, can we make variable capacitors?" or "is Otago in Dunedin?" (Yeah, sometimes I really wonder myself. . .) Thanks for all the advice and insight, for your wicked sense of humor, for laughing and joking all the time and making our research group so much fun. You're really awesome – thank you!

Next, this is to everyone who taught me Physics for the last three years.

We get here as little stage one-ers, *feeling* how mighty awesome Physics really is, but not being able to fully grasp the magnitude of it, nor the details or its extent. Then, you come along, and unravel the world, explaining one thing after the other. There is nothing more wonderful than these moments when all of a sudden, one new little piece of the puzzle falls into place. When we understand a new thing about how the world works. Your classes have always been exciting and inspiring, your passion and love of Physics catchy.

Here is a (probably poor) list of everyone I can think of to thank (no offense if you're not on it – I have the memory of a gold-fish!).

Geoff Austin – for your great sense of humor and kind nature (and view on Global Warming!!); Paul Barker – for being a realist and an idealist at the same time, for your cool jokes, sarcasm and cynicism and simultaneous unwavering fairness and honesty – you see the world without bias and accept it; Gary Bold – for being the nuttiest, funniest professor who cheers us up by just walking into the room; Mark Conway – for showing us all those demos and fun-as experiments. You really do brighten up undergrad classes and bring a spark of wonder into everyday phenomena; Maarten Hoogerland – for being the nice, friendly, casual, honest and simple guy that you are. For laughing with us, for understanding us. David Krofcheck – for your jokes and friendliness, the Einstein quotes, and for talking American (I miss it!). And finally, to Lionel Watkins who taught me healthy respect for experimental Physics and many, many other things. Thanks for the thousands of jokes and stories, for telling me about Feynman, for Jedi skul and all the fun times!

I want to also say a huge thanks to Sze Tan, although he will probably never read this. I've never even *met* Sze, and yet I admire him greatly! Thank you for being a real Physicist, for *wanting* to teach and share your knowledge and help us find things out. I have read many of your course notes and I can *feel* your enthusiasm and passion for Physics beaming at me from every line! Not only do you love Physics and are real damn good at it, you're also a brilliant teacher, making everything super clear and easy, yet always telling the full story without "babyfying" it. I can only say that I *hope* you will one day return to academia because – let's face it – you were *born* for it! Thanks heaps for the QO Toolbox too, I would've been a goner without it! I owe you big time!

Next, to Simon who's been baby-sitting me for as long as I can remember. You are the only non-professor guy I know who really, really *gets* it. How wonderful Physics is. We both share the same passion for it, but its been you who's been saving my neck over the years! Its also been your influence in helping me decide to take on this project which I have enjoyed infinitely. Thank-you for giving me those notes on the Master equation, I couldn't resist referencing them because they are just so damn good! I've also used your dissertation quite extensively so thank you for making it so brilliant. Where would I be without you?

To everyone at home for not making me do any house work and letting me spend all my time working. To my brother Danny especially, for being there with me for the last 22 years.

To everyone – THANK-YOU!!!

Sophie S.S. , Auckland, June 2009

email: sophie.s.s@hotmail.com

3

Contents

Chapter 1

Introduction

The global framework into which this dissertation fits is *Quantum Optics*, which is a very big, very well established area of Physics. Quantum Optics (in contrast to classical Optics where light is treated as a wave) basically deals with understanding light as photons. The much celebrated theory of Quantum Electrodynamics is then clearly closely related, as it addresses the interaction of photons with matter.

More specifically, our discussion will be set in the context of Cavity Quantum Electrodynamics, which is a particular branch off from QED. Because the interaction strength between matter and single photons in free space is very weak at optical frequencies, in Cavity QED we confine the electromagnetic field together with an atom to a mirrored cavity. This increases the interaction strength by a few orders of magnitude, thereby making quantum effects dominant. The idea is that we can now directly observe and make measurements on a system which is to a great extent determined by this interaction of light with matter, making it possible to test the theory of QED. Now, this field of Physics has existed for many decades and much progress has been made, mostly with *actual* atoms in *actual* mirror cavities.

In the last ten years, with advances in micro-technology and superb production techniques, a new context for the same theory has sprung up, namely: Solid-State Physics. It is possible to construct an equivalent system to our atom-in-a-cavity in what is essentially a miniature electric circuit. In this Circuit QED, it is possible to easily attain coupling strengths *much* greater than in the standard set-up, and hence (higher order) quantum effects that we are so interested in observing become accessible to measurement.

It is these recent advances that form the inspiration for our work. A very fundamental model in Quantum Optics, the *Jaynes-Cummings* model, will be used to describe our system. Furthermore, we shall have to use the theory of "Open Quantum Systems" to develop an appropriate mathematical treatment. Once we are familiar with the model and framework, we will begin discussing interesting Quantum effects and their significance. I will first introduce concepts and phenomena in "standard" problems, and only *then* begin discussing original results in our particular case.

Chapter 2

The Jaynes-Cummings Model

The Jaynes-Cummings Model (JCM) has been central in Quantum Optics ever since it was first proposed [1]. It describes the interaction of a two-level atom with a mode of electromagnetic radiation. Usually, in order to realize this model experimentally, both the atom and the field mode are confined to a mirrored cavity, whereby we enter the realm of what is known as *Cavity Quantum Electrodynamics* (CQED). This model is very simple, which in fact constitutes its biggest virtue. Because we can solve it analytically, our understanding of the system is very profound. However, this did not hinder physicists – both theoreticians and experimentalists – from investigating it for decades. On the contrary: it *stimulated* more and more research as new angles on old problems were explored. Moreover, practically all of the more complicated models have at their roots some connection to the JCM. That is, to describe a complex system, one begins from a very simple idea which is understood completely, and then builds on top of that.

For these reasons, the JCM is highly important. Even more so to us, as it is essentially *the* basis for our work. Hence, in this chapter, we shall derive the relevant Hamiltonian and then solve the problem analytically.

2.1 Derivation of the Hamiltonian

The general method of this section was inspired by [2]. Also note that Gaussian units are used.

The system Hamiltonian can be written in the form

$$H_{JC} \;\; = \;\; H_A + H_F + H_I \tag{2.1.1}$$

where the terms on the right-hand side stand for the free atomic, free field and the interaction Hamiltonians, in that order. Our task is to find expressions for these three terms.

2.1.1 Free Hamiltonians

The two-level atom has only two states by assumption, so let us denote them $|g\rangle$ for ground and $|e\rangle$ for excited. Because this Hilbert space is two-dimensional, we will introduce Pauli

operators to simplify the notation. Thus, define

$$
\begin{aligned}
\sigma_+ &= |e\rangle \langle g|, \\
\sigma_- &= |g\rangle \langle e|, \\
\sigma_z &= [\sigma_+, \sigma_-].
\end{aligned}
\tag{2.1.2}
$$

Now, we will choose the zero of our energy scale to coincide with the ground state of the atom. Therefore, since every operator can be expanded in terms of its eigenstates and eigenvalues as $A = \sum_i a_i |a_i\rangle \langle a_i|$, we can write the free atomic Hamiltonian

$$
H_A = \hbar\omega_A |e\rangle \langle e| = \hbar\omega_A \sigma_+ \sigma_-,
\tag{2.1.3}
$$

where ω_A is the transition frequency between the two states.

Next, consider a single mode of electromagnetic (EM) radiation. The quantization of Electromagnetism is not in the scope of this work (for example, see [3] Chapter 2), however, it should not be too surprising that EM fields can be described by a collection of Harmonic Oscillators. The basic Hamiltonian for a quantized Harmonic Oscillator can of course be written in terms of the ladder operators, a and $a^\dagger$. It has the well-known form

$$
H = \hbar\omega(a^\dagger a + 1/2)
\tag{2.1.4}
$$

with ω being the oscillator frequency. Recall that this Hamiltonian has Fock (also known as number) states as its eigenstates, with eigenvalues $\hbar\omega(n + 1/2)$, according to

$$
H |n\rangle = \hbar\omega(n + \frac{1}{2}) |n\rangle.
$$

In the above, $|n\rangle$ is the n-photon Fock state, and the effect of the ladder operators on number states is

$$
\begin{aligned}
a |n\rangle &= \sqrt{n} |n - 1\rangle \\
a^\dagger |n\rangle &= \sqrt{n + 1} |n + 1\rangle.
\end{aligned}
$$

As one can see, a ($a^\dagger$) destroys (creates) one quantum of excitation in the oscillator and hence is termed the *annihilation* (*creation*) operator.

In general, we need an annihilation operator a for each mode – that is, per wave-vector $\mathbf{k}$ and polarization state λ. However, because all of these modes are orthogonal, the total Hamiltonian for a collection of modes is simply the *sum* over all possible wave-vectors and polarizations. This means the above eqn (2.1.4) should be replaced by

$$
H = \sum_{\mathbf{k},\lambda} \hbar\omega_{\mathbf{k}} (a_{\mathbf{k}\lambda}^\dagger a_{\mathbf{k}\lambda} + 1/2).
\tag{2.1.5}
$$

Although this is simple enough to do, we will only be needing one mode in the work that follows, and the extra indices and summations tend to make equations look more complicated then they really are. So I will specialize at this early stage to the case of a single mode of EM radiation. Therefore, let us define the free cavity field (of resonant frequency ω_c) Hamiltonian

$$
H_F = \hbar\omega_c a^\dagger a
\tag{2.1.6}
$$

where we have dropped the $1/2\hbar\omega_c$. This is the zero-point energy of the field, which is a constant and does not contribute to the energy measured by a photon absorbing detector[1].

---

[1]This is not to say it is not experimentally detectable. The zero-point energy can be observed in the Casimir Effect as vacuum fluctuations (virtual-photon processes).

2.1.2   Interaction Hamiltonian

Our next goal is to find an expression for the interaction Hamiltonian – some form of coupling between the cavity and the atom. We will take the perhaps slightly longer route out of the traditional two, but it is the more fundamental. It will allow us to explicitly see all the approximations being made – an important point to be aware of since each approximation holds under different conditions; one would be ill-advised to apply the same simplified model globally to *all* physical situations.

2.1.2.1   Minimal-Coupling approach

From our experience with classical EM fields, we may expect to see something like

$$\mathbf{E}(\mathbf{r}, t) \;=\; \hat{\mathbf{e}} E_o \cos(\omega t - \mathbf{k} \cdot \mathbf{r}) \tag{2.1.7}$$

for the electric field. In fact, the quantized version of this equation can also be written as a traveling wave expansion [2]. It becomes

$$\mathbf{E}(\mathbf{r}) \;=\; \hat{\mathbf{e}} \sqrt{\frac{2\pi\hbar\omega_c}{V}} \left\{ a e^{i\mathbf{k}\cdot\mathbf{r}} + a^\dagger e^{-i\mathbf{k}\cdot\mathbf{r}} \right\}. \tag{2.1.8}$$

In the above, $\hat{\mathbf{e}}$ is the unit polarization vector which is real, corresponding to plane polarized light. Linear polarization can be assumed without loss of generality. ε_o is the permittivity of free space and V is the effective mode volume of the cavity. Note that eqn (2.1.8) gives us a Schrödinger picture operator, which is therefore time-independent. Similarly, it turns out that the vector potential $\mathcal{A}$ can be written [2]

$$\mathcal{A}(\mathbf{r}) \;=\; \hat{\mathbf{e}} \sqrt{\frac{2\pi\hbar c^2}{\omega_c V}} \left\{ a e^{i\mathbf{k}\cdot\mathbf{r}} + a^\dagger e^{-i\mathbf{k}\cdot\mathbf{r}} \right\}. \tag{2.1.9}$$

We will make immediate use of the expression for the vector potential, but eqn (2.1.8) will turn up naturally in the course of the derivation, so it is helpful to see it before-hand.

Imagine a Hydrogen-like atom interacting with an EM field. The Hamiltonian for the free atom has the familiar form

$$H \;=\; \frac{\mathbf{p}_m^2}{2\mu} + \mathcal{V} \tag{2.1.10}$$

where μ is the reduced mass of the nucleus-electron system and $\mathcal{V}$ is the electrostatic potential due to the nucleus. Now, classically, an EM field can be described by a scalar potential Φ and a vector potential $\mathcal{A}$. When such a field is present, the canonical momentum $\mathbf{p}_c$ is related to the mechanical momentum $\mathbf{p}_m$ via $\mathbf{p}_c = \mathbf{p}_m + \frac{q}{c}\mathcal{A}$. Here q is the charge. In the case of an electron, we adopt the convention that $q = -e = -1.6 \times 10^{-19}$ C, i.e. $e = 1.6 \times 10^{-19}$ C is positive. Therefore, the changes needed in eqn (2.1.10) are:

- swap $\mathbf{p}_m$ for $\mathbf{p}_c + \frac{e}{c}\mathcal{A}$, the effective mechanical momentum (from now on, we write $\mathbf{p}$ for the canonical momentum, dropping the subscript),

- add the electrostatic energy due to the additional scalar potential, and

- add the free Hamiltonian for the field, since we are interested in the atom-field system.

It is also understood that we will be treating all the classical quantities such as $\mathcal{A}$ as quantum-mechanical *operators*. Making these changes leads us to

$$H \;=\; \frac{1}{2\mu}\left(\mathbf{p}+\frac{e}{c}\mathcal{A}\right)^2 + \mathcal{V} - e\Phi + H_F. \tag{2.1.11}$$

Because we have no external electrostatic potential, we set Φ to zero. Also, since $\mathbf{p}$ and $\mathcal{A}$ are operators, we need to be careful about their order when expanding the square. Taking this into account, eqn (2.1.11) becomes

$$H \;=\; \frac{1}{2\mu}\mathbf{p}^2 + \mathcal{V} + \hbar\omega_c a^\dagger a + \frac{e}{2\mu c}\left[\mathbf{p}\cdot\mathcal{A}+\mathcal{A}\cdot\mathbf{p}\right] + \frac{e^2}{2\mu c^2}\mathcal{A}^2. \tag{2.1.12}$$

Recognizing the first two terms as the Hamiltonian of the free atom, and the third as the free Hamiltonian of the field, that leaves us with the fourth and fifth terms as resulting from the interaction.

Now, the $\mathcal{A}^2$ term corresponds to two-photon processes in the quantum-mechanical sense. Under "normal" parameter regimes (those that are practically achievable), this term contributes very little and is usually dropped. So, the term of interest to us is

$$H_I \;=\; \frac{e}{2\mu c}\left[\mathbf{p}\cdot\mathcal{A}+\mathcal{A}\cdot\mathbf{p}\right]. \tag{2.1.13}$$

2.1.2.2 Dipole Approximation

Recall our expression for the vector potential from eqn (2.1.9):

$$\mathcal{A}(\mathbf{r}) \;=\; \hat{\mathbf{e}}\,\sqrt{\frac{2\pi\hbar c^2}{\omega_c V}}\left\{ae^{i\mathbf{k}\cdot\mathbf{r}} + a^\dagger e^{-i\mathbf{k}\cdot\mathbf{r}}\right\}.$$

We would like to use it here, but before we do, there is a further simplification to be made: the *Dipole Approximation*. One can think of $\mathbf{r}$ as the position of the electron from our Hydrogenic atom and introduce $\mathbf{r}_A$ to denote the position of the COM of the entire atom (so effectively, the position of the nucleus). If the wavelength is much greater than the size of the atom (which is reasonable since $\lambda = \mathcal{O}(500\ nm)$ and the Bohr radius is $\mathcal{O}(0.5\ \text{Å})$), i.e. $\lambda \gg |\mathbf{r}-\mathbf{r}_A|$, it is sufficient to evaluate the exponential at $\mathbf{r}_A$ instead of $\mathbf{r}$. Mathematically, this can be seen from

$$\begin{aligned}
e^{\pm i\mathbf{k}\cdot\mathbf{r}} \;&=\; e^{\pm i\mathbf{k}\cdot(\mathbf{r}_A+(\mathbf{r}-\mathbf{r}_A))}\\
&=\; e^{\pm i\mathbf{k}\cdot\mathbf{r}_A}\left(1\pm 2\pi i\frac{|\mathbf{r}-\mathbf{r}_A|}{\lambda}\frac{\mathbf{k}\cdot(\mathbf{r}-\mathbf{r}_A)}{|\mathbf{k}|\,|\mathbf{r}-\mathbf{r}_A|}\cdots\right)\\
&\approx\; e^{\pm i\mathbf{k}\cdot\mathbf{r}_A}. \tag{2.1.14}
\end{aligned}$$

Physically, this approximation reduces the full interaction energy to just that of the electric-*dipole* interaction (hence the name). The electric-quadrapole and magnetic-dipole energies are smaller by a factor of the fine structure constant $\alpha = 1/137$ and indeed can be neglected.

Because we have swapped $\mathbf{r}$ for $\mathbf{r}_A$, the phases in $\mathcal{A}$ are now constant so the field mode (we can make the same approximation in eqn (2.1.8)) is independent of the cavity geometry[2]. This is a humongous simplification! Let us see how far that takes us.

Using the above approximation then, the interaction Hamiltonian becomes

$$H_I \;=\; \frac{e}{\mu c}\sqrt{\frac{2\pi\hbar c^2}{\omega_c V}}\;\mathbf{p}\cdot\hat{\mathbf{e}}\left\{ae^{i\mathbf{k}\cdot\mathbf{r}_A}+a^\dagger e^{-i\mathbf{k}\cdot\mathbf{r}_A}\right\}. \tag{2.1.15}$$

We would like to express $\mathbf{p}$ through $\mathbf{r}$, and so to this end, consider the Heisenberg equation of motion for $\mathbf{r}$

$$\dot{\mathbf{r}} \;=\; \frac{1}{i\hbar}\left[\mathbf{r}, H_A\right] \qquad \Rightarrow$$

$$\mathbf{p} \;=\; \frac{\mu}{i\hbar}\left[\mathbf{r}, H_A\right], \qquad \text{as } \mathbf{p}=\mu\dot{\mathbf{r}}. \tag{2.1.16}$$

Moreover, we can insert two identity operators expanded over the atomic states, and write

$$\mathbf{p} \;=\; \sum_{\alpha=g,e}\sum_{\alpha'=g,e}\left|\alpha\right\rangle\left\langle\alpha\right|\mathbf{p}\left|\alpha'\right\rangle\left\langle\alpha'\right|$$

$$= \;\left\langle g\right|\mathbf{p}\left|g\right\rangle\left|g\right\rangle\left\langle g\right|+\left\langle e\right|\mathbf{p}\left|e\right\rangle\left|e\right\rangle\left\langle e\right|+\left\langle g\right|\mathbf{p}\left|e\right\rangle\left|g\right\rangle\left\langle e\right|+\left\langle e\right|\mathbf{p}\left|g\right\rangle\left|e\right\rangle\left\langle g\right|. \tag{2.1.17}$$

Now, from eqn (2.1.16), we can write explicitly

$$\mathbf{p} \;=\; -i\omega_A\mu\left(\mathbf{r}\left|e\right\rangle\left\langle e\right|-\left|e\right\rangle\left\langle e\right|\mathbf{r}\right). \tag{2.1.18}$$

Evaluating the four terms in eqn (2.1.17),

$$\begin{aligned}
\left\langle g\right|\mathbf{p}\left|g\right\rangle &\;=\; 0, \\
\left\langle e\right|\mathbf{p}\left|e\right\rangle &\;=\; 0, \\
\left\langle g\right|\mathbf{p}\left|e\right\rangle &\;=\; -i\omega_A\mu\left\langle g\right|\mathbf{r}\left|e\right\rangle, \\
\left\langle e\right|\mathbf{p}\left|g\right\rangle &\;=\; i\omega_A\mu\left\langle e\right|\mathbf{r}\left|g\right\rangle.
\end{aligned} \tag{2.1.19}$$

If we further define $\mathbf{d}_{ge}=-e\left\langle g\right|\mathbf{r}\left|e\right\rangle$, we can write $\mathbf{p}$ through the raising and lowering atomic Pauli operators as

$$\mathbf{p} \;=\; \frac{i\omega_A\mu}{e}\left(\mathbf{d}_{ge}\sigma_- - \mathbf{d}_{ge}^*\sigma_+\right). \tag{2.1.20}$$

Substituting the above into eqn (2.1.15), we obtain

$$H_I \;=\; \frac{e}{\mu c}\sqrt{\frac{2\pi\hbar c^2}{\omega_c V}}\;\frac{i\omega_A\mu}{e}\left(\mathbf{d}_{ge}\sigma_- - \mathbf{d}_{ge}^*\sigma_+\right)\cdot\hat{\mathbf{e}}\left\{ae^{i\mathbf{k}\cdot\mathbf{r}_A}+a^\dagger e^{-i\mathbf{k}\cdot\mathbf{r}_A}\right\}. \tag{2.1.21}$$

This is in fact the starting point of the second approach to deriving H_I mentioned in the introduction. It is simply the electric field from eqn (2.1.8) dotted with the dipole operator $-e\sum_{n=1}^{Z}\mathbf{r}_n$ where the summation is over all the electrons.

---

[2]I have been using the plane waves expansion for the field from the beginning, but in fact, the form of the mode depends on the cavity shape. Plane wave are just particularly nice to deal with, and as we see now, it does not matter anyway. Incidentally, experimentalists *do* tend to use spherical mirrors in practice.

We will now use a very common "trick" which will come in handy countless times during our subsequent work. The basic idea is that we can absorb phases into operators since in Quantum Mechanics, kets which differ by absolute phase only are equivalent. Thus, the operator $\hat{A}$ and $\hat{A}\,e^{i\phi}$ can be considered as essentially the same physical operator. However, if one chooses to absorb a phase of ϕ into $\hat{A}$, one better also absorb a phase of $-\phi$ into $\hat{A}^\dagger$! Other than that, the absorb-a-phase-into-an-operator procedure is trivial and so we will not detail how it is done from now on, but rather just mention it in passing when we use it.

To simplify the notation then, let us write $\mathbf{d}_{ge} \cdot \hat{\mathbf{e}} \equiv d_{ge}e^{i\eta}$ and recall that $\pm i = e^{\pm i\pi/2}$. So, we can absorb a phase of $\pm(\eta + \pi/2)$ into $\sigma_\mp$ and $\pm\mathbf{k} \cdot \mathbf{r}_A$ into a and $a^\dagger$. Finally, define the coupling strength (atom-field)

$$g = \sqrt{\frac{2\pi}{\omega_c V \hbar}}\;\omega_A d_{ge}, \tag{2.1.22}$$

and with this, we can write

$$H_I = \hbar g \left(\sigma_+ + \sigma_-\right)\left(a^\dagger + a\right). \tag{2.1.23}$$

2.1.2.3 Rotating-Wave Approximation

While this is a very *simple* form for the interaction Hamiltonian, it is not yet analytically solvable. There still remains one approximation to be made: the Rotating-Wave Approximation (RWA). Expanding eqn (2.1.23) we have four terms:

$$\sigma_+ a^\dagger, \quad \sigma_+ a, \quad \sigma_- a^\dagger, \quad \sigma_- a.$$

Under the RWA, the first and last terms are neglected. We will now briefly discuss the physical justification, and then illustrate these arguments mathematically. In the process, we will get the chance to familiarize ourselves with the Dirac (also known as the Interaction) picture, which will be constantly used throughout the dissertation.

To begin with, we note that both $\sigma_+ a^\dagger$ and $\sigma_- a$ either create or destroy *two* quanta of excitation in the atom-field system. On the other hand, $\sigma_+ a$ and $\sigma_- a^\dagger$ leave the total excitation of the system unchanged, they simply transfer one quantum of excitation between the atom and field. Hence the first and last terms do not conserve energy to first order. These terms correspond to virtual or two (and more) photon processes which clearly contribute very little. In fact, the RWA is really justified if $g \ll \omega_A \sim \omega_c$, and we shall see why in a moment.

2.1.2.4 Digression: Interaction Picture

Let us now see how the RWA comes about mathematically. To do this, we need to transform the interaction Hamiltonian into a convenient Dirac picture. In this particular case, the transformation is very simple and so we can do it in detail this first time to demonstrate the key ideas.

Define the free Hamiltonian

$$H_o = H_A + H_c = \hbar\omega_A\sigma_+\sigma_- + \hbar\omega_c a^\dagger a. \tag{2.1.24}$$

We shall use H_o to generate the unitary operator for the transformation

$$U = \exp\left(-\frac{i}{\hbar}H_o t\right). \tag{2.1.25}$$

An operator A in the Schrödinger picture becomes in the Dirac picture (denoted traditionally by a tilde),

$$\tilde{A} = U^\dagger A U. \tag{2.1.26}$$

To find this (time-dependent) transformed operator, one can adopt either of two approaches, depending on which is easier. One is to just follow the definition, while the other is to solve the equivalent of Heisenberg's equation of motion. It has the usual form (if A is not explicitly time-dependent in the Schrödinger picture)

$$\frac{d\tilde{A}}{dt} = \frac{1}{i\hbar}\left[\tilde{A}(t), H_o\right], \tag{2.1.27}$$

except that we notice that in place of the total Hamiltonian, we have only H_o. We will take this second approach, as in our case the calculation becomes trivial. We begin by finding $\tilde{a}$. Recall that H_o is the same in both pictures and that

$$\left[a, a^\dagger a\right] = \left[a, a^\dagger\right] a + a^\dagger \left[a, a\right] = a. \tag{2.1.28}$$

Now, the commutator $[\tilde{a}(t), H_o]$ which is in the Dirac picture can be found by first taking the commutator in the Schrödinger picture and then transforming the result. Putting everything together then:

$$\frac{d\tilde{a}}{dt} = -i\omega_c\tilde{a} \quad \text{with initial condition} \quad \tilde{a}(0) = a$$
$$\Rightarrow \quad \tilde{a} = a\, e^{-i\omega_c t}. \tag{2.1.29}$$

Of course this immediately gives us $\tilde{a}^\dagger = a^\dagger e^{i\omega_c t}$. Similarly, we can find $\tilde{\sigma}_-$.
Since $[\sigma_-, \sigma_+\sigma_-] = \sigma_-$,

$$\frac{d\tilde{\sigma}_-}{dt} = -i\omega_A\tilde{\sigma}_- \quad \text{with initial condition} \quad \tilde{\sigma}_-(0) = \sigma_-$$
$$\Rightarrow \quad \tilde{\sigma}_- = \sigma_-\, e^{-i\omega_A t} \quad \text{and} \quad \therefore \quad \tilde{\sigma}_+ = \sigma_+\, e^{i\omega_A t}. \tag{2.1.30}$$

2.1.2.5 Back to the RWA

Now that we have the operators in the Dirac picture, we can transform all of H_I. Assuming for the moment that $\omega_o = \omega_c = \omega_A$[3], we get

$$\tilde{H}_I = \hbar g\left(\sigma_+ a + a^\dagger\sigma_-\right) + \hbar g\left(\sigma_- a e^{-2i\omega_o t} + \sigma_+ a^\dagger e^{2i\omega_o t}\right). \tag{2.1.31}$$

_____

[3]Approximately, this is normally the case. If any detuning is present, it is insignificant on the scale that is important here. Using ω_o simply make the argument more transparent.

The terms that are neglected in the RWA are oscillating at a very high frequency compared with the other two (which are stationary in this particular Interaction picture). Solving for the dynamics of the system typically involves an integration of the Hamiltonian over time. Because the rest of the Hamiltonian evolves on a much longer time-scale, these fast oscillations get averaged out fairly quickly. That is, the effect due to the so-called *counter-rotating* terms – those neglected in the RWA – is insignificant.

This gives us the second argument for why the RWA is valid, so we can, at last, write the final form of the interaction Hamiltonian

$$H_I = \hbar g \left(\sigma_+ a + a^\dagger \sigma_- \right) \tag{2.1.32}$$

where we have transformed back into the Schrödinger picture. Thus, the final result of this section is the Jaynes-Cummings Hamiltonian:

$$H_{JC} = H_A + H_F + H_I = \hbar \omega_A \sigma_+ \sigma_- + \hbar \omega_c a^\dagger a + \hbar g \left(\sigma_+ a + a^\dagger \sigma_- \right). \tag{2.1.33}$$

2.1.3 External Driving

The JC Hamiltonian as found above indeed encapsulates the essential physics of the system. The key elements of the model are already in place. However, from a practical point of view, the system as it is at the moment is not very useful. This is because there is no clear way to make measurements on it, to probe its dynamics. It is very common to consider an external driving field which is driving the cavity. The external driving is controlled by the experimentalist, allowing us to interact with the atom-cavity system, thus allowing for a controlled investigation.

However, the driving term (which we will derive shortly) is capable of producing some very interesting effects. We will discuss those when the time comes. Just keep in mind that the driving, although not strictly part of the original JCM, is capable of generating very interesting phenomena under the correct circumstances.

2.1.3.1 Cavity-Laser interaction

The driving field can be classically described by a vector potential [2]

$$\mathcal{A} = \hat{\mathbf{e}} \frac{c \mathcal{E}_o}{\omega_L} \cos(\omega_L t - \mathbf{k} \cdot \mathbf{r} + \phi) \tag{2.1.34}$$

where $\mathcal{E}_o$ is the amplitude of the laser field, ω_L is its frequency, and I have deliberately used the same symbol for the polarization unit vector as we had in the previous section. This is because we will later on have to assume that the driving field interacts with a cavity mode of the same polarization only, so we may as well use the same symbol from the start.

Now, consider the $\mathbf{k} \cdot \mathbf{r} + \phi$ term in eqn (2.1.34). Since to a good approximation there is no spatial variation, we can set these equal to some constant phase, say ϕ_o. Under near-resonant conditions ($\omega_o \approx \omega_L$), the coupling of the cavity and external field can be taken to be linear with coupling constant ε. Then the cavity-laser interaction Hamiltonian is [2]:

$$H_d = \varepsilon \frac{c \mathcal{E}_o}{2\omega_L} \hat{\mathbf{e}} \left(e^{-i(\omega_L t + \phi_o)} + e^{i(\omega_L t + \phi_o)} \right) \cdot \hat{\mathbf{e}} \sqrt{\frac{2\pi \hbar c^2}{\omega_c V}} \left(a e^{i\psi_o} + a^\dagger e^{-i\psi_o} \right). \tag{2.1.35}$$

Next, absorbing the phases into the ladder operators and making a RWA, the driving term reduces to

$$H_d = \varepsilon \frac{c\mathcal{E}_o}{2\omega_L} \sqrt{\frac{2\pi\hbar c^2}{\omega_c V}} \left(a e^{i\omega_L t} + a^\dagger e^{-i\omega_L t} \right). \tag{2.1.36}$$

Finally, define

$$\mathcal{E} = \varepsilon \frac{c\mathcal{E}_o}{2\omega_L} \sqrt{\frac{2\pi c^2}{\hbar \omega_c V}}, \tag{2.1.37}$$

so that we get

$$H_d = \hbar\mathcal{E} \left(a e^{i\omega_L t} + a^\dagger e^{-i\omega_L t} \right). \tag{2.1.38}$$

2.1.4 Overview

Thus, we have now completed the derivation of the model that will be investigated in this thesis. All together, our Hamiltonian is

$$H = \hbar\omega_A \sigma_+ \sigma_- + \hbar\omega_c a^\dagger a + \hbar g \left(\sigma_+ a + a^\dagger \sigma_- \right) + \hbar\mathcal{E} \left(a e^{i\omega_L t} + a^\dagger e^{-i\omega_L t} \right). \tag{2.1.39}$$

2.2 Analytic Solution of the JCM

The approach to the problem is the same as presented by Carmichael (unpublished lecture notes).

We will now find the eigenvalue spectrum and eigenvectors of the on-resonance[4] ($\omega_o = \omega_c = \omega_A$) JCM specified by

$$H_{JC} = \hbar\omega_o \sigma_+ \sigma_- + \hbar\omega_o a^\dagger a + \hbar g \left(\sigma_+ a + a^\dagger \sigma_- \right). \tag{2.2.40}$$

This is a very important calculation because it arms us with intuition, i.e. helps us visualize and understand physical systems which may be different to the above and yet "close enough" to the JCM so that the ideas are essentially the same.

We have already introduced the eigenkets of H_A – they are $|g\rangle$ and $|e\rangle$ with eigenvalues 0 and $\hbar\omega_o$ respectively. The eigenstates of H_F are Fock states $|n\rangle$ with eigenvalues $n\hbar\omega_o$. Clearly, the ground state of the system must be $|g\rangle |0\rangle$ since there are no excitations in this state. When the coupling is turned off (i.e. $g = 0$), all the excited states are doubly degenerate. For example, $|g\rangle |1\rangle$ and $|e\rangle |0\rangle$ both have one quantum of excitation of the same energy $\hbar\omega_o$. In fact, all pairs of (excited) states $|g\rangle |n\rangle$ and $|e\rangle |n-1\rangle$ are doubly degenerate. These are called 'bare' states.

When the coupling is turned on, these pairs of states are coupled. As a result, two new eigenstates are formed – the so-called 'dressed' states, which are shifted in energy above

---

[4]The non-resonant case can be solved by following exactly the same procedure.

and below from the previously degenerate eigenvalue. Let us see how this comes out from a simple calculation.

We begin by observing the effect of H_{JC} on $|g\rangle\,|n\rangle$ and $|e\rangle\,|n-1\rangle$:

$$
\begin{aligned}
H_{JC}\,|g\rangle\,|n\rangle &= \hbar\omega_o n\,|g\rangle\,|n\rangle + \hbar g\sqrt{n}\,|e\rangle\,|n-1\rangle\,, \\
H_{JC}\,|e\rangle\,|n-1\rangle &= \hbar\omega_o n\,|e\rangle\,|n-1\rangle + \hbar g\sqrt{n}\,|g\rangle\,|n\rangle\,.
\end{aligned}
\tag{2.2.41}
$$

Next, assume that the eigenvectors of H_{JC} are linear combinations of $|g\rangle\,|n\rangle$ and $|e\rangle\,|n-1\rangle$:

$$
\begin{aligned}
|E_n\rangle &= a_n\,|g\rangle\,|n\rangle + b_n\,|e\rangle\,|n-1\rangle\,, \quad \text{with} \tag{2.2.42} \\
H_{JC}\,|E_n\rangle &= E_n\,|E_n\rangle\,. \tag{2.2.43}
\end{aligned}
$$

Now substitute eqn (2.2.42) into eqn (2.2.43) and evaluate the left-hand side by making use of eqn (2.2.41). Then, equating coefficients of the same states on both sides, we get the following system of equations:

$$
\begin{pmatrix} n\omega_o - \frac{E_n}{\hbar} & \sqrt{n}g \\ \sqrt{n}g & n\omega_o - \frac{E_n}{\hbar} \end{pmatrix}
\begin{pmatrix} a_n \\ b_n \end{pmatrix} = \vec{0}.
\tag{2.2.44}
$$

To solve this linear algebra problem, write down the characteristic equation (i.e. set the determinant to zero), which immediately gives

$$
E_n^\pm = \hbar\left(n\omega_o \pm \sqrt{n}g\right).
\tag{2.2.45}
$$

Having obtained the eigenvalues, the eigenkets are found (by inspection) to be

$$
|n\pm\rangle = \frac{1}{\sqrt{2}}\left(|g\rangle\,|n\rangle \pm |e\rangle\,|n-1\rangle\right).
\tag{2.2.46}
$$

2.2.1   Summary

Thus, our final result is as follows: the on-resonance Jaynes-Cummings system described by H_{JC} has the ground state $|g,0\rangle$ with eigenvalue zero and excited eigenkets $|n\pm\rangle = \frac{1}{\sqrt{2}}\left(|g\rangle\,|n\rangle \pm |e\rangle\,|n-1\rangle\right)$ with corresponding eigenvalues $E_n^\pm = \hbar\left(n\omega_o \pm \sqrt{n}g\right)$ where $n \in \mathbb{N}$. The eigenvalue spectrum is commonly referred to as the JC *ladder* with the dressed states as the *rungs*. The states $|1\pm\rangle$ are traditionally referred to as the vacuum Rabi states (for historical reasons) and I, too, shall adopt this terminology. To illustrate this spectrum, it is depicted in fig. 2.1 showing the first five dressed states and the important frequencies.
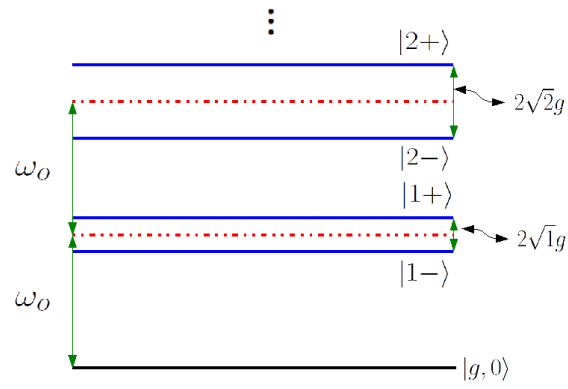
Figure 2.1: Spectrum of the JCM: in red, we see the degenerate, uncoupled atomic and field levels. In blue, we have the final dressed states of the system which form closely spaced doublets, the splitting of which is proportional to the coupling, g.

Chapter 3

Open Quantum Systems

In our undergraduate years, we are taught about quantum systems: how to describe them in the language of Hilbert spaces, beautiful rules for their manipulation, how they evolve in time. We look at different pictures – Schrödinger, Heisenberg and Dirac, and how to transform between them. Everything adds up, all the little pieces come together and we begin to feel that we *understand* Quantum Mechanics. The fundamental concepts – the essential foundations – are, at this stage, already in place.

However, this is not the full story. There is still one step forward to be made, a step that links realistic experimental conditions and the immaculate theory we have developed. That step is the introduction of *ignorance*.

The theory as we have seen it so far is applicable to systems which are at once both *pure* and *closed*, i.e. we know everything there is to know about them. Of course, there is intrinsic quantum uncertainty present which gives rise to the probabilistic nature of Quantum Mechanics. But one cannot make that uncertainty go away. No matter how many times you measure the position and momentum of a particle in a particular state, or with what precision, the Heisenberg Uncertainty Principle (HUP) is still there.

On the other hand, consider a fundamentally different situation: what if we don't exactly *know* what state the particle is in? Then, how do we know with respect to what state we must take the expectation value and variance? How to compare theory with experiment when you are aware, for example, of the imperfection of your state-preparing apparatus?

An equivalent situation is realized when the system of interest is interacting with some other system which, to us, is inaccessible. This occurs all the time in practice; to fully isolate a system is difficult, to say the least. There is a formalism which accommodates the additional classical ignorance which we are presently faced with. This is the subject of first section in this chapter.

Once we have seen how to describe these so-called *mixed* states, we will find the equation of motion that governs their time evolution. We will allow our system to interact with a reservoir – loosing energy to it, in fact, through dissipation (thus the name *open* quantum systems). As the end result, we shall derive the *Master equation in Lindblad form*.

3.1 Density Operators

Here I partly follow [4], but a few arguments and proofs were also borrowed from [5] and [6].

Consider an ensemble of identical particles, all in the same quantum-mechanical state $|\psi\rangle$. Let A be some observable with a complete set of eigenkets $|a_1\rangle$, $|a_2\rangle$, $|a_3\rangle$ and eigenvalues a_1, a_2, a_3. Suppose $|\psi\rangle = c_1 |a_1\rangle + c_2 |a_2\rangle + c_3 |a_3\rangle$. If we now measure the expectation value of A, the result will differ between the individual particles. Some will give a_1, some a_2 and others a_3, despite the fact that they were all initially prepared in exactly the same state.

More precisely, if enough particles are measured (to give representative statistics), we will notice that a_1 turns up with a probability of $|c_1|^2$, a_2 with $|c_2|^2$ and so on, for obvious reasons.

Alternatively, think of a situation (as discussed in the introduction) where there is only *one* particle, but its initial state is not completely known. Say we can only specify the probability that our apparatus prepared this or that state. Suppose our apparatus specifications tell us that the output state is $|a_1\rangle$ with probability $|c_1|^2$, $|a_2\rangle$ with probability $|c_2|^2$, and similarly for $|a_3\rangle$. Then when we ask the question "what is the expectation value of A in the output state?", the best answer we can give is: a_1 with probability $|c_1|^2$, a_2 with $|c_2|^2$, etc...

This type of uncertainty regarding exactly what the state of the system is can result not only from imperfect preparation, but also if the system interacts with some environment which we have no way of measuring. That is, even if my initial state is unambiguously determined, if the following evolution has (small) contributions from an outside environment (which I have no knowledge of), I can no longer claim to know the state of the system with certainty.

All three of the above scenarios are equivalent in terms of their consequences. We call such states (with added classical uncertainty) *mixed* states, as opposed to *pure* states which can be described by a single ket. Motivated by this discussion and realizing that expectation values are the key quantities in Quantum Mechanics as they connect experiment to theory, we proceed to introduce the formal mathematical framework.

3.1.1 Definition and expectation values

Suppose we have a mixed state specified by probabilities (sometimes called *fractional populations*) w_i to have state $|\alpha^{(i)}\rangle$. The different $|\alpha^{(i)}\rangle$'s do not have to be orthogonal. For example, I could specify a mixed state for a spin-$\frac{1}{2}$ system by saying it has some probability to be in the $|z+\rangle$ state, some other fractional population to be in $|x-\rangle$, and yet some third probability to be in the $|y+\rangle$ state. However, we do require a normalization condition on the weight factors: $\sum_i w_i = 1$.

The ensemble average of some operator A with eigenvalues a' and eigenvectors $|a'\rangle$ in this mixed state is

$$\langle A \rangle \;=\; \sum_i w_i \langle \alpha^{(i)}| A |\alpha^{(i)}\rangle \;=\; \sum_i \sum_{a'} w_i \left|\langle a'|\alpha^{(i)}\rangle\right|^2 a'. \tag{3.1.1}$$

Note that two probability concepts are present in this expression:

1. $\langle a'|\alpha^{(i)}\rangle$ represents the amplitude of being in state $\left|\alpha^{(i)}\right\rangle$ and then being found in a state $|a'\rangle$; quantum uncertainty stems from the coherent superposition of states, as opposed to

2. the classical chance of being in state $\left|\alpha^{(i)}\right\rangle$ which enters through the weight factors w_i.

To reinforce the difference between a coherent superposition and a probabilistic mixture, recall that coherent superpositions can exhibit interference while probabilistic mixtures cannot. These concepts are in fact central not only to our discussion here, but globally in Quantum Mechanics.

For reasons which will become apparent in a moment, we next write the ensemble average of A in some arbitrary complete basis $|b\rangle$.

$$
\begin{aligned}
\langle A \rangle \;&=\; \sum_i w_i \sum_{b'} \sum_{b''} \left\langle \alpha^{(i)}|b'\right\rangle \left\langle b'\right| A \left|b''\right\rangle \left\langle b''|\alpha^{(i)}\right\rangle \\
&=\; \sum_{b'} \sum_{b''} \left(\sum_i w_i \left\langle b''|\alpha^{(i)}\right\rangle \left\langle \alpha^{(i)}|b'\right\rangle \right) \left\langle b'\right| A \left|b''\right\rangle \qquad (3.1.2)
\end{aligned}
$$

We notice that the term in the brackets is a general property of the ensemble, completely independent of the fact that we chose to look at observable A. It is a matrix element of an operator that characterizes the mixed state. We call this the *density* operator, defined as

$$
\rho \;=\; \sum_i w_i \left|\alpha^{(i)}\right\rangle \left\langle \alpha^{(i)}\right| . \qquad (3.1.3)
$$

Clearly then, interpreting eqn (3.1.2) as matrix multiplication,

$$
\langle A \rangle \;=\; tr\left[\rho A\right]. \qquad (3.1.4)
$$

This is a very powerful result. It tells us that once the density operator for a mixed state is obtained, we can calculate the expectation value of any operator.

3.1.2 Properties

First, since the trace is representation independent, we can do the calculations in the most convenient basis for the problem. Second, note that ρ is Hermitian and therefore possesses a complete set of eigenkets with real eigenvalues. The reader should not be surprised to find that these are, of course, $\left|\alpha^{(i)}\right\rangle$ and w_i. Finally, since $\sum_i w_i = 1$, it is evident that $tr\left[\rho\right] = 1$.

At this point, a note of caution is in order. Naturally, any pure state can be represented by a density operator, and this density operator is unique for a given pure state. However, the converse is not true. Mixed states cannot be represented by a single ket, and there are many *different* ensembles that give the *same* density operator.

Given a density operator, one can perform a simple check to determine whether it corresponds to a pure or mixed state. Specifically, we calculate $tr\left[\rho^2\right]$. If the result is one, the state is pure. If the state is mixed, the result will be between zero and one. Below is a short proof of this rather cute fact.

Lemma: $\sum_i w_i^2 \leq 1$ and $\sum_i w_i^2 = 1 \Leftrightarrow w_i = \delta_{ik}$ for some index k, i.e. only one of the w_i's, w_k, is non-zero.

We can see this from

$$1 = \left(\sum_i w_i\right)\left(\sum_j w_j\right) = \sum_{i,j} w_i w_j = \sum_i w_i^2 + \sum_{i \neq j} w_i w_j. \tag{3.1.5}$$

Now, since all $0 \leq w_i \leq 1$, $\sum_{i \neq j} w_i w_j \geq 0$. Then, from the above equality, we conclude that $\sum_i w_i^2 \leq 1$. But $\sum_{i \neq j} w_i w_j$ is only non-zero if more than one of the w_i's is non-zero. Thus $\sum_i w_i^2 = 1$ only if one of the w_i's is non-zero. This proves the lemma, and since

$$tr\left[\rho^2\right] = \sum_i w_i^2, \tag{3.1.6}$$

we have proved the above stated criterion for distinguishing pure from mixed states. $\square$

A quick note is appropriate before we discuss the next topic. A very handy property of the trace (constantly used in practice) is that it is invariant under cyclic permutations of its arguments. That is, for example,

$$tr\left[ABC\right] = tr\left[CAB\right] = tr\left[BCA\right]. \tag{3.1.7}$$

Naturally, this can be extended to any number of matrices.

Now we move on to look at the time evolution of the density operator. Recall that

$$\rho = \sum_i w_i \left|\alpha^{(i)}\right\rangle \left\langle\alpha^{(i)}\right|.$$

If we do not disturb the ensemble, the only time evolution will have to come from the $\left|\alpha^{(i)}\right\rangle$'s. Luckily, we already have the Schrödinger equation to tell us how they evolve. We have

$$\frac{d\rho}{dt} = \sum_i w_i \left[\frac{d\left|\alpha^{(i)}\right\rangle}{dt}\left\langle\alpha^{(i)}\right| + \left|\alpha^{(i)}\right\rangle\frac{d\left\langle\alpha^{(i)}\right|}{dt}\right]. \tag{3.1.8}$$

But by Schrödinger,

$$\frac{d\left|\alpha^{(i)}\right\rangle}{dt} = \frac{1}{i\hbar}H\left|\alpha^{(i)}\right\rangle \tag{3.1.9}$$

$$\frac{d\left\langle\alpha^{(i)}\right|}{dt} = -\frac{1}{i\hbar}\left\langle\alpha^{(i)}\right|H. \tag{3.1.10}$$

Putting this back into eqn (3.1.8), we see that

$$\frac{d\rho}{dt} = \frac{1}{i\hbar}\sum_i w_i \left[H\left|\alpha^{(i)}\right\rangle\left\langle\alpha^{(i)}\right| - \left|\alpha^{(i)}\right\rangle\left\langle\alpha^{(i)}\right|H\right]$$

$$= \frac{1}{i\hbar}\left(H\rho - \rho H\right)$$

$$= \frac{1}{i\hbar}\left[H,\rho\right]. \tag{3.1.11}$$

This is called the *Von Neumann* equation. It is hard to miss the similarity to Heisenberg's equation of motion except for the reverse order in the commutator. However, we are in the Schrödinger picture and hence there is no direct connection.

3.1.3   Reduced Density Operators

In the introduction of §3.1 we considered the case where our system was to be interacting with an environment which is inaccessible to measurements. This idea can be developed further and is the topic for this final section on density matrices.

Assume that we have two sub-systems A and B with Hilbert spaces $\mathcal{H}_A$ and $\mathcal{H}_B$. Then the Hilbert space of the two sub-systems together is the tensor product space $\mathcal{H} = \mathcal{H}_A \otimes \mathcal{H}_B$. Let $|\psi_i\rangle$ be some set of kets on $\mathcal{H}$. Then the density operator describing the joint system $A \oplus B$ may be written in the form

$$\rho = \sum_i w_i |\psi_i\rangle \langle\psi_i| . \tag{3.1.12}$$

Quite often, one of these sub-systems – say B – is the environment or reservoir which we cannot measure. We do not *want* to measure it as we are only interested in system A. Thus, a compact description of A is needed. Essentially, we would like to somehow include B as part of our uncertainty regarding the state of A.

What we do is called taking the partial trace over B (or tracing out B). This process can be thought of as performing an imaginary complete measurement on B and then ignoring the result. We discard the quantum nature of B and only retain its presence as the possible effects it can have on A. As long as we have no knowledge of the actual state B is in, we are left with a mixed ensemble for A described by some new density operator which is now only on $\mathcal{H}_A$.

Let us give the mathematical definition then. Suppose that we have a complete set of kets $|b_n\rangle$ spanning $\mathcal{H}_B$. Then the *reduced density operator* of system A alone is defined as

$$\rho_A = \sum_n \langle b_n| \rho |b_n\rangle = tr_B [\rho] . \tag{3.1.13}$$

It is easy to see that ρ_A has all of the properties we discussed above – after all, it is just another density operator. In practice, almost all the time, we use reduced density operators. This especially applies in the case we will consider in the following section where a system of interest is damped into a reservoir and we wish to only concern ourselves with that system.

The density operator formalism is not merely an easier way of keeping track of things, it is the *only* way complicated physical situations can be reduced to a simple model and solved to yield highly accurate predictions. We have gained a very powerful tool in this section, and it is time to use it in the derivation of the next key element of open quantum systems, namely the Master equation.

3.2 The Master Equation

In this section we will mainly follow the derivation given by [2] and [7] – [9].

Consider a system S interacting with a reservoir R. The reservoir is assumed to be some really big system at thermal equilibrium and is of no interest to us – it is just the environment surrounding our thought-experiment. We are wanting to follow the evolution of the system S. But because S and R interact, S is not a closed system. In fact, it is loosing energy to the reservoir through dissipation. This is a completely ordinary idea: think of a mass on a spring, set oscillating in the lab. We all know that after some time it will come to rest. This is because it is interacting with the air around it and looses energy through the process of friction (for the sake of the analogy we pretend the spring is perfectly elastic). However, if you were asked to solve for the dynamics of this mass (and given such information as the cross-sectional area of the mass and the constant of air resistance), you would not have to think twice – we know how to insert this environment into the problem by including a decay term in Newton's law.

What we are trying to do here is find a quantum-mechanical analogue for the above mass example into which the environment enters as parameters only (e.g. air resistance). We are interested in the reduced density matrix for S, but the Von Neumann equation alone will not do, just like it is insufficient to naïvely apply Hooke's law to our mass ignoring the damping. The equation we will get as the end result is called the Master equation in Lindblad form, and (like the modified Newton's law) is essentially the Von Neumann equation with some additional decay terms. The fact that this equation may be written down in such a general way is very powerful – it means that instead of having to re-derive a slightly different Master equation for each problem, we can (at least in most cases) write it down immediately according to the rule we shall find.

Thus, although the derivation is somewhat lengthly, it is *not* difficult and will save a lot of time in the long run. Let us begin then.

3.2.1 Von Neumann: integro-differential form

Assume that the total Hamiltonian H for the system plus reservoir can be written

$$H \quad = \quad H_S + H_R + H_{SR} \tag{3.2.14}$$

where H_S is the Hamiltonian of S, H_R of R, and H_{SR} is the interaction Hamiltonian. Let $\chi(t)$ be the density operator for the $S \oplus R$ system and the reduced density matrix for S be denoted ρ. That is,

$$\rho(t) \quad = \quad tr_R \left[\chi(t) \right]. \tag{3.2.15}$$

As one may trivially verify, once $\rho(t)$ is obtained, the expectation value of any operator A on the Hilbert space of S alone can be found by taking $tr_S \left[A\rho(t) \right]$. This is why we seek an equation of motion for ρ.

However, we start from the only thing we know so far – the equation of motion for χ:

$$\dot{\chi}(t) \;=\; \frac{1}{i\hbar}\left[H, \chi(t)\right]. \tag{3.2.16}$$

Note that χ obeys the Von Neumann equation because the system of $S \oplus R$ together *is* closed, so the results of §3.1 apply. Next, we need to transform into an interaction picture (recall we have already met the Dirac picture in §2.1.2.4). Define $H_o = H_S + H_R$ to generate the transformation. Then in this Dirac picture

$$\tilde{\chi}(t) \;=\; e^{\frac{i}{\hbar}H_o t}\chi(t)e^{-\frac{i}{\hbar}H_o t}. \tag{3.2.17}$$

Taking the time derivative of $\tilde{\chi}(t)$ and using the product rule

$$\begin{aligned}
\dot{\tilde{\chi}}(t) \;&=\; \frac{i}{\hbar}H_o\tilde{\chi}(t) + e^{\frac{i}{\hbar}H_o t}\dot{\chi}(t)e^{-\frac{i}{\hbar}H_o t} - \frac{i}{\hbar}\tilde{\chi}(t)H_o \\
&=\; \frac{i}{\hbar}\left[H_o, \tilde{\chi}(t)\right] + e^{\frac{i}{\hbar}H_o t}\dot{\chi}(t)e^{-\frac{i}{\hbar}H_o t}.
\end{aligned} \tag{3.2.18}$$

Now substitute the RHS of eqn (3.2.16) for $\dot{\chi}(t)$ in the second term above

$$\begin{aligned}
\dot{\tilde{\chi}}(t) \;&=\; \frac{i}{\hbar}\left[H_o, \tilde{\chi}(t)\right] + \frac{1}{i\hbar}\, e^{\frac{i}{\hbar}H_o t}\left[H, \chi(t)\right]e^{-\frac{i}{\hbar}H_o t} \\
&=\; \frac{i}{\hbar}\left[H_o, \tilde{\chi}(t)\right] - \frac{i}{\hbar}\left[H_o, \tilde{\chi}(t)\right] + \frac{1}{i\hbar}\left[\tilde{H}_{SR}(t), \tilde{\chi}(t)\right] \\
&=\; \frac{1}{i\hbar}\left[\tilde{H}_{SR}(t), \tilde{\chi}(t)\right],
\end{aligned} \tag{3.2.19}$$

where we have used $H = H_o + H_{SR}$ and $\tilde{H}_o = H_o$. Physically, transforming into this picture separates the fast evolution due to H_o from the slow evolution caused by H_{SR}. Mathematically, it will allow us to identify and make some legitimate approximations.

We now formally integrate eqn (3.2.19) to get

$$\tilde{\chi}(t) \;=\; \tilde{\chi}(0) + \frac{1}{i\hbar}\int_0^t dt' \left[\tilde{H}_{SR}(t'), \tilde{\chi}(t')\right]. \tag{3.2.20}$$

If we then take this solution and substitute it back into eqn (3.2.19), we obtain

$$\dot{\tilde{\chi}}(t) \;=\; \frac{1}{i\hbar}\left[\tilde{H}_{SR}(t), \tilde{\chi}(0)\right] - \frac{1}{\hbar^2}\int_0^t dt' \left[\tilde{H}_{SR}(t), \left[\tilde{H}_{SR}(t'), \tilde{\chi}(t')\right]\right]. \tag{3.2.21}$$

3.2.2 Master equation for the reduced density operator

As the next step, we assume that the interaction between S and R is turned on at $t = 0$, and as a consequence, at this initial time the system and reservoir are uncorrelated. This is just a different way of saying the total state of the $S \oplus R$ system can be factorized as

$$\tilde{\chi}(0) \;=\; \chi(0) \;=\; \rho(0)\mathcal{R}(0), \tag{3.2.22}$$

where ρ is the reduced density matrix of S (as defined above) and similarly, $\mathcal{R}$ for R. Also, clearly, $\tilde{\rho}(t) = tr_R[\tilde{\chi}(t)]$.

Now we return our attention to eqn (3.2.21). We would like to trace out R on both sides, but we would like to get rid of the first term on the RHS for later convenience and simplicity. That is, we would like to have

$$tr_R\left\{\left[\tilde{H}_{SR}(t), \tilde{\chi}(0)\right]\right\} = 0. \tag{3.2.23}$$

Since the trace is over R and $\tilde{\chi}(0)$ factorizes as we have assumed above, this is certainly the case if

$$tr_R\left\{\tilde{H}_{SR}(t)\mathcal{R}(0)\right\} = 0. \tag{3.2.24}$$

In words, eqn (3.2.24) is saying that we get to drop the term we want if the reservoir operators that make up H_{SR} have an expectation value (i.e. mean) of zero in the initial state of the reservoir. But what if they do not? Then all we must do is observe that after taking the partial trace over R, $tr_R\left\{\tilde{H}_{SR}(t)\mathcal{R}(0)\right\}$ is an operator on the Hilbert space of S alone. Therefore, it can be *shifted* to be part of H_S. This means that we can always arrange for eqn (3.2.23) to hold. Thus, taking the partial trace over R on both sides of eqn (3.2.21),

$$\dot{\rho}(t) = -\frac{1}{\hbar^2}\int_0^t dt'\, tr_R\left\{\left[\tilde{H}_{SR}(t), \left[\tilde{H}_{SR}(t'), \tilde{\chi}(t')\right]\right]\right\}. \tag{3.2.25}$$

3.2.3   The Born Approximation

Now, we know $\tilde{\chi}(0)$ factorizes because there is no prior interaction between S and R. But as time goes on the presence of coupling means this will no longer be true (S and R will become *entangled*). If the coupling is weak, though, we can assume that $\chi(t)$ will not be very different from the uncorrelated state it would have been without coupling. "Very" can be quantified as "to first order in H_{SR}". Furthermore, we are assuming the reservoir is a large system maintained at thermal equilibrium, difficult to perturb, and thus *its* state can be assumed to remain unchanged, i.e. $\mathcal{R}(0)$. Putting these arguments together into a mathematical statement:

$$\tilde{\chi}(t) = \tilde{\rho}(t)\mathcal{R}(0) + \mathcal{O}(H_{SR}). \tag{3.2.26}$$

In analogy to a similar sort of assumption in scattering theory, this is called the *Born Approximation*. Next, we intend to substitute eqn (3.2.26) into eqn (3.2.25). However, there is no need to keep the $\mathcal{O}(H_{SR})$ – after the commutators are expanded it would become third order in H_{SR}, while we only wish to keep terms up to second order in the Born Approximation. After substitution, we get

$$\dot{\rho}(t) = -\frac{1}{\hbar^2}\int_0^t dt'\, tr_R\left\{\left[\tilde{H}_{SR}(t), \left[\tilde{H}_{SR}(t'), \tilde{\rho}(t')\mathcal{R}(0)\right]\right]\right\}. \tag{3.2.27}$$

3.2.4 The Markov Approximation

Inspecting the above equation, it becomes evident that it is not Markovian. In other words, $\tilde{\rho}$ depends on its past history. This memory of the system is present through the integration over t'. On the other hand, the future evolution of a Markovian system depends only on its present state. Physically, it is of course possible that past values of the system affect its future: the system affects the reservoir thus imprinting the state of S onto R, then the reservoir affects the system in return. But, if R is large and maintained at thermal equilibrium, any information imprinted on it by the system will be erased very quickly. The reservoir will re-equilibrate on a time-scale much shorter than that which is significant for the evolution of S. If this condition is true, i.e. the time-scales for the (fast) decay of R and the (slow) evolution of S are widely separated, we can make the next approximation.

This is called the *Markov Approximation* and comes down to replacing $\tilde{\rho}(t')$ by $\tilde{\rho}(t)$ in eqn (3.2.27):

$$\dot{\tilde{\rho}}(t) \;=\; -\frac{1}{\hbar^2} \int_0^t dt' \, tr_R \left\{ \left[\tilde{H}_{SR}(t), \left[\tilde{H}_{SR}(t'), \tilde{\rho}(t)\mathcal{R}(0) \right] \right] \right\}. \tag{3.2.28}$$

3.2.4.1 A model for H_{SR}

It is possible to express the requirement of the Markov Approximation mathematically; without this statement we will not be able to finish the derivation. However, to do this and to proceed in general, we need to re-state our model more specifically. We write

$$H_{SR} \;=\; \sum_i s_i \Gamma_i \tag{3.2.29}$$

where the s_i's are operators on the Hilbert space of S and the Γ_i's on that of R. This is the expression we will use, but allow me to justify and explain this a little. First of all, the operators s_i must obey a special condition[1], namely

$$[s_i, H_S] \;=\; \hbar w_i s_i, \quad \text{and} \quad w_i \neq w_{i'} \quad \text{unless} \quad i \;=\; i'. \tag{3.2.30}$$

Of course this means that in the Dirac picture, the time evolution of the $\tilde{s}_i$'s is governed by

$$\dot{\tilde{s}}_i(t) \;=\; \frac{1}{i\hbar} \left[\tilde{s}_i(t), H_S \right], \tag{3.2.31}$$

with the trivial solution

$$\tilde{s}_i(t) \;=\; s_i e^{-iw_i t}. \tag{3.2.32}$$

Now, this is all very well, but there still remain many hidden omissions I have not justified yet. In fact, the most general expansion of H_{SR} would have to be of the form

$$H_{SR} \;=\; \hbar \sum_{ijk} \alpha_{ijk} s_{ij} \Gamma_k. \tag{3.2.33}$$

---

[1]The special condition is, as one can see, of the eigen-problem type. Think of a *super operator* which acts on ordinary operators. It is defined entirely by its action: take the commutator of the argument with H_S. This motivates calling s_i the set of eigen-*operators* of this super operator.

The difference here is that we have allowed the eigen-operators (see footnote 1) s_i to have a degeneracy which is labeled through the index j (the α's are constants). Because there are three sums now, we are allowing for all possible pairing up of s_i's and Γ_i's. But, if one carries through the subsequent arguments using this general expression, eventually we would have to make one (reasonable) assumption after the other, and at the end of the process end up with a result that can be derived straight-forwardly if one assumes eqn (3.2.29) from the beginning. An example of this full process can be found in [2] while a clearer version is contained in [9].

I will *not* do this here. Instead we simply accept eqn (3.2.29) and go on from there. So then, in the Interaction picture,

$$\tilde{H}_{SR}(t) \;=\; \sum_i \tilde{s}_i(t)\tilde{\Gamma}_i(t). \tag{3.2.34}$$

If we substitute this back into eqn (3.2.28),

$$\dot{\tilde{\rho}}(t) \;=\; -\sum_i\sum_j \int_0^t dt'\, tr_R\left\{\left[\tilde{s}_i(t)\tilde{\Gamma}_i(t), \left[\tilde{s}_j(t')\tilde{\Gamma}_j(t'), \tilde{\rho}(t)\mathcal{R}(0)\right]\right]\right\}. \tag{3.2.35}$$

Now, expanding commutators, realizing that the trace is only over R and using the cyclic property of the trace, we get

$$\dot{\tilde{\rho}}(t) \;=\; -\sum_i\sum_j \int_0^t (\tilde{s}_i(t)\tilde{s}_j(t')\tilde{\rho}(t) - \tilde{s}_j(t')\tilde{\rho}(t)\tilde{s}_i(t))\, tr_R\left\{\mathcal{R}(0)\tilde{\Gamma}_i(t)\tilde{\Gamma}_j(t')\right\}$$

$$+ (\tilde{\rho}(t)\tilde{s}_j(t')\tilde{s}_i(t) - \tilde{s}_i(t)\tilde{\rho}(t)\tilde{s}_j(t'))\, tr_R\left\{\mathcal{R}(0)\tilde{\Gamma}_j(t')\tilde{\Gamma}_i(t)\right\}\, dt'. \tag{3.2.36}$$

Finally, we are able to state the requirement of the Markov Approximation mathematically. Note that the condition we will shortly impose on $tr_R\left\{\mathcal{R}(0)\tilde{\Gamma}_i(t)\tilde{\Gamma}_j(t')\right\}$ also applies to $tr_R\left\{\mathcal{R}(0)\tilde{\Gamma}_j(t')\tilde{\Gamma}_i(t)\right\}$, for reasons that will become apparent in a moment.

We need to have these two correlation functions decaying very rapidly on the time-scale on which $\tilde{\rho}(t)$ evolves if the Markov Approximation is to be valid. To do this, we will take them proportional to the delta function with a complex proportionality constant (to be discussed later)

$$tr_R\left\{\mathcal{R}(0)\tilde{\Gamma}_i(t)\tilde{\Gamma}_j(t')\right\} \;\propto\; \delta(t-t'). \tag{3.2.37}$$

3.2.5 The Secular Approximation

We may now proceed from eqn (3.2.36). We shall play a little trick which will simplify the notation later. What we want to do is replace all the operators with index i in the first term and index j in the second term, by their adjoints. That is, we would like to write

$$\dot{\tilde{\rho}}(t) \;=\; -\sum_i\sum_j \int_0^t \left(\tilde{s}_i^\dagger(t)\tilde{s}_j(t')\tilde{\rho}(t) - \tilde{s}_j(t')\tilde{\rho}(t)\tilde{s}_i^\dagger(t)\right) tr_R\left\{\mathcal{R}(0)\tilde{\Gamma}_i^\dagger(t)\tilde{\Gamma}_j(t')\right\}$$

$$+ \left(\tilde{\rho}(t)\tilde{s}_j^\dagger(t')\tilde{s}_i(t) - \tilde{s}_i(t)\tilde{\rho}(t)\tilde{s}_j^\dagger(t')\right) tr_R\left\{\mathcal{R}(0)\tilde{\Gamma}_j^\dagger(t')\tilde{\Gamma}_i(t)\right\}\, dt'. \tag{3.2.38}$$

Let us consider why this is allowed. In our expansion of the *Hermitian* H_{SR} as

$$H_{SR} = \sum_i s_i \Gamma_i,$$

for each $s_i \Gamma_i$, there is some other index i' for which $s_{i'} \Gamma_{i'} = s_i^\dagger \Gamma_i^\dagger$. This must be the case for H_{SR} to be Hermitian. So clearly the following are equivalent:

$$H_{SR} = \sum_i s_i \Gamma_i = \sum_i s_i^\dagger \Gamma_i^\dagger.$$

I hope it is now evident that eqn (3.2.38) is perfectly valid. Next, we use a piece of information we already have, namely our knowledge of the time dependence of the $\tilde{s}_i$'s from eqn (3.2.32),

$$\tilde{s}_i(t) = s_i e^{-iw_i t}.$$

When we substitute this into eqn (3.2.38), we still have a double sum over i and j. However, the reservoir is large and in thermal equilibrium and we expect that different reservoir operators are uncorrelated. In other words, the only coherences are between an operator and its adjoint. Thus we are assuming that the correlation functions from eqn (3.2.37) vanish unless $i = j$. Neglecting all terms for which $i \neq j$ is called making the *Secular Approximation*. We shall make this approximation, carrying out the sum over i, which gives

$$
\begin{aligned}
\dot{\tilde{\rho}}(t) = & -\sum_j \int_0^t \left(\tilde{s}_j^\dagger(t)\tilde{s}_j(t')\tilde{\rho}(t) - \tilde{s}_j(t')\tilde{\rho}(t)\tilde{s}_j^\dagger(t) \right) tr_R \left\{ \mathcal{R}(0)\tilde{\Gamma}_j^\dagger(t)\tilde{\Gamma}_j(t') \right\} \\
& + \left(\tilde{\rho}(t)\tilde{s}_j^\dagger(t')\tilde{s}_j(t) - \tilde{s}_j(t)\tilde{\rho}(t)\tilde{s}_j^\dagger(t') \right) tr_R \left\{ \mathcal{R}(0)\tilde{\Gamma}_j^\dagger(t')\tilde{\Gamma}_j(t) \right\} dt' \\
= & -\sum_j \left(s_j^\dagger s_j \tilde{\rho}(t) - s_j \tilde{\rho}(t) s_j^\dagger \right) \int_0^t dt' e^{iw_j(t-t')} tr_R \left\{ \mathcal{R}(0)\tilde{\Gamma}_j^\dagger(t)\tilde{\Gamma}_j(t') \right\} \\
& + \left(\tilde{\rho}(t) s_j^\dagger s_j - s_j \tilde{\rho}(t) s_j^\dagger \right) \int_0^t dt' e^{-iw_j(t-t')} tr_R \left\{ \mathcal{R}(0)\tilde{\Gamma}_j^\dagger(t')\tilde{\Gamma}_j(t) \right\}. \quad (3.2.39)
\end{aligned}
$$

3.2.5.1 Decay rates

The next step is also based on a piece of information we have already discussed. We are interested in "evaluating" the integrals over t'. But remember that from eqn (3.2.37) we know the correlation functions are proportional to $\delta(t - t')$. It is easy to see that in this case the integrals come out equal to the proportionality constant and are complex conjugates of each other. For concreteness, denote

$$\int_0^t dt' e^{iw_j(t-t')} tr_R \left\{ \mathcal{R}(0)\tilde{\Gamma}_j^\dagger(t)\tilde{\Gamma}_j(t') \right\} = \frac{1}{2}(\gamma_j + i\Delta_j), \quad (3.2.40)$$

with γ_j, $\Delta_j \in \mathbb{R}$. One could carry on with this more general approach, allowing the proportionality constant to be complex, as is done in [2] and [9]. Now, at the end of this process, it becomes clear that a non-zero Δ_j enters the final result as an energy shift of the

system Hamiltonian H_S. But, this energy shift is usually very small and can be neglected. Therefore, there is no harm in assuming from the beginning that $\Delta_j = 0$.

What this means is that the two integrals are not merely complex conjugates, but equal to each other, both being $\gamma_j/2$. We shall continue with this assumption. Putting this into eqn (3.2.39), we see that

$$\dot{\tilde{\rho}}(t) \;=\; -\sum_j \frac{\gamma_j}{2}\left(-2s_j\tilde{\rho}(t)s_j^\dagger + s_j^\dagger s_j\tilde{\rho}(t) + \tilde{\rho}(t)s_j^\dagger s_j\right). \tag{3.2.41}$$

Remark: Actually, the proportionality to the delta function is an approximation. An alternative way of interpreting eqn (3.2.40) is the following. We are basically computing the rate of dissipation from the system into the environment. Recall Fermi's Golden Rule from time-dependent perturbation theory. There, the probability for a transition into a group of "similar" states is found by treating the density of states in this group as roughly constant, which then allows one to take this average value outside the integral. The point is that it is the availability of energy states in the reservoir of the *relevant frequency* that is important. Hence, in reality, the decay rates γ_j depend on the density of states in the reservoir around the resonant frequency w_j. This idea is not emphasized if one simply assumes eqn (3.2.37), but the conclusion is unchanged.

3.2.6   The final result

As the last step, we must transform back from the Dirac into the Schrödinger pictures. Seeing as we have traced over R in the equation for ρ, the reduced density matrix for S, this conversion is achieved through the equation

$$\dot{\rho}(t) \;=\; \frac{1}{i\hbar}[H_S, \rho(t)] + e^{-\frac{i}{\hbar}H_S t}\dot{\tilde{\rho}}(t)e^{\frac{i}{\hbar}H_S t} \tag{3.2.42}$$

as can be readily proved by following the exact same logic applied in eqn (3.2.18). The final result is thus

$$\dot{\rho}(t) \;=\; \frac{1}{i\hbar}[H_S, \rho(t)] + \sum_j \frac{\gamma_j}{2}\left(2s_j\rho(t)s_j^\dagger - s_j^\dagger s_j\rho(t) - \rho(t)s_j^\dagger s_j\right). \tag{3.2.43}$$

This is also sometimes written in terms of *collapse* operators that absorb γ_j into their definition: $C_j = \sqrt{\gamma_j}s_j$. With this notation, the Master equation becomes

$$\dot{\rho}(t) \;=\; \frac{1}{i\hbar}[H_S, \rho(t)] + \sum_j \left(C_j\rho(t)C_j^\dagger - \frac{1}{2}C_j^\dagger C_j\rho(t) - \frac{1}{2}\rho(t)C_j^\dagger C_j\right). \tag{3.2.44}$$

Yet another very common (and handy!) notation makes use of a super operator, called the (generalized) *Liouvillian* and denoted $\mathcal{L}$. The idea is that $\mathcal{L}$ acts on ρ – an ordinary operator – and is defined by its action, specified by the RHS of eqn (3.2.44). Explicitly, we can write

$$\mathcal{L} \;=\; \frac{1}{i\hbar}[H_S, \cdot] + \sum_j \left(C_j\cdot C_j^\dagger - \frac{1}{2}C_j^\dagger C_j\cdot - \frac{1}{2}\cdot C_j^\dagger C_j\right), \tag{3.2.45}$$

in which case the Master equation is just

$$\dot{\rho}(t) = \mathcal{L}\rho(t). \tag{3.2.46}$$

This completes the derivation. We will use this equation time and again in the following chapters.

3.3 Quantum Regression Theorem

Here we will closely follow [8].

Having done so much work to derive the Master equation, it would be a shame not to identify any "free bonuses" we can get out of it. The Quantum Regression Theorem (QRT) is one of those. Actually, it isn't truly a theorem, but more like a lemma, a consequence of our work in the previous section. The Master equation will allow us to solve for $\rho(t)$ which in turn allows us to compute any expectation value we like *at any one time.* But how about two-time averages? It turns out there is a simple way to compute them directly from ρ_{ss} and $\mathcal{L}$, so let us see how this comes about.

What we wish to find is this:

$$\langle A(t)B(t')C(t)\rangle, \tag{3.3.47}$$

where A, B, C are operators on the Hilbert space of S and $t' \geq t$. A quantity of this sort is important for evaluating two-time correlation functions which carry much information about, and characterize some aspects of, the system. Thus, in practice, we find ourselves needing to compute these two-time averages all the time. Luckily, this is not too difficult.

Because the operators in eqn (3.3.47) are time-dependent, it is to be interpreted in the Heisenberg picture, but at the end of the calculation we shall transform back. The superscript '(H)' will denote an operator in the Heisenberg picture and no superscript denotes a Schrödinger operator. We have then

$$
\begin{aligned}
\langle A(t)B(t')C(t)\rangle &= tr_{S\otimes R}\left[\chi^{(H)}A^{(H)}(t)B^{(H)}(t')C^{(H)}(t)\right] \\
&= tr_{S\otimes R}\left[\chi^{(H)}e^{\frac{i}{\hbar}Ht}Ae^{\frac{i}{\hbar}H(t'-t)}Be^{-\frac{i}{\hbar}H(t'-t)}Ce^{-\frac{i}{\hbar}Ht}\right].
\end{aligned} \tag{3.3.48}
$$

We now use the cyclic property of the trace to rearrange the order to

$$
\begin{aligned}
\langle A(t)B(t')C(t)\rangle &= tr_{S\otimes R}\left[Be^{-\frac{i}{\hbar}H(t'-t)}Ce^{-\frac{i}{\hbar}Ht}\chi^{(H)}e^{\frac{i}{\hbar}Ht}Ae^{\frac{i}{\hbar}H(t'-t)}\right] \\
&= tr_{S\otimes R}\left[Be^{-\frac{i}{\hbar}H(t'-t)}C\chi(t)Ae^{\frac{i}{\hbar}H(t'-t)}\right] \\
&= tr_S\left[B\, tr_R\left[e^{-\frac{i}{\hbar}H(t'-t)}C\chi(t)Ae^{\frac{i}{\hbar}H(t'-t)}\right]\right].
\end{aligned} \tag{3.3.49}
$$

Now define $\tau = t' - t$ and

$$\chi_{CA}(\tau) = e^{-\frac{i}{\hbar}H\tau}C\chi(t)Ae^{\frac{i}{\hbar}H\tau} \tag{3.3.50}$$

31

which allows us to write eqn (3.3.49) as

$$\langle A(t)B(t')C(t) \rangle = tr_S \left[B \, tr_R \left[\chi_{CA}(\tau) \right] \right]. \tag{3.3.51}$$

Recall that in the derivation of the Master equation, we assumed that $\chi(0)$ was factorisable. Using the same arguments we can do this here too.

$$
\begin{aligned}
\chi_{CA}(0) &= C\chi(t)A = \mathcal{R}(0)C\rho(t)A = \mathcal{R}(0)tr_R \left[C\chi(t)A \right] \\
&= \mathcal{R}(0)tr_R \left[\chi_{CA}(0) \right] = \mathcal{R}(0)\rho_{CA}(0).
\end{aligned} \tag{3.3.52}
$$

Thus we have defined $tr_R \left[\chi_{CA}(\tau) \right] = \rho_{CA}(\tau)$. Finally, since the differentiation is with respect to τ (not t), it is easy to see that

$$\frac{d}{d\tau}\chi_{CA}(\tau) = \frac{1}{i\hbar} \left[H, \chi_{CA}(\tau) \right]. \tag{3.3.53}$$

Now consider: our definition of the reduced density operator $\rho_{CA}(\tau)$, the factorisability of $\chi_{CA}(0)$ and the Von Neumann equation for $\chi_{CA}(\tau)$ are completely analogous to our starting points in deriving the Master equation! To be precise, they are equivalent to eqns (3.2.15), (3.2.22) and (3.2.16), respectively.

Furthermore, the evolution Hamiltonian H is the same in both Von Neumann equations. So, without doing any more work, we know that the differential equation for $\rho_{CA}(\tau)$ will be the same as that for $\rho(t)$, namely the Master equation with the same Liouvillian. So,

$$\frac{d}{d\tau}\rho_{CA}(\tau) = \mathcal{L}\rho_{CA}(\tau), \tag{3.3.54}$$

with the formal solution

$$\rho_{CA}(\tau) = e^{\mathcal{L}\tau}\rho_{CA}(0) = e^{\mathcal{L}\tau}(C\rho(t)A). \tag{3.3.55}$$

From here we can state the QRT directly

$$\langle A(t)B(t+\tau)C(t) \rangle = tr_S \left[Be^{\mathcal{L}\tau}(C\rho(t)A) \right] \tag{3.3.56}$$

with ρ as obtained from solving the Master equation, $\dot{\rho}(t) = \mathcal{L}\rho(t)$.

This result is the backbone of calculations of two-time correlation functions. We continue discussing correlation functions in the next chapter.

Chapter 4

Concepts and Definitions

The first three sections in this chapter will introduce and define some useful concepts. First, we give a brief summary regarding two-time correlation functions and photon statistics, followed by first-order correlation functions and spectra. These are fundamental tools for analysis in Quantum Optics and we shall make use of them when we come to do computer simulations. Next, we give a brief review of Quantum Trajectory theory which is utilized later on in the thesis for illustrating some of the ideas.

The following section will review the basic idea from a paper of Tian and Carmichael [10]. The work that follows (which is original to this dissertation) has strong connections to the key results presented in this publication. Therefore, before we move on to discussing numerical results, it is instructive to understand the phenomena that we are observing.

The final section will present a classical/traditional analytic calculation of intensity correlation functions, which is useful to understand as background to our work.

4.1   Photon Statistics

In this section I mostly follow [8] and [2].

The QRT gives us a tool to extract various information from the Master equation. In particular, we can get information about photon statistics. For example, we might ask: what is the probability of detecting a photon (emitted from some source) at time t_1 and then another photon at a later time t_2? We will now see how this issue can be approached by first looking at classical intensity correlation functions and then their quantum mechanical versions. We shall discover that some particular properties of correlation functions are possible in Quantum Mechanics but have no classical analogues. Historically, this has been the cause of much excitement in the Quantum Optics community. More importantly though, by analyzing correlation functions we can gain a better understanding of the system under investigation.

Consider a classical light beam of intensity $I(t)$. Define the second-order intensity corre-

lation function

$$g^{(2)}(\tau) = \frac{\langle I(t)I(t+\tau)\rangle}{\langle I(t)\rangle\,\langle I(t+\tau)\rangle}. \tag{4.1.1}$$

In the above, angular brackets denote a time-average. We can write $I(t)$ as a sum of its average and the fluctuations as

$$I(t) = \langle I(t)\rangle + \Delta I(t) \tag{4.1.2}$$

with the understanding that fluctuations average to zero, i.e. $\langle \Delta I(t)\rangle = 0$. Substituting this gives

$$g^{(2)}(\tau) = 1 + \frac{\langle \Delta I(t)\Delta I(t+\tau)\rangle}{\langle I\rangle^2} \tag{4.1.3}$$

and in particular,

$$g^{(2)}(0) = 1 + \frac{\langle \Delta I(t)^2\rangle}{\langle I\rangle^2} \geq 1. \tag{4.1.4}$$

Moreover, by using Cauchy's inequality $I(t_1)^2 + I(t_2)^2 \geq 2I(t_1)I(t_2)$, one can show that $g^{(2)}(0) \geq g^{(2)}(\tau) \; \forall\tau$ (note that $\tau \geq 0$). Now, lastly, we expect that for τ greater than the coherence time of the source, there will be no correlation between $I(t)$ and $I(t+\tau)$. Thus,

$$\lim_{\tau \to \infty} g^{(2)}(\tau) = 1. \tag{4.1.5}$$

For a coherent source $g^{(2)}(\tau) = 1 \; \forall\tau$. In fact, $g^{(2)}(\tau) < 1$ is not classically possible.

Now, the quantum mechanical definition of the second-order correlation function takes the form

$$g^{(2)}_{a_1 a_2}(\tau) = \frac{\left\langle a_1^\dagger(t)a_2^\dagger(t+\tau)a_2(t+\tau)a_1(t)\right\rangle}{\left\langle a_1^\dagger(t)a_1(t)\right\rangle \left\langle a_2^\dagger(t+\tau)a_2(t+\tau)\right\rangle}. \tag{4.1.6}$$

Here the angular brackets denote expectation values. We have added subscripts 1 and 2 to our field operators to label detection at two different detectors but in general one can consider $a_1 = a_2$, this would be a auto-correlation as opposed to a cross-correlation. As before, the denominator is present for normalization. What is more interesting is the particular order of the operators in the numerator. Whenever all the annihilation operators are written to the left of the creation operators, this is called *normal ordering*. Also, when operators are ordered from the outside in with increasing time, this is called *time ordering*. The numerator has both these properties. It is a consequence of the photoelectric detection process – a photon is incident, destroyed, and its energy converted to a photocurrent.

There is a simple classification scheme for light based on the properties of the two-time correlation function. It is as follows:

- $g^{(2)}(0) > 1$. Bunched light. In this case the probability of detecting two photons with a short time interval between them is higher than if the time interval is long. The photon arrives in clumps or bunches. A thermal source is an example.

- $g^{(2)}(0) = 1$. Coherent light. Random gaps between photons.

- $g^{(2)}(0) < 1$. Antibunched light (although the definition is somewhat controversial!). The opposite of bunched; photons are more evenly spread out in time than a coherent source would produce. This is not possible classically but definitely *is* quantum mechanically. An example is a source of single photons. This can be seen from the following: it is trivial to show that for a Fock state $|n\rangle$, $g^{(2)}(0) = \frac{n(n-1)}{n^2}$ and so $n = 1$ gives $g^{(2)}(0) = 0$.

There is a further classification of light according to its photon number statistics. Let $\bar{n}$ be the mean number of photons and $(\Delta n)^2$ the variance of the photon number distribution of the field. Then:

- $(\Delta n)^2 > \bar{n}$ – super-poissonian statistics.

- $(\Delta n)^2 = \bar{n}$ – poissonian statistics.

- $(\Delta n)^2 < \bar{n}$ – sub-poissonian statistics. This is also not possible classically.

Note that sub-poissonian Statistics and antibunching are independent phenomena that can be present either together or separately.

Now let us go back to eqn (4.1.6). Taking the limit $t \to \infty$ means the expectation values will be taken with respect to the steady-state density matrix. It also means that t is no longer relevant (for so-called *stationary sources*) and can be set to zero. We shall distinguish the long-time limit correlation function from that in eqn (4.1.6) by adding a subscript 'ss' for steady-state. Hence the steady-state cross-correlation of two operators μ and ν is

$$\left[g_{\mu\nu}^{(2)}(\tau)\right]_{ss} = \frac{\left\langle \mu^\dagger(0)\nu^\dagger(\tau)\nu(\tau)\mu(0)\right\rangle_{ss}}{\left\langle \mu^\dagger\mu\right\rangle_{ss}\left\langle \nu^\dagger\nu\right\rangle_{ss}}. \tag{4.1.7}$$

This is the expression we will want to calculate in the next chapter, so we may as well see how it is done now. Recall the QRT

$$\langle A(t)B(t+\tau)C(t)\rangle = tr_S\left[Be^{\mathcal{L}\tau}(C\rho(t)A)\right]$$

with ρ obtained from solving the Master equation, $\dot{\rho}(t) = \mathcal{L}\rho(t)$. Now let ρ_{ss} be the steady-state solution of the Master equation, i.e. $\mathcal{L}\rho_{ss} = 0$. Direct application of the QRT leads immediately to

$$\left[g_{\mu\nu}^{(2)}(\tau)\right]_{ss} = \frac{1}{\left\langle \mu^\dagger\mu\right\rangle_{ss}\left\langle \nu^\dagger\nu\right\rangle_{ss}} tr\left[\nu^\dagger\nu e^{\mathcal{L}\tau}\left(\mu\rho_{ss}\mu^\dagger\right)\right]. \tag{4.1.8}$$

In particular, we shall be especially interested in the case where $\nu = \mu = a$:

$$\left[g_{aa}^{(2)}(\tau)\right]_{ss} = \frac{\left\langle a^\dagger(0)a^\dagger(\tau)a(\tau)a(0)\right\rangle_{ss}}{\left\langle a^\dagger a\right\rangle_{ss}^2}. \tag{4.1.9}$$

Equation (4.1.8) is the final result of the section, and together with the classification scheme above prepares us to analyze correlation function results when we come to simulations.

4.2 Optical Spectra

We have seen how the QRT has allowed us to almost trivially calculate an important quantity, the second-order intensity correlation function. However, its application also allows us to obtain another very important result, namely the spectrum of the field. We might ask what frequency components are present in the radiated field from some system of interest, which will be a key characteristic of that system. Classically, quantities such as the energy or power spectral densities are Fourier Transforms (FT) of auto-correlation functions of the signal function, even in the presence of some random noise component.

In fact, the full Quantum Mechanical approach is not so different, except that we need to replace classical correlation functions by quantum-mechanical ones. They take the form of first-order two-time averages. A typical example would be the field from a cavity mode, $\langle a^\dagger(t+\tau)a(t)\rangle$. Its complex conjugate is $\langle a^\dagger(t)a(t+\tau)\rangle$, which is often used as an alternative definition. In practice, they can be used interchangeably. Just as in the previous section, we take the limit $t \to \infty$ to find the long-time correlation function $\langle a^\dagger(\tau)a(0)\rangle$, independent of t. The FT of this yields the spectrum.

We shall denote first-order correlation functions by $G^{(1)}$, using a capital letter because we have not yet normalized this quantity. Thus, in general, the first-order correlation of observables ν and μ is

$$G^{(1)}_{\nu\mu}(\tau) = \langle \nu^\dagger(t+\tau)\mu(t)\rangle, \tag{4.2.10}$$

$$\left[G^{(1)}_{\nu\mu}(\tau)\right]_{ss} = \langle \nu^\dagger(\tau)\mu(0)\rangle. \tag{4.2.11}$$

Note that if we wished to normalize these, we would simply divide $\left[G^{(1)}_{\nu\mu}(\tau)\right]_{ss}$ by $\langle \nu^\dagger\mu\rangle_{ss}$ to get $\left[g^{(1)}_{\nu\mu}(\tau)\right]_{ss}$.

But how does one calculate an expression of this sort? Actually, we already know the answer. Going back to the QRT formula on the previous page, if we set $A(t) \equiv 1$, the identity operator, then we arrive at

$$\langle B(t+\tau)C(t)\rangle = tr_S\left[Be^{\mathcal{L}\tau}(C\rho(t))\right]. \tag{4.2.12}$$

Alternatively, if we chose to look at $\langle \nu^\dagger(t)\mu(t+\tau)\rangle$ instead, just set $C(t) \equiv 1$ to get the corresponding formula.

We will soon need to calculate the FT, defined by: the FT of $f(t)$ is $F(\nu)$, with

$$F(\nu) = \int_{-\infty}^{\infty} f(t)\exp(-2\pi i\nu t)\,dt, \quad \text{and the inverse relationship} \tag{4.2.13}$$

$$f(t) = \int_{-\infty}^{\infty} F(\nu)\exp(2\pi i\nu t)\,d\nu. \tag{4.2.14}$$

Now, observe that we will be taking the FT of a *steady state* quantity, having taken the limit $t \to 0$. However, fluctuations away from this steady state are also possible. One could define the so-called covariance function, which is simply given by $\langle \nu^\dagger(\tau)\mu(0)\rangle - \langle \nu^\dagger\rangle\langle \mu\rangle$. It

is easy to see that this quantity, the covariance of ν and μ, is basically the correlation with the mean subtracted, and describes the above mentioned fluctuations from the steady state.

Although the *total* spectrum is the FT of the correlation function, it can be decomposed as a sum of two quantities. One is the *coherent* part of the spectrum, arising from the steady state average. The second, is the FT of the covariance, the *incoherent* part, present due to fluctuations away from this steady state. The coherent component can be shown to be proportional to a delta function and gives us no new information. The incoherent component is in fact what we are after and contains all the essential information. Thus, in practice, we will focus on calculating the incoherent spectrum by taking the FT (with respect to τ) of the normalized covariance given by

$$\frac{\left\langle \nu^\dagger(\tau)\mu(0)\right\rangle - \left\langle \nu^\dagger\right\rangle \left\langle \mu\right\rangle}{\left\langle \nu^\dagger\mu\right\rangle_{ss}}$$

which we can compute by using eqn (4.2.12).

4.3   Quantum Trajectory Theory

So far, we have seen how to use density operators and the Master equation to describe the dynamics of an open quantum system. In Cavity QED, the need for these concepts arises due to interaction of our system with a large reservoir to which it loses energy through decay. Essentially, the "problem" is this: given some particular initial state of the system (assume it is known exactly), we do not precisely know how it will evolve. For example, will there be a decay into the reservoir? If so, at what time and through which dissipative channel? We cannot predict these things exactly because the reservoir is inaccessible to us. Hence a large number of possible outcomes for the same initial conditions can occur. The best we can do is take an *ensemble average* and incorporate the damping into the equation of motion, as we have done.

However, it is not the only possible way of dealing with this situation. Here we present the alternative; the theory is called Quantum Trajectories. The basic idea is simple and goes as follows. Suppose we are given a system Hamiltonian H_S and appropriate collapse operators C_j's as in eqn (3.2.44). Assume for a moment that we can find a way of incorporating the decay processes into some effective Hamiltonian H_{eff}, so that H_{eff} carries information both about H_S and about the decay rates with their corresponding channels.

We would like to do away with density matrices and Master equations, and solve the Schrödinger equation instead, using H_{eff}. But a pure evolution will lack the element of stochastic decays into the reservoir! We must add this element into our theory in the following way. Suppose we track our system continuously through ideal detectors that are constantly monitoring its output field. We shall have an imaginary detector for each possible decay channel. As soon as a photon is incident on detector j, we know that the system has undergone a collapse through the jth channel. We can then manually apply the collapse operator to our state ket, and then continue evolving the result under H_{eff}.

Thus we have a continuous evolution between collapses governed by the effective Schrödinger equation, with collapses conditioned on stochastic signals at the detectors. But we need to

realize that a sequence of clicks at the detectors is just a particular manifestation of the process. If we try to repeat the thought experiment, we will get a different evolution because of the stochastic ("random") nature of the decay processes. Every *trajectory* is just a particular manifestation of all possible ways the evolution can proceed. We must *average* over many, many such trajectories to get an answer regarding ensemble averages and be able to give predictions.

Before we proceed to give a little more detail about the theory, I would like to draw the reader's attention to the advantages of this method over the Master equation treatment. Consider problems where the dimensionality of the Hilbert space is very large – call it N. Then to solve for the density matrix, we need to solve for each of its elements and hence we have N^2 equations. If we solve the Schrödinger equation, then we need only determine the ket, which has N elements, so the number of coupled ODEs is significantly reduced.

For small and moderate Hilbert space dimensions the Master equation may be preferable because we only need to do the calculation once whereas for the Quantum Trajectory approach, we would have to repeat the computation over and over. But when the basis size gets so big that a computer simply *cannot* handle solving N^2 equations (or does it extremely slowly), Quantum Trajectories provide a way out.

A second, highly important advantage of Trajectory theory is the new perspective. It gives us a more direct, easier way to think about what is really happening in our system, and time and again provides priceless insight and understanding. A parallel can be drawn between this approach and Feynman's path integral formulation of Quantum Mechanics – the connection is, I believe, very strong.

Let us now give a more in depth description of the method. First of all, it turns out that

$$H_{eff} = H_S - \frac{i\hbar}{2}\sum_j C_j^\dagger C_j. \qquad (4.3.15)$$

I shall not prove that this is indeed the appropriate form of the effective Hamiltonian (or anything else in this section, really. I simply summarize the results; see [2] for a much more complete discussion). However, we will get a chance to see an effective Hamiltonian of this form "in action" in the final section of the chapter, which may help the reader accept that this is indeed the correct form.

Between collapses, the evolution is given by

$$\frac{d\psi(t)}{dt} = \frac{1}{i\hbar}H_{eff}\psi(t). \qquad (4.3.16)$$

We simulate (using a Monte-Carlo method) sequences of photons arriving at the detectors. If a photon is detected at time t' at the kth detector, we artificially collapse the wave-function:

$$\psi(t'_+) = \frac{C_k\,\psi(t'_-)}{||C_k\,\psi(t'_-)||}. \qquad (4.3.17)$$

Notice that the state must be renormalized "by hand" after a collapse. In general, the Monte-Carlo approach requires working with the unnormalized wave function since the probability

for decay is contained in the norm of the state. We only need to normalize the ket when a computation of an expectation value is required, for all other purposes we can work with a non-unit norm. In particular, the probability for the kth collapse in time interval dt is $||C_k \, \psi(t)||^2 \, dt$.

Thus, we can simulate individual trajectories quite straight-forwardly. An ensemble average over sufficiently many trajectories reproduces the results of the Master equation – the two approaches are, of course, equivalent. We will use trajectories for concept illustration in the next chapter.

4.4   Dressing of dressed-states

In chapter 2 we derived the driven JC Hamiltonian

$$H \;\; = \;\; \hbar\omega_A\sigma_+\sigma_- + \hbar\omega_c a^\dagger a + \hbar g\left(\sigma_+ a + a^\dagger\sigma_-\right) + \hbar\mathcal{E}\left(ae^{i\omega_L t} + a^\dagger e^{-i\omega_L t}\right).$$

We then also derived the eigenkets and energy levels of the undriven JC system and found an anharmonic ladder of dressed states. The same spectrum is a good approximation to the spectrum of H above as long as the drive strength is weak and only serves to slightly perturb the situation. Here we specialize to the resonant case: $\omega_o = \omega_A = \omega_c$. We now consider the following scenario.

Suppose the driving frequency is tuned very closely to the lower vacuum Rabi state (or alternatively the upper). By that we mean the state $|1-\rangle$, and so $\omega_L = \omega_o - g$. Because the spectrum is so strongly anharmonic, only the transition between $|g,0\rangle$ and $|1-\rangle$ is excited, as the drive frequency does not match any other transitions. When this is the case, it is reasonable to assume that only transitions between these two states are important. Essentially, only two states *matter*, and we can approximate the situation by neglecting all but the privileged two states.

Of course such a two-state approximation is only valid as long as the other states do not contribute significantly. It will break down as the drive is increased. But our purpose here is to adopt this two-state model and use it to explain the phenomena that will be discussed shortly. The comparison of the full to the two-state model will not be analyzed, that can be found in [10]; we just want to make clear the basic principle responsible for what we shall call (after [10]) *dressing of dressed-states*.

The observation that we shall try to explain is as follows. With the cavity and atom on resonance and the laser driving the lower vacuum state, there are three frequency components in the system. Actually, the incoherent spectrum shows a so-called *Mollow triplet* with characteristic sidebands [7]. The central frequency is at $\omega = \omega_o - g$, as might be naïvely expected, but we also get two additional sidebands at frequencies which are proportional to the drive strength! More precisely, these two additional frequencies are symmetrically arranged about the central frequency at $\omega = \omega_o - g \pm \sqrt{2}\mathcal{E}$.

This is not so difficult to understand qualitatively. The situation of a two-state system driven by, or in other words coupled to, a field is precisely the starting point in the derivation of the JCM. We can expect therefore that the two states are coupled and mixed, and

new states are formed. Moreover, just like the splitting between pairs of dressed states is proportional to g, the coupling, so it must be here but g is replaced by $\mathcal{E}$ (actually, $\mathcal{E}$ is the equivalent of $g \langle n \rangle$, n being the number operator). The authors in [13] have termed this phenomenon *super-splitting* because what essentially happens is that each of the two states $|g, 0\rangle$ and $|1-\rangle$ is super-split into a doublet by the AC Stark Effect.

And now let us go through the calculation to see why and how this happens. To begin with, we need to restrict our Hamiltonian to two states only: $|g, 0\rangle$ and $|1-\rangle$. Since $|1-\rangle = \frac{1}{\sqrt{2}} (|g\rangle |1\rangle - |e\rangle |0\rangle)$, it is trivial to calculate the four matrix elements of a and σ_-. Defining $\ell_- = |g, 0\rangle \langle 1-|$, the operators of interest become $a = \frac{1}{\sqrt{2}} \ell_-$ and $\sigma_- = -\frac{1}{\sqrt{2}} \ell_-$. The Hamiltonian becomes

$$H = \hbar(\omega_o - g)\ell_+\ell_- + \hbar\frac{\mathcal{E}}{\sqrt{2}} \left(\ell_+ e^{-i(\omega_o - g)t} + \ell_- e^{i(\omega_o - g)t}\right). \qquad (4.4.18)$$

Next we would like to transform to an interaction picture with $H_o = \hbar(\omega_o - g)\ell_+\ell_-$, so that the second term above (which we shall call H_D) becomes time independent. This type of transformation is elementary and differs in no way at all from the example worked out in §2.1.2.4. It is easy to see that

$$\tilde{H}_D = \hbar\frac{\mathcal{E}}{\sqrt{2}} (\ell_+ + \ell_-). \qquad (4.4.19)$$

The next, also extremely simple step is to find the eigenkets and eigenvalues of $\tilde{H}_D$. Skipping the algebra we get

$$|\psi_{1,2}\rangle = \frac{1}{\sqrt{2}} (|1-\rangle \pm |g, 0\rangle) \quad \text{with eigenvalues}$$

$$E_{1,2} = \pm\hbar\frac{\mathcal{E}}{\sqrt{2}} . \qquad (4.4.20)$$

Now we need to somehow convert this information in the *Dirac* picture to useful information in the *Schrödinger* picture. For this purpose we appeal to the recipe given in [11]: each eigenket of $\tilde{H}_D$ must be multiplied from the left by $e^{-\frac{i}{\hbar}Et}e^{-\frac{i}{\hbar}H_o t}$ where E is its eigenvalue in the Dirac picture. This will give us periodic states of the system (the closest equivalent of "steady-states") with their frequency as the quasi-energies of the system.

First then, we realize that $U^\dagger = e^{-\frac{i}{\hbar}H_o t}$ is extremely easy to find because we are working in the basis of eigenvectors of H_o. If we choose the basis ordering $|g, 0\rangle$, $|1-\rangle$,

$$U^\dagger = \begin{pmatrix} 1 & 0 \\ 0 & e^{-i(\omega_o - g)t} \end{pmatrix}. \qquad (4.4.21)$$

Doing the multiplication as per the prescription above, we get (in the Schrödinger picture)

$$|\psi_{1,2}\rangle = \frac{1}{\sqrt{2}} \left\{ |1-\rangle e^{-i(\omega_o - g \mp \frac{\mathcal{E}}{\sqrt{2}})t} \pm |g, 0\rangle e^{\pm i\frac{\mathcal{E}}{\sqrt{2}}t} \right\}. \qquad (4.4.22)$$

The frequencies in the exponentials give us the dynamic Stark shifted frequencies. Each of the eigen-frequencies is "split" into a doublet at $\pm\frac{\mathcal{E}}{\sqrt{2}}$ from the unshifted frequency. Diagrammatically, eqn (4.4.22) is represented as shown in fig. 4.1. We see that there are three
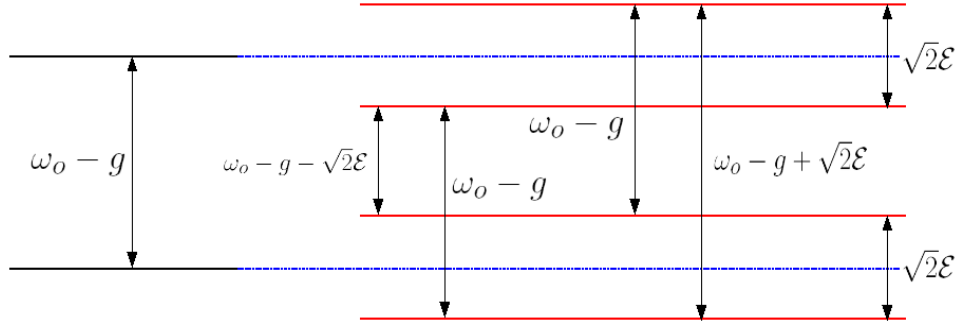
Figure 4.1: Stark-shifted levels of the two-state model driven by an external field.

possible transition frequencies between the quasi-energies present in the system. They are $\omega_o - g$ and $\omega_o - g \pm \sqrt{2}\mathcal{E}$, as we "knew" they had to be.

Remark: Fig. 4.1 is the usual way of representing the situation, but it is a little misleading. The red lines cannot be interpreted as actual steady states – they are *not*. The red lines are best thought of as representing the quasi-eigen-frequencies of the system, stemming from our two periodic solutions. When we say the energy levels are split into a doublet, we do not actually literally mean that there are now four new steady-states (after all, the levels had no degeneracy to begin with). Instead, we have periodic states (of the entire system) that oscillate with eigen-mode frequencies given by the exponents in eqn (4.4.22). In fact, these are common ideas and techniques that are part of what is known as *Floquet theory* [12].

Incidentally, because of the phase relationship in the cycle of our periodic solutions, the transitions at the central frequency of $\omega_o - g$ occur 90° out-of-phase with the transitions at $\omega_o - g \pm \sqrt{2}\mathcal{E}$. This means that in the above mentioned Mollow triplet, the light that contributes to the central peak is at quadrature to the light that contributes to the sidebands. This can be seen by looking at the so-called Homodyne spectrum, which allows one to separate the two out-of-phase components via controlling the phase of the *local oscillator*, θ. When $\theta = 0$, only the central peak is seen while $\theta = \frac{\pi}{2}$ gives the sidebands only. We will briefly come back to this in the next chapter.

It is also important to emphasize that this super-splitting phenomenon is a non-linear *saturation* effect. We can explain it physically in the following way. There are two main processes we need to consider: coherent exchange of excitation between the driving field and the (effective) two-level system, as well as irreversible decays into the reservoir. When the driving is very weak, the most important coupling process is a one-photon excitation. One photon of the driving field is absorbed, consequently the system is in the excited state, and it then emits this photon irreversibly into the environment.

However, when the driving strength is increased somewhat, second order processes become important. A process such as a *coherent exchange* of a photon between the two-state system and the driving field contributes strongly too. That is, an instantaneous two-photon process occurs: the driving field "puts" a photon into the system and takes it back immediately, *before* an irreversible decay can occur. One can imagine that with a stronger drive still, two of these instantaneous photon exchanges can happen simultaneously, as one process. Even-

tually, with increasing drive strength, higher and higher order processes dominate because essentially the coupling strength is much greater than the decay rates. The driving field and two-level system exchange many, many photons before the chain of loop-like (up and down) exchanges is interrupted by a collapse into the reservoir.

It is exactly this non-linear saturation that causes the dynamic Stark-shift. Thus, we have gained an understanding of the behavior observed when the JC system is driven very close to resonance with one of the vacuum states. We shall come back to super-splitting again later, when numerical results will be presented.

4.5 Correlation functions – reduced model

We have already met intensity correlation functions on several occasions, mainly in §4.1. We discussed the definition and classification, pointing out interesting Quantum effects such as antibunching as a possibility. Moreover, we have worked out how to calculate them using the QRT. Our own results will make extensive use of correlation functions where we shall explore parameter regimes previously considered inaccessible. However, before we launch into this new territory, it is wise to look over some well established work in the more usual parameter regime.

To this end, in this section we shall consider an analytically solvable reduced model. We stress that it is not going to be able to explain the results we shall present in the next chapter, but it is a nice approach and the method is quite general and hence instructive for other problems as well. Furthermore, historical reasons alone justify including the following brief calculation in this dissertation. Once again, we will follow [8].

4.5.1 Cavity QED

Consider the driven JC Hamiltonian, but this time we let $\omega_o = \omega_c = \omega_A$. In order to use the Master equation, we need to introduce the relevant collapse operators. Recall that in eqn (3.2.43), there is a sum over all damping terms in the problem. In the case of an atom coupled to a cavity mode there are two possible dissipation routes: either energy is lost to the environment from the field or it is lost from the atom.

The two operators that correspond to the s_j's are a and σ_-[1], the two lowering operators that can take energy out of the system and transfer it to the reservoir. We now need some decay rates, γ_j's. Define κ as the rate at which energy is lost to the reservoir due to emission through the cavity *mirrors*, i.e. $\kappa/2$ is the decay rate for the field. Similarly, define γ as the rate at which energy is lost to the reservoir due to emission through the cavity *sides*, i.e. $\gamma/2$ is the decay rate for the atom. This defines our collapse operators.

Most of our discussion in general will be applicable to the *strong coupling regime* in which we have the condition that $g \gg \kappa$ and $g \gg \gamma$. That is, the coupling is stronger than the damping so that dissipation does not obscure the quantum character of the system.

---

[1]Note that the requirement that the s_j's be eigen-operators in the sense discussed in chapter 3 is fulfilled.

Now, using previous conventions we would write the Hamiltonian of interest as

$$H = \hbar\omega_o \left(\sigma_+\sigma_- + a^\dagger a\right) + \hbar g \left(\sigma_+ a + a^\dagger\sigma_-\right) + \hbar\mathcal{E}\left(a e^{i\omega_o t} + a^\dagger e^{-i\omega_o t}\right). \quad (4.5.23)$$

On occasion, it turns out to be more numerically stable, and more convenient for calculation to re-write the interaction and drive terms with a slight modification. Recall that on page 13 we learned the absorb-a-phase-into-an-operator trick. This argument can be run backwards in the sense that a phase can be introduced at will. It is thus equally valid to write

$$H = \hbar\omega_o \left(\sigma_+\sigma_- + a^\dagger a\right) + i\hbar g \left(a^\dagger\sigma_- - \sigma_+ a\right) + i\hbar\mathcal{E}\left(a^\dagger e^{-i\omega_o t} - a e^{i\omega_o t}\right). \quad (4.5.24)$$

We would like to transform to a Dirac picture so that the Hamiltonian becomes time independent. Having already gained considerable experience with this particular type of transformation, it should seem quite natural to define $H_o = \hbar\omega_L \left(\sigma_+\sigma_- + a^\dagger a\right)$. Note that we are using the *driving* frequency because it is the time dependence at ω_L that we want to get rid of. As the reader may trivially verify, the Hamiltonian in the Interaction picture with the drive then is given by

$$H = \hbar\Delta \left(\sigma_+\sigma_- + a^\dagger a\right) + i\hbar g \left(a^\dagger\sigma_- - \sigma_+ a\right) + i\hbar\mathcal{E}\left(a^\dagger - a\right) \quad (4.5.25)$$

where $\Delta = \omega_o - \omega_L$. It is then this Hamiltonian which enters the Master equation.

4.5.2   Weak drive limit

The model we shall develop is going to be appropriate for the weak excitation limit, i.e. we shall assume $\mathcal{E}$ is very small indeed, allowing a perturbative expansion in the drive strength and leading to a number of approximations.

The first of these is neglection of the $-i\hbar\mathcal{E}a$ term in the Hamiltonian as it only contributes to terms of order higher than one in $\mathcal{E}$ while we are only going to do the calculation to *first* order. This gives the approximate Hamiltonian

$$H_S = \hbar\Delta \left(\sigma_+\sigma_- + a^\dagger a\right) + i\hbar g \left(a^\dagger\sigma_- - \sigma_+ a\right) + i\hbar\mathcal{E}a^\dagger. \quad (4.5.26)$$

Next, we have already introduced the idea of collapse operators and a Liouvillian super-operator at the end of the the section on the Master equation. For our system, we have two collapse operators given by $C_a = \sqrt{\kappa}a$ and $C_{\sigma_-} = \sqrt{\gamma}\sigma_-$. Thus, from eqn (3.2.45), we get

$$\mathcal{L} = \frac{1}{i\hbar}[H,\cdot] + \sum_{j=a,\sigma_-} \left(C_j \cdot C_j^\dagger - \frac{1}{2}C_j^\dagger C_j \cdot - \frac{1}{2}\cdot C_j^\dagger C_j\right). \quad (4.5.27)$$

The terms $C_j \cdot C_j^\dagger$ represent collapses due to interaction with the reservoir, i.e. a photon being emitted from the cavity. However, if the driving is weak, there are seldom quanta of excitation in the system to be lost and hence collapses are rare. In fact, we can approximate the states as *pure*, instead of mixed (recall that it was precisely the interaction with the reservoir which required the use of density operators in the description of our previously *open* system). Therefore, we drop the $C_j \cdot C_j^\dagger$ terms from the Liouvillian, thereby making the evolution of the system pure.

Thus, the approximate Liouvillian can be written

$$\mathcal{L}' = \frac{1}{i\hbar}[H_S, \cdot] - \frac{1}{2}\sum_{j=a,\sigma_-}\left\{C_j^\dagger C_j, \cdot\right\} \tag{4.5.28}$$

where the $\{\ldots\}$ brackets denote the anti-commutator, which determines our approximate Master equation: $\partial\rho/\partial t = \mathcal{L}'\rho$. We can easily prove that this equation of motion produces pure evolution under some effective Hamiltonian, H_e. Let us define

$$H_e = H_S - i\hbar\frac{1}{2}\sum_{j=a,\sigma_-}C_j^\dagger C_j,$$

$$\rho(t) = |\psi(t)\rangle\langle\psi(t)| \tag{4.5.29}$$

and then show that evolution of $\rho(t)$ under $\mathcal{L}'$ is fully equivalent to evolution of $|\psi(t)\rangle$ under H_e. Incidentally, since H_e is non-Hermitian, the evolution is non-unitary and the norm of the state is not preserved, but to first order in $\mathcal{E}$, it will be.

Proof:
Clearly, the bra corresponding to $(H_e|\psi(t)\rangle)$ is $(\langle\psi(t)|H_e^\dagger)$, and from the Schrödinger equation,

$$i\hbar\frac{\partial}{\partial t}|\psi(t)\rangle = H_e|\psi(t)\rangle,$$

$$i\hbar\frac{\partial}{\partial t}\langle\psi(t)| = -\langle\psi(t)|H_e^\dagger. \tag{4.5.30}$$

Thus, the time derivative of $\rho(t)$ can be computed directly:

$$i\hbar\frac{\partial\rho(t)}{\partial t} = \left(i\hbar\frac{\partial}{\partial t}|\psi(t)\rangle\right)\langle\psi(t)| + |\psi(t)\rangle\left(i\hbar\frac{\partial}{\partial t}\langle\psi(t)|\right)$$

$$= H_e|\psi(t)\rangle\langle\psi(t)| - |\psi(t)\rangle\langle\psi(t)|H_e^\dagger. \tag{4.5.31}$$

Then substitute H_e and $\rho(t)$ from eqn (4.5.29) and re-arrange to immediately get $\mathcal{L}'$ from eqn (4.5.28) acting on ρ.

Hence, what we have learned from the above is that the (approximate) system development can be specified by the Hamiltonian H_e evolving the pure state $|\psi\rangle$. Our goal is to find an analytic formula for $\left[g_{aa}^{(2)}(\tau)\right]_{ss}$ from eqn (4.1.9). In order to do this, we adopt the following strategy. Since we have taken out emission processes from our equations, we must find the steady state of the system, induce a collapse manually by annihilating a photon, and then observe the probability for a second emission while the system relaxes back to the steady state.

For an exactly solvable problem, we shall have to restrict our basis. We choose to work in the tensor product basis of atomic and field states, keeping only up to two quanta of excitation. Thus the states in which we shall expand $|\psi\rangle$ are: $\{|g\rangle|0\rangle, |g\rangle|1\rangle, |g\rangle|2\rangle, |e\rangle|0\rangle, |e\rangle|1\rangle\}$.

Moreover, we will choose normalization such that the coefficient of the ground state in the expansion is always one *despite* the fact that this clearly cannot be exactly true since the

other states will contribute to the norm as well. But, to first order in $\mathcal{E}$, the approximation certainly holds and is reasonable. So, we write

$$|\psi(t)\rangle \;=\; |g\rangle\,|0\rangle + \alpha(t)\,|g\rangle\,|1\rangle + \beta(t)\,|e\rangle\,|0\rangle + \eta(t)\,|g\rangle\,|2\rangle + \xi(t)\,|e\rangle\,|1\rangle\,. \qquad (4.5.32)$$

Writing out the Schrödinger equation under the effective Hamiltonian, we have

$$\frac{\partial}{\partial t}|\psi(t)\rangle \;=\; \left\{\mathcal{E}a^\dagger - i\Delta(\sigma_+\sigma_- + a^\dagger a) + g(a^\dagger\sigma_- - \sigma_+ a) - \frac{\kappa}{2}a^\dagger a - \frac{\gamma}{2}\sigma_+\sigma_-\right\}|\psi(t)\rangle\,. \qquad (4.5.33)$$

Next, if one substitutes the expansion for our wave-function from eqn (4.5.32) into the above equation of motion, we get a set of ODEs for the state amplitudes. They are:

$$\begin{aligned}
\dot{\alpha} &= -\frac{\kappa}{2}\alpha + g\beta - i\Delta\alpha + \mathcal{E},\\
\dot{\beta} &= -\frac{\gamma}{2}\beta - g\alpha - i\Delta\beta,\\
\dot{\eta} &= -\kappa\eta + \sqrt{2}g\xi - 2i\Delta\eta + \sqrt{2}\mathcal{E}\alpha,\\
\dot{\xi} &= -\frac{\kappa}{2}\xi - \frac{\gamma}{2}\xi - \sqrt{2}g\eta - 2i\Delta\xi + \mathcal{E}\beta.
\end{aligned} \qquad (4.5.34)$$

As previously mentioned, we shall assume that at $\tau = 0$, the system is in the steady-state $|\psi\rangle_{ss}$ which can be found by solving for the steady state of the above system of ODEs. However, this is immediately followed by a photon emission, so that at $\tau = 0$ the state collapses to

$$|\phi(0)\rangle \;=\; \frac{a\,|\psi\rangle_{ss}}{\sqrt{\langle a^\dagger a\rangle_{ss}}}, \quad \text{with subsequent short-term evolution} \qquad (4.5.35)$$

$$|\phi(\tau)\rangle \;=\; |g\rangle\,|0\rangle + \alpha(\tau)\,|g\rangle\,|1\rangle + \beta(\tau)\,|e\rangle\,|0\rangle \qquad (4.5.36)$$

which now has a maximum of one remaining excitation. Presently, we shall take a moment to explain the next step in some detail. We know that an expression of the form $tr\left[\hat{A}\rho(t)\right]$ would essentially give us $\left\langle\hat{A}(t)\right\rangle$. Furthermore, the formal solution of the Master equation allows us to write $\rho(t) = e^{\mathcal{L}t}\rho(0)$, so $\left\langle\hat{A}(t)\right\rangle = tr\left[\hat{A}e^{\mathcal{L}t}\rho(0)\right]$.

Recalling our eqns (4.1.8) & (4.1.9), we see that it is equally valid to write the following. First, define

$$\rho'_{ss} \;=\; \frac{a\rho_{ss}a^\dagger}{\langle a^\dagger a\rangle_{ss}}. \qquad (4.5.37)$$

Then, rewrite eqn (4.1.8) (with $\nu = \mu = a$) as

$$\left[g_{aa}^{(2)}(\tau)\right]_{ss} \;=\; \frac{1}{\langle a^\dagger a\rangle_{ss}} tr\left[a^\dagger a e^{\mathcal{L}\tau}\rho'_{ss}\right] \;=\; \frac{\left\langle a^\dagger(\tau)a(\tau)\right\rangle_{\rho(0)=\rho'_{ss}}}{\langle a^\dagger a\rangle_{ss}}. \qquad (4.5.38)$$

In the numerator, we have the expectation value of $a^\dagger a$ taken with respect to (wrt) the state that *had been* ρ'_{ss} at $\tau = 0$ but was then evolved for a duration τ. We note that our definitions of $|\phi(0)\rangle$ and ρ'_{ss} imply that $\rho'_{ss} = |\phi(0)\rangle\langle\phi(0)|$, so in fact, the expectation value in the numerator is wrt $|\phi(\tau)\rangle$. In the denominator, we have the same expectation value, but this time taken wrt $|\phi\rangle_{ss}$. Putting all of this together, it is the case that

$$\left[g_{aa}^{(2)}(\tau)\right]_{ss} \;=\; \frac{\langle\phi(\tau)|\,a^\dagger a\,|\phi(\tau)\rangle}{\langle\phi|\,a^\dagger a\,|\phi\rangle_{ss}}. \qquad (4.5.39)$$

Soon, we are going to require some initial conditions (ICs) in order to solve for $\alpha(\tau)$ and $\beta(\tau)$ so that we can obtain $|\phi(\tau)\rangle$. We may as well find them now. If the steady state of the system at $\tau = 0$ just prior to the collapse is

$$|\psi\rangle_{ss} = |g\rangle |0\rangle + \alpha_{ss} |g\rangle |1\rangle + \beta_{ss} |e\rangle |0\rangle + \eta_{ss} |g\rangle |2\rangle + \xi_{ss} |e\rangle |1\rangle, \qquad (4.5.40)$$

calculating $|\phi(0)\rangle$ as in eqn (4.5.35) quickly yields

$$\begin{aligned}
\alpha(0) &= \frac{\sqrt{2}\eta_{ss}}{\alpha_{ss}}, \\
\beta(0) &= \frac{\xi_{ss}}{\alpha_{ss}}, \\
\eta(0) &= 0, \\
\xi(0) &= 0. \qquad (4.5.41)
\end{aligned}$$

Finally, we can substitute our expansions for $|\phi(\tau)\rangle$ and $|\phi\rangle_{ss}$ into eqn (4.5.39), and readily obtain

$$\left[g_{aa}^{(2)}(\tau) \right]_{ss} = \frac{|\alpha(\tau)|^2}{|\alpha_{ss}|^2}. \qquad (4.5.42)$$

Our goal becomes to first find the steady state solution of eqns (4.5.34) and then their general solution, which will enable computation of the second-order intensity correlation function from the above formula.

Define $x = \frac{\kappa}{2} + i\Delta$, $y = \frac{\gamma}{2} + i\Delta$ and

$$\begin{aligned}
\vec{A}(t) &= (\alpha(t),\ \beta(t),\ \eta(t), \xi(t))^T, \\
\vec{d}(t) &= (\mathcal{E},\ 0,\ 0, 0)^T, \\
\mathbf{D} &= \begin{pmatrix}
-x & g & 0 & 0 \\
-g & -y & 0 & 0 \\
\sqrt{2}g & 0 & -2x & \sqrt{2}g \\
0 & \mathcal{E} & -\sqrt{2}g & -(x+y)
\end{pmatrix}. \qquad (4.5.43)
\end{aligned}$$

Our set of ODEs in eqns (4.5.34) can then be compactly written as

$$\dot{\vec{A}}(t) = \mathbf{D}\vec{A}(t) + \vec{d}. \qquad (4.5.44)$$

For the steady state case, $\dot{\vec{A}}_{ss}(t) = 0$ so $\vec{A}_{ss}(t) = -\mathbf{D}^{-1}\vec{d}$. After some algebra, we get

$$\vec{A}_{ss}(t) = \begin{pmatrix}
\dfrac{y\mathcal{E}}{xy+g^2} \\[4mm]
\dfrac{-g\mathcal{E}}{xy+g^2} \\[4mm]
\dfrac{\frac{1}{\sqrt{2}}\mathcal{E}^2(y^2+xy-g^2)}{x^3y+x^2y^2+2xyg^2+g^2x^2+g^4} \\[4mm]
\dfrac{-g\mathcal{E}^2(x+y)}{x^3y+x^2y^2+2xyg^2+g^2x^2+g^4}
\end{pmatrix}. \qquad (4.5.45)$$

So now we can compute the ICs from eqn (4.5.41) as well as the denominator in eqn (4.5.42) and what remains is to find the general solution $\vec{A}(t)$ from eqn (4.5.44). But this is a linear, first order set of ordinary differential equations! We are thus guaranteed that a solution exists and is unique. I will not bother the reader with the details, but rather present the final answer. After some considerably tedious but straight-forward mathematics, we arrive at

$$
\begin{aligned}
f &= \sqrt{(x-y)^2 - 4g^2}, \\
v &= x^2 + xy + g^2, \\
\left[g_{aa}^{(2)}(\tau) \right]_{ss} &= \left| \frac{1}{y^4 f^2 v^2} \left(y^2 f v - g^4 e^{-\frac{1}{2}(x+y)t} \left\{ (x+y)\sinh(ft/2) + f\cosh(ft/2) \right\} \right)^2 \right|.
\end{aligned}
\tag{4.5.46}
$$

This is the final result, which we shall use in the next chapter for comparison to numerical calculations in the appropriate weak excitation limit: $\mathcal{E} \ll \kappa, \gamma$.

Chapter 5

Results

5.1 Introduction

In chapter 2, we have derived the JCM which describes the system of a two-level atom coupled to a single mode of electromagnetic radiation, all confined to a cavity. However, the "atom" need not necessarily *be* an atom. Any two level system will do, and these are generally referred to as *qubits.* In recent years, a new experimental branch of CQED has developed called *Circuit QED.* Here, the qubit can be any one of a wide variety of man-made devices. The investigations in this chapter draw inspiration from this new generation of experiments.

In this thesis we shall not go into any amount of detail regarding how the experiments are done, but rather just highlight some of their key achievements, which then form the motivation for our work. In particular, we shall briefly discuss the results presented in [13], but note that there have been other publications along similar lines – for example, see [14].

The realization of the JCM in the Circuit QED set-up has essentially opened up a new era in Quantum Optics. This is because the parameter regimes that are now made accessible are truly extreme compared to conditions that were experimentally realistic in the past. The damping rates – κ and γ – are reduced drastically thereby increasing the resolution of any measurements on the system. Conversely, the coupling, g, is very much increased relative to the damping contributing to the same effect. Moreover, in contrast to the optical frequency atomic set-up, the experimenter has a more precise control over the system, parameters are more accurately determined and can be held constant in time, while noise is significantly reduced.

All these factors add up to give us the end result of a physical set-up capable of a resolution so far considered unattainable. The focus of the latest research on the experimental front has thus become probing the *non-linearities* of the JCM. The work published by Bishop et al. [13] demonstrates two of these effects. We now review them briefly as they lead on directly to our own investigation.

5.1.1   Super-Splitting and Multi-Photon Transitions

We continue working with the driven JCM, with the Hamiltonian in the Schrödinger picture given by eqn (4.5.23), that is

$$H \;\; = \;\; \hbar\omega_o \left(\sigma_+\sigma_- + a^\dagger a\right) + \hbar g \left(a^\dagger \sigma_- + \sigma_+ a\right) + \hbar\mathcal{E} \left(a^\dagger e^{-i\omega_L t} + a e^{i\omega_L t}\right). \qquad (5.1.1)$$

We then transform to an Interaction picture at the drive frequency which leads to an equivalent of eqn (4.5.25):

$$H \;\; = \;\; \hbar\Delta \left(\sigma_+\sigma_- + a^\dagger a\right) + \hbar g \left(a^\dagger \sigma_- + \sigma_+ a\right) + \hbar\mathcal{E} \left(a^\dagger + a\right) \qquad (5.1.2)$$

where $\Delta = \omega_o - \omega_L$. We also have dissipation through two channels with collapse operators $C_a = \sqrt{\kappa}a$ and $C_{\sigma_-} = \sqrt{\gamma}\sigma_-$. Finally, our Master equation is determined by the Liouvillian

$$\mathcal{L} \;\; = \;\; \frac{1}{i\hbar}\left[H, \cdot\right] + \sum_{j=a,\sigma_-} \left(C_j \cdot C_j^\dagger - \frac{1}{2}C_j^\dagger C_j \cdot - \frac{1}{2}\cdot C_j^\dagger C_j\right). \qquad (5.1.3)$$

This defines the (by now quite familiar) problem, and we can begin our discussion.

In §4.4, we met a phenomenon that we have termed "dressing of dressed-states" or "super-splitting". We saw that if one of the vacuum Rabi states is driven strongly on resonance, the system can be approximated as a two-level one, which then led to saturation and Stark splitting of each of the two states. We have mentioned that this can be observed by inspecting the incoherent spectrum which should show a clear Mollow triplet: a central frequency with sidebands similar to that of Resonance Fluorescence.

But this is not the only way the presence of the effect can be detected. Bishop and his group have observed this experimentally by measuring the quantity $|\langle a \rangle|^2$[1]. They have clearly and indisputably demonstrated the two-state behavior predicted by Carmichael et al. This saturation phenomenon is certainly non-linear and hence quite interesting, although fully understood thanks to the work in [10].

Furthermore, this two-state approximation leads to another very important consequence. Consider for a minute such a two-level system described by Pauli operators $s_\pm$. Also, imagine monitoring the radiated field from this system with some ideal detector. It is easy to see that $s_\pm^2 = 0$, identically, which simply means that two photons cannot be absorbed or emitted simultaneously as only one quantum of excitation can be stored in the system at all times. So what does this imply for the value of $\left[g^{(2)}_{s_- s_-}(0)\right]_{ss}$? Similarly to the argument regarding the Fock state $|1\rangle$ on page 35, since the numerator vanishes while the denominator does not, $\left[g^{(2)}_{s_- s_-}(0)\right]_{ss} = 0$.

Hence, we expect antibunched, sub-poissonian light when we drive the vacuum Rabi states on resonance. It is a well known property of two-state systems, and is clearly predicted from our analytical formula (4.5.46). We shall come back to this issue shortly.

Actually, this phenomenon which we have so far been referring to as just "two-state behavior" has a name – it is called *Photon Blockade*. Photon Blockade, as the name suggests,

---

[1]Note that while $\langle a^\dagger a \rangle$ is the total intensity, $|\langle a \rangle|^2$ is the *coherent* part of the light.

simply implies that a system with many states driven at some particular frequency will be excited up to a particular state, but not higher. This will be due to the fact that the frequency of the driving laser is far detuned from the next energy level gap in the system. Hence photons are easily excited to this special state, but cannot get past that level! It is also usually characterized by the following description: coherent laser light is incident on the system (at the driven mirror of the cavity), and at the output (the other mirror through which light leaks out of the cavity), antibunched and sub-poissonian light comes out. Thus a random stream of photons is converted to a more evenly spaced, regular output.

The other highly exciting point demonstrated in [13] is direct probing of the higher dressed states, i.e. those with two or more quanta of excitation. The observation was in the form of *multi-photon transitions* (MPT). What we mean by that is the following: imagine we drive the cavity field at frequency ω_L with strength $\mathcal{E}$, and suppose that we tune this frequency such that $\omega_L = \omega_o \pm g$. That is, to either the lower or upper vacuum states. Then one intuitively expects that the transition $|g, 0\rangle \rightarrow |1\pm\rangle$ is excited. This is a one-photon process, and therefore linear in every sense.

But now consider a slightly different situation. What if we drive the system with $\omega_L = \omega_o \pm g/\sqrt{n}$ where $n \in \mathbb{N}$? The reader may observe that in this case, $n\omega_L = n\omega_o \pm \sqrt{n}g$. Hence, if n photons of the driving frequency are absorbed all at once, the transition $|g, 0\rangle \rightarrow |n\pm\rangle$ can be excited. We immediately need to make two comments. First, since n photons are required for such a process to take place, we need many photons to be available, i.e. we expect $\mathcal{E}$ will need to be quite high before we can observe this. Second, this is a *non-linear* process in the Quantum Mechanical sense because it involves two or more photons[2].

So then, if we drive with $\omega_L = \omega_o \pm g/\sqrt{n}$ strongly enough, the corresponding transition *is* excited, n photons *are* absorbed simultaneously, but the linear nature of our interaction Hamiltonian implies that probability for the transition will depend on the energies of the intermediate states, i.e. those between $|g, 0\rangle$ and $|n\pm\rangle$. More precisely, it will depend on the detunings of the gaps between actual intermediate states and ω_L. Moreover, once a multi-photon excitation occurs, the system subsequently decays back down to the ground state by going through the intermediate levels. Hence the intermediate levels cannot be ignored (at least not *all* of them).

Bishop et al. observed MPT processes by once again measuring $|\langle a \rangle|^2$ which, if plotted as a function of ω_L, shows clear and distinct resonance peaks at the frequencies of the MPT. Note that this is an effect that requires quite strong drive and yet high quality data so that each peak can be resolved individually. This is clearly possible in Circuit QED and hence a further experimental investigation of the strong coupling, strong drive regime in the near future is imminent. In this thesis, we shall attempt to make some theoretical predictions regarding what might be found.

We will begin our investigation by inquiring about the behavior of the system when strongly driven on a multi-photon resonance. We are interested to see if something similar to the

---

[2]To avoid possible confusion, allow me to point out that the occurrence of MPT in the JCM is a completely different situation to the so-called Multi-Photon Jaynes-Cummings Model! This latter model is similar to the usual JCM, except the interaction Hamiltonian is replaced by $\hbar g \left(a^{\dagger n}\sigma_- + \sigma_+ a^n \right)$. This has no direct relation to the MPT we are discussing. In this case, unlike ours, one does not *need* to have intermediate levels in the model for a MPT to occur.

saturation effect discussed in §4.4 will be found. Also, we are looking to characterize the system according to its photon statistics and check whether non-classical light is possible.

5.2 Numerical Simulations

We have finally arrived at the long-awaited point when we can (and need) to solve some of the problems we have discussed on a computer. All simulations are performed within the Matlab environment, using the Quantum Optics Toolbox developed by Dr. Sze M. Tan [15].

5.2.1 Dimensionless Master equation

Whenever differential equations are solved numerically, they are usually non-dimensionalized. The idea is to scale dependent and independent variables by their typical value to then arrive at a differential equation where all terms are unit-less and roughly of the same order of magnitude. This is done for several reasons one of which is avoiding having very small and very large numbers in the same expression which causes numerical error. We must then choose an angular frequency such that (preferably) the period associated with it is of a typical time-scale in the problem.

It is usual to select κ for this purpose as we are normally interested in the light leaking out of the cavity mirror, a process which happens on the characteristic time-scale of $\frac{2\pi}{\kappa}$. We shall do this here. Thus we will define $t' = \kappa t$ and $\omega' = \omega/\kappa$ where ω is any quantity with the dimensions of angular frequency. Then, for simplicity, we do not write the dashes on the variables; thus from now on, scaling by κ is implied unless stated otherwise.

5.2.2 Parameters

Next, we need to choose some parameter values as a starting point for exploration of the dynamics. Table 5.1 shows the default parameters, which are based on realistic experimental values. We shall deviate from these on occasion, mostly when a small change in a parameter can cause a qualitative change in the system behavior. Δ and $\mathcal{E}$ will be varied.

Parameter	Value
g	500
κ	1
γ	1

Table 5.1: Default parameter values for numerical investigation.

5.2.3 Basis truncation and the steady-state

In general, to do calculations on a computer, we shall have to truncate the infinite Hilbert space of the field mode to some finite number, N. We then usually expand the problem

in the tensor product states, and since the qubit only has two levels, this results in a total number of $2N$ basis states. For example, if we choose $N = 2$, we only keep states $|0, g\rangle$, $|0, e\rangle$, $|1, g\rangle$, $|1, e\rangle$.

A common alternative truncation is to specify the maximum number of *excitations* a tensor product state can have. Thus, if we choose a maximum of two excitations, we only keep the states $|0, g\rangle$, $|0, e\rangle$, $|1, g\rangle$, $|1, e\rangle$, $|2, g\rangle$.

Yet a third very handy choice is to use dressed-states directly as basis states instead of tensor product states. In this case, we simply specify which states we have kept. For example, if we only require the ground and first pair of excited states of the system, then we write the problem in the representation of $|g, 0\rangle$, $|1-\rangle$, $|1+\rangle$.

Most of the time I shall use the first alternative for basis states with $N = 10$. When more states will have to be included to get accurate results, I will specify the truncation explicitly. For the following general discussion, let us suppose that the total number of basis states in use is $\mathcal{N}$.

We will constantly be required to compute the steady-state solution to the Master equation. In fact, this is done by writing out the elements of ρ ($\mathcal{N}^2$ of them) as a vector and the Liouvillian as an $\mathcal{N}^2 \times \mathcal{N}^2$ matrix. ρ_{ss} is then simply the nullspace of this matrix. Unless Hilbert space dimensions are extremely large, this is normally a straight-forward calculation.

5.2.4 Overview

We shall begin our investigation by looking at three very important quantities: $\langle \sigma_+ \sigma_- \rangle$, $\langle a^\dagger a \rangle$ and $\left[g_{aa}^{(2)}(0) \right]_{ss}$. Notice that to compute them one only requires the steady-state solution to the Master equation. Surface plots are shown in fig. 5.1. Here I only scan Δ through the "positive" half of the spectrum because the negative half is a mirror image – the plots are symmetric.

Consider first the plots of $\langle \sigma_+ \sigma_- \rangle$ and $\langle a^\dagger a \rangle$. The peaks seen are resonance peaks corresponding to transitions to the *lower* dressed states (because $\Delta > 0$, and $\Delta = \omega_o - \omega_L = \omega_o - (\omega_o \pm g/\sqrt{n}) = -(\pm)g/\sqrt{n}$). One can easily verify that the detunings at which the resonances are observed are equal to those discussed above in connection to MPT (the peak at $\Delta = 500$ is the lower Rabi vacuum peak). Notice also that for MPT, the resonances in $\langle a^\dagger a \rangle$ are higher than in $\langle \sigma_+ \sigma_- \rangle$ since the atom can only store one quantum of excitation and the field must store the rest.

I would like to point out that figs. 5.1 (a) and (b) show a dynamic evolution of the peaks as a function of drive strength. The particular heights and widths should be, in principle, explained by direct connection to physical processes occurring in the system. Unfortunately, this investigation is outside the scope of the present work, but it is important to be aware of exactly what we do and do not (yet) understand.

Next, we inspect the third figure, that of $\left[g_{aa}^{(2)}(0) \right]_{ss}$. There is a lot more to be said about
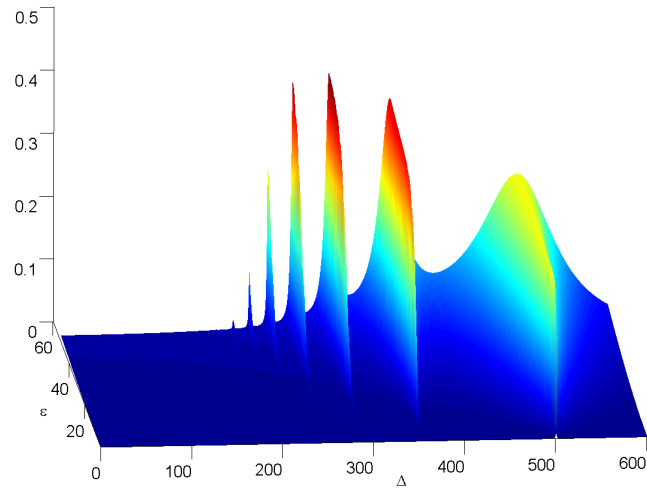
(a)
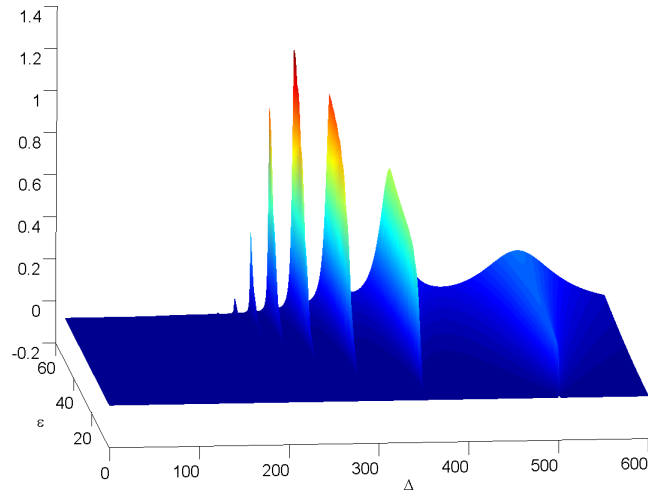
(b)
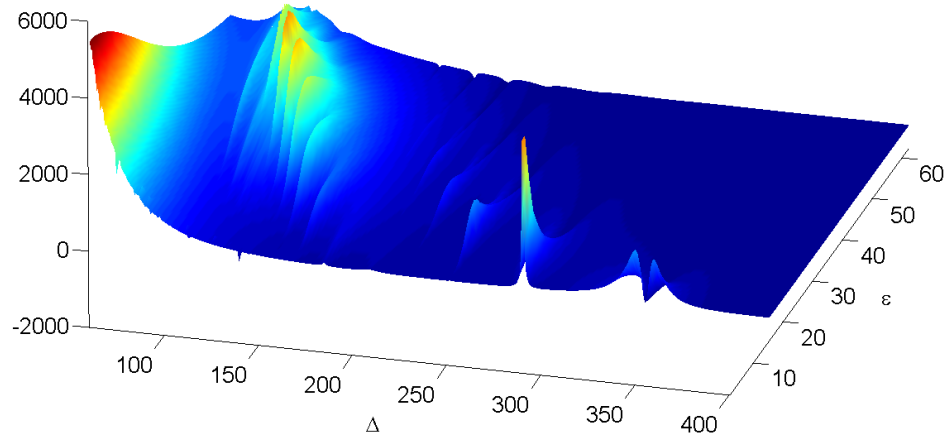
(c)

Figure 5.1: (a) $\langle \sigma_+ \sigma_- \rangle$, (b) $\langle a^\dagger a \rangle$ and (c) $\left[g_{aa}^{(2)}(0) \right]_{ss}$ plotted as functions of drive strength $(\mathcal{E})$ and detuning (Δ).

this plot, much of which will require further investigation. First, I must mention that the surface was essentially flat for $\Delta > 400$ which is not very exciting and hence not shown. In particular, the vacuum peak is most definitely antibunched as expected, since $\left[g_{aa}^{(2)}(0)\right]_{ss} < 1$ for $\Delta = 500$ at all drive strengths. For smaller drive, the numerics were somewhat unstable and had to be left out, as was the case with the small detuning region. Furthermore, for $\Delta < 170$ we see a region of cascaded, high peaks which I shall not discuss at all in this thesis.

We focus on understanding the structure present for the higher values of Δ. We observe the same pattern for each of the MPT shown, but note that we only see the later development stages of the two-photon peak. In general, what happens is this: for very low drive, there are not enough photons in the cavity to excite the MPT and so initially, the surface is flat. Of course, this does not mean at *zero* but at some background value. However, since at this stage there is no evidence of the presence of the resonance, this background value tells us nothing critical regarding the nature of MPT. Then, the transition is gradually more and more excited and $\left[g_{aa}^{(2)}(0)\right]_{ss}$ as a function of $\mathcal{E}$ climbs up to a maximum.

Having reached this turning point, the curve then begins its descent. Closely following the maximum, we have another characteristic event: the peak begins to split into a doublet when viewed as a cut through the surface at constant $\mathcal{E}$. The splitting deepens, the sub-peaks broaden and eventually level off.

I must mention at this early stage that the two-photon peak is special in the following way. Despite the fact that numerics are not very helpful for the extremely small $\mathcal{E}$ regime, there is reason to believe that $\left[g_{aa}^{(2)}(0)\right]_{ss}$ as a function of drive strength has the above mentioned maximum when $\mathcal{E} = 0$. This claim is based on an analytic calculation with the model restricted to the dressed states $|g, 0\rangle$, $|1-\rangle$, $|2-\rangle$, covered in the next chapter.

In any case, every MPT peak eventually becomes very strongly bunched[3]. Depending on the number of the peak (only referring to MPT in this instance), the maximum value decreases going to higher excitation. Note that the actual peaks shift slightly along the Δ axis when the drive strength is increased. This is a consequence of the fact that the strong drive is affecting the energy levels – recall that the dressed-state energies are eigenvalues of the *undriven* Hamiltonian, H_{JC}. Table 5.2 summarizes the characteristic points for each of the first five multi-photon peaks.

Next, the first question that comes to mind is: does the light from the cavity *actually* become antibunched when driven strongly enough on a MPT? i.e. does $\left[g_{aa}^{(2)}(0)\right]_{ss}$ go below one? For our particular parameter choice, the simple answer is no, only the two-photon peak shows real antibunching. But some thought and experimentation leads to the following comments. The value to which $\left[g_{aa}^{(2)}(0)\right]_{ss}$ settles under very strong drive is determined by nothing but the *background*, the value of which is higher the smaller the detuning. Hence we cannot draw any conclusion regarding the nature of the process; there is, in principle, no fundamental difference between a two and a three photon transition. Furthermore, in support of the same argument, if we change the atomic linewidth to $\gamma = 0.5$, the three-photon process also

---

[3]As I said, since the background is usually much higher than one, technically the light has been bunched from the beginning, but that has nothing to do with the process of a Multi-Photon Transition.

Peak No.	2	3	4	5	6
$\mathcal{E}_{max}$	0	3.6	11.1	19.3	26.6
Δ_{max}	353.6	288.7	250.16	224.025	204.8
h_{max}	4.104×10^5	4279	1340	817.7	631.5
$\mathcal{E}_{ss}$	0.32	4.8	12.7	21	28.9
Δ_{ss}	353.6	288.7	250.22	224.1	204.95
h_{ss}	1.22×10^5	3155	1154	743.9	569.2

Table 5.2: Characteristic points for the MPT peaks on the plot of $\left[g_{aa}^{(2)}(0)\right]_{ss}$. "max" refers to maximum reached, "ss" indicates the point where the peaks begins splitting into sub-peaks (see text). $\mathcal{E}$ and Δ have their usual meanings, while h refers to the *actual value* of $\left[g_{aa}^{(2)}(0)\right]_{ss}$ calculated at the characteristic point. All other parameters were default (see table 5.1).

shows antibunching. Likewise, when $\gamma = 0$ the fourth peak exhibits antibunching as well, etc.

Thus, although strictly speaking for our default parameters only peak two shows genuine antibunching, we can (and will) speak of antibunching for all MPT peaks in general. It is simply the simultaneous presence of other, more global processes in the system that obscure the effect. We shall then have to find a simple explanation for the following: in contrast to a two-state system which always radiates antibunched light, a multi-level system driven on a multi-photon transition shows strong bunching for small drive which then is transformed to antibunching with increasing drive. The next chapter will address this issue in detail. For now, we move on to a more complete set of numerical results.

5.2.5   Quantum Trajectories

We will now use the technique described in §4.3 to help us visualize the above mentioned transition from bunching to antibunching. Thus, we shall be literally *looking* at instances of the process the statistics of which we are trying to understand. Fig. 5.2 shows three examples of trajectories, obtained by driving the system on the two-photon peak.

We know that as soon as an n-photon absorption occurs, the system will have to decay back to its ground state so these n photons should be emitted through one or the other channel on a time-scale of the inverse of the linewidths. Naturally, when the drive is weak, $\langle a^{\dagger}a \rangle_{ss}$ is very small. That is, on average, the number of photons emitted from the cavity is low because it is rarely excited. But, whenever it *is* excited, a "clump" of photons comes out, so the probability to detect two photons with a short time interval between them is quite high. Now since

$$\left[g_{aa}^{(2)}(\tau)\right]_{ss} = \frac{\langle a^{\dagger}(0)a^{\dagger}(\tau)a(\tau)a(0) \rangle_{ss}}{\langle a^{\dagger}a \rangle_{ss}^2}, \tag{5.2.4}$$

we recognize these as ideal ingredients for bunching – the numerator is reasonably big while the denominator is tiny. Note that this is exactly what is seen in fig 5.2 (blue): photon emissions are rare but almost always come in closely spaced pairs. As the drive increases, emissions become more and more common, to such an extent that photons are more evenly
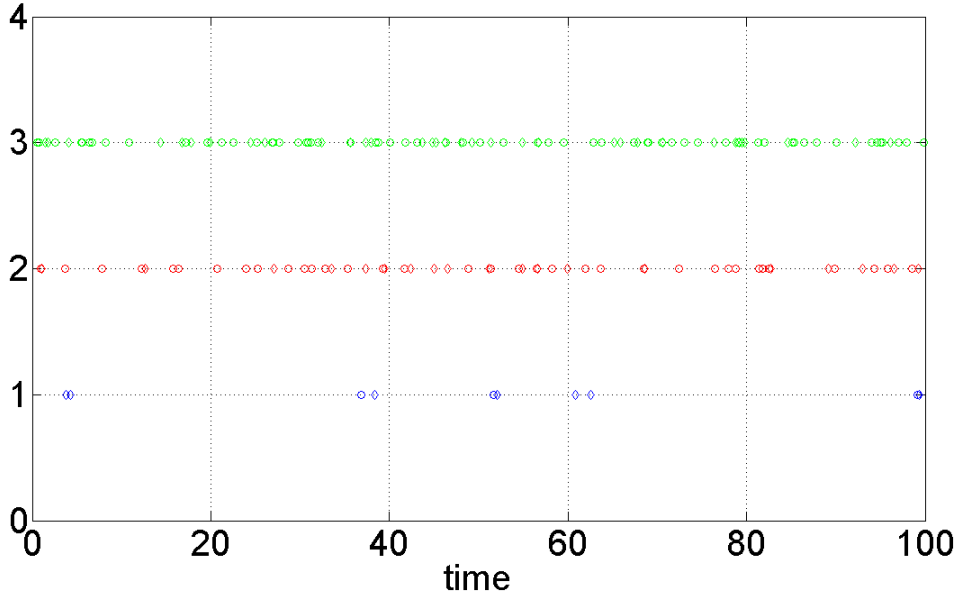
Figure 5.2: An example of Quantum Trajectories showing times and channels of collapse: $\diamond$ – atom, o – field; blue – ($\mathcal{E} = 5$, $\Delta = 353.6$, $\left[g_{aa}^{(2)}(0)\right]_{ss} = 8.6474$), red – ($\mathcal{E} = 10$, $\Delta = 353.825$, $\left[g_{aa}^{(2)}(0)\right]_{ss} = 1.1601$), green – ($\mathcal{E} = 15$, $\Delta = 354.2$, $\left[g_{aa}^{(2)}(0)\right]_{ss} = 0.7634$).

spaced. This makes for antibunched light, as suggested by the value of $\left[g_{aa}^{(2)}(0)\right]_{ss}$ [4].

In fact, it is the competing rates of excitation and decay that are responsible for this effect. Consider a two-photon transition from $|g,0\rangle$ to $|2-\rangle$, which "puts" two quanta of excitation into $|2-\rangle$. When the drive strength is weak, two photons are emitted and the system relaxes back to the ground state long before the next excitation event. When the drive strength is high (as is in the third case shown in fig. 5.2) however, the next excitation either follows immediately after the system decays to the ground state, or even *before* these two photons are emitted.

At first, this might seem contradictory, but remember that once two photons occupy $|2-\rangle$, the system can either decay back down through the lower or upper vacuum Rabi states. Indeed, depending on the polarity of the dressed state we are driving (i.e. $|n-\rangle$ or $|n+\rangle$), the smallest detuning path is of the same polarity. That is, either $|g,0\rangle \rightarrow |1-\rangle \rightarrow \ldots \rightarrow |n-\rangle$ or $|g,0\rangle \rightarrow |1+\rangle \rightarrow \ldots \rightarrow |n+\rangle$. The amplitude for excitation along the path of least detuning will naturally dominate. Thus, both excitation and decay can happen simultaneously as long as the decay occurs along the alternate path.

Specifically, for the two-photon transition, this means that if one photon has already been emitted, there is (at least an equal) chance of the system decaying to the $|1+\rangle$ and the dominant amplitude excitation path remaining clear for the next two-photon transition.

---

[4]However, *perfect* antibunching – $\left[g_{aa}^{(2)}(0)\right]_{ss} = 0$ – will not be seen for any MPT as it is a one photon effect.

5.2.6 Intensity correlations and spectra

We will now track the developing peaks (as a function of the drive strength) by plotting $\left[g_{aa}^{(2)}(\tau)\right]_{ss}$ and both the atomic and field incoherent spectra. Among other things, this will allow us to put our analytic formula from §4.5 to the test. Recall that we expect the formula to only be valid for $\mathcal{E} \ll \kappa, \gamma$. Moreover, we will look for a possible development of a Mollow triplet and a slow oscillation in the second-order correlation function at the corresponding frequency. These are sure signs of saturation which one might expect.

5.2.6.1 Vacuum Rabi peak

Let us start from the vacuum Rabi peak, the behavior of which we understand. Please refer to fig. 5.3. In (a) and (d) we see plots of $\langle a^\dagger a \rangle$ and $\langle \sigma_+ \sigma_- \rangle$ as a function of the detuning, Δ, for different drive strengths. We easily recognize the resonance peak corresponding to the transition $|g, 0\rangle \rightarrow |1-\rangle$ at $\Delta = g$, as the mean excitation of the field and atom indicate. In (d), I have also added a plot of the second-order correlation function at zero delay, which shows us that the light is indeed antibunched even as the drive is increased[5].

Plots (b) and (e) give us the intensity correlation function as found from numerical calculation, compared to the prediction from our analytic formula. In both cases, we have antibunched, sub-poissonian light, as expected. For $\mathcal{E} = 0.1$, the agreement is very good. For higher drive, $\left[g_{aa}^{(2)}(\tau)\right]_{ss}$ develops a slow oscillation as a consequence of the dynamic Stark splitting discussed in §4.4. This is always seen for an ordinary two-state system: super-splitting is manifested in $\left[g_{s_-s_-}^{(2)}(\tau)\right]_{ss}$ as a slow oscillation component at the frequency of the sidebands in the corresponding incoherent spectrum. However, as one may easily observe, eqn (4.5.46) is independent of $\mathcal{E}$ (as it must be, considering the method used to obtain it!) and therefore cannot be expected to reproduce this dependence on drive strength.

Next, plots (c) and (f) show us the incoherent spectra obtained from the normalized auto-covariance of a and σ_-. Note that the frequency axis is with respect to ω_L. Once again, these results agree with what we have grown to anticipate. For low drive, there is only one frequency component in the system – at the drive frequency. For higher drive, we see a clear example of a Mollow triplet. Moreover, the oscillation frequency in the correlation function is in fact equal to the sideband frequency seen in these spectra. This is also the case for MPT, as we shall see.

It is curious to note that a certain asymmetry is observed between the two sidebands. Our Mollow triplet from fig. 5.3 *appears* symmetric, but if we look closer... The field and atomic spectra are asymmetric in a complementary way: the sub-peak which is weaker for the field is stronger for the atom and vice versa. Moreover, two extremely weak doublets are found at frequencies of $\pm 2g$ (not illustrated), all in accordance with previous results from [10].

I have not been able to determine precisely the cause of the asymmetry in the spectrum.

---

[5]It is even *more* antibunched in (a), $\left[g_{aa}^{(2)}(0)\right]_{ss}$ is zero for the entire range shown. However, somewhat unstable numerics do not allow us to see this clearly and so I have not added this curve to (a).
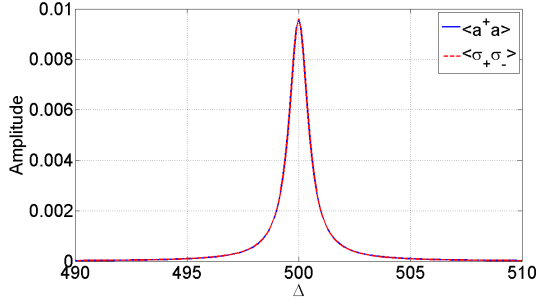
(a) Mean excitation vs. detuning.
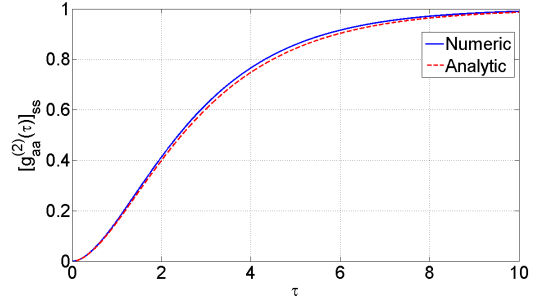
(b) Second-order intensity correlation function.
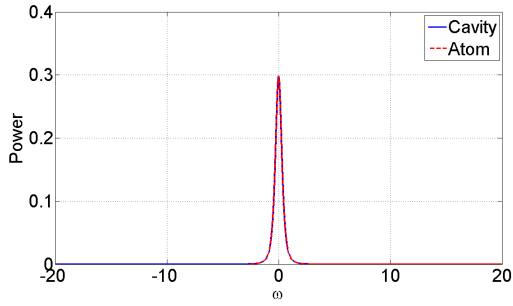
(c) Incoherent spectra.
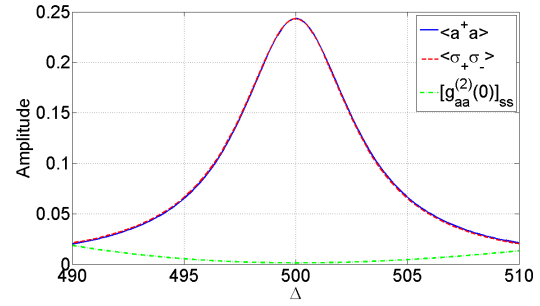
(d) Mean excitation and second-order intensity correlation function at zero delay vs. detuning.
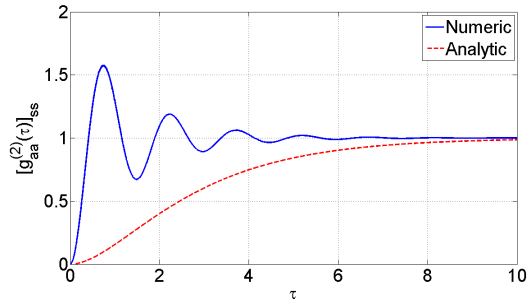
(e) Second-order intensity correlation function.
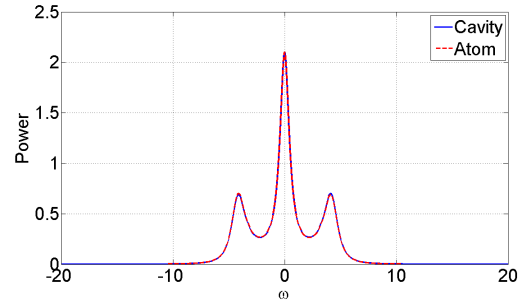
(f) Incoherent spectra.

Figure 5.3: Peak 1, $\Delta = 500$; (a)–(c) $\mathcal{E} = 0.1$, (d)–(f) $\mathcal{E} = 3$.

However, some experimentation does provide suggestive insight, which I will now describe.

- The amplitude relation is flipped when we drive the other vacuum Rabi state.

- If the basis is truncated to $|g, 0\rangle$ and $|1-\rangle$ only, the spectrum is perfectly symmetric.

- Adding either of $|1+\rangle$ or $|2-\rangle$ produces an asymmetry of the same kind as observed in the full model, but the effect of $|2-\rangle$ is opposite to that of $|1+\rangle$ and dominates the total asymmetry.

- The Homodyne spectra (I will give a formula with some plots later in the chapter) for the two quadratures are identical to those of Resonance Fluorescence.

- The asymmetry increases with increasing drive, measured by the ratio of the difference in heights to the maximum height. This may be expected since it is probably present due to higher order processes the contribution from which will grow with the drive strength.

Thus, we know the asymmetry is due mostly to the presence of the next dressed state up with the same polarity because it is the next closest to resonance with the drive. No further conclusions are possible at this stage – a more in-depth investigation is needed, but this detail is not so crucial to our main arguments and so I leave it to be discussed elsewhere.

Incidentally, we can easily explain the presence of the *doublets* at $\pm 2g$ mentioned above. The splitting between these sub-peaks is equal to the sideband frequency of the Mollow triplet. Let us for the moment denote the Stark super-splitting frequency $S(\mathcal{E})$ (so that the Mollow sidebands are at $\pm 2S(\mathcal{E})$). The doublets correspond to transitions between the dynamically Stark-shifted quasi-energy levels of the ground state and the upper vacuum Rabi level. Naturally, these occur at frequencies of $\pm\left[(\omega_o + g) \pm S(\mathcal{E}) - (\omega_o - g)\right] = \pm(2g \pm S(\mathcal{E}))$, so the splitting between the two peaks at $\pm 2g$ is $2S(\mathcal{E})$ (remember that the frequency axis is wrt ω_L).

Extremely tiny peaks at $\pm 2g$ are also seen in the spectra calculated below when the system is driven on a multi-photon resonance, but they are, of course, no longer doublets.

5.2.6.2 Two-photon peak

It is time to examine the behavior of the two-photon peak. Firstly, we would like to compare numerical and analytic results for the second-order correlation function. In principle, this should be perfectly possible for our default parameter choice. However, as mentioned in footnote 5, at low enough drive strengths, the numerical computation of $\left\langle a^{\dagger 2} a^2 \right\rangle / \left\langle a^\dagger a \right\rangle^2$ is somewhat unstable. To get unambiguously good agreement, we shall have to reduce our value of g.

Therefore, working with $g = 100$, in fig. 5.4 we observe the two-photon peak. In (a), both the analytic and numeric results tell us the light is very strongly bunched. The second-order correlation function plotted at the peak value shows the long-time characteristics expected for super-poissonian and bunched light, but it also possesses a very fast frequency component. This frequency is practically the same in the numeric and analytic plots. Moreover, MPT with more than two photons *also* possess this fast oscillation, at nearly the same frequency. However, as n (number of photons in the MPT) deviates from 2, this frequency

starts *slightly* deviating from the one present for the two-photon transition.

The rapid oscillations can be understood as a beating effect between two very close frequencies. This is called a *quantum beat*: a photon emission sets up a superposition of states with different energies which then causes a beat frequency to show up in the subsequent Schrödinger evolution.

In particular, this fast frequency is none other than $2g$, the splitting between the vacuum Rabi states. This is the case for the following reason. Consider first the two-photon transition. Say the system is excited into one of $|2\pm\rangle$ and one photon is emitted. Subsequently, the second-order correlation (which gives us the dynamic probability of detecting a second photon) is then either calculated from the initial condition "the system is in state $|1-\rangle$" or "the system is in state $|1+\rangle$".

Therefore, it is not surprising that the frequency $2g$ is present in $\left[g_{aa}^{(2)}(\tau)\right]_{ss}$. But now, let us consider the higher order MPT. Applying the above logic directly would lead to an apparent discrepancy. What we must realize is that the "Initial Condition" argument, although particularly nice for the two-photon peak, is not completely general. The second-order intensity correlation function depends, of course, on the dynamic probability of detecting another photon with a delay of τ after the first one. This means that, say for the three-photon peak, *all* the transitions – 3rd excited dressed state to the 2nd pair, 2nd to 1st, 1st to ground – contribute! After all, the "first" photon at the detector could be the second in the cascade of emissions just as well as it could be the first.

What this tells us is that we expect the fast frequency in $\left[g_{aa}^{(2)}(\tau)\right]_{ss}$ to be that of the splitting between the pair of dressed states with the highest *relative* population among the intermediate states at any given time. Elementary logic suggests that population of the intermediate excited states would decrease going to higher excitation, and therefore it is sensible that we see this fast oscillation at the splitting of the lowest doublet.
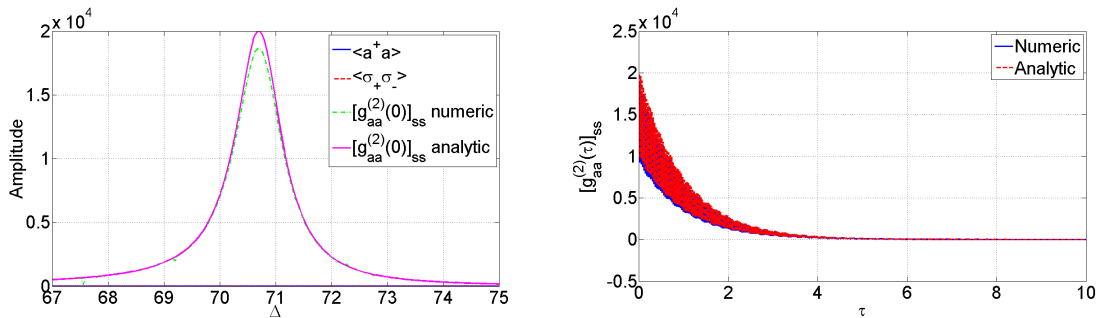
(a) Mean excitation and second-order intensity correlation function at zero delay vs. detuning.

(b) Second-order intensity correlation function.

Figure 5.4: Peak 2, $g = 100$, $\Delta = 70.7$, $\mathcal{E} = 0.1$.

Note that we will not attempt to compare results of the *third* peak with the analytic formula, because remember – to arrive at the end result, we truncated the basis at the two quanta of excitation level! Thus, our formula cannot be expected to "be aware of" more-than-two-photon-transitions.

So, having shown agreement with the analytic formula for very low drive in the vicinity of the second peak, we now go back to the default parameter values and continue our investigation. With reference to fig. 5.5, plots (a)–(b) are the equivalents of fig. 5.4 but with $g = 500$. The reader can now see what I meant by "numerical instability". Although it is quite clear what the $\left[g_{aa}^{(2)}(0)\right]_{ss}$ curve is supposed to look like, it is considerably nicer to deal with either the higher-drive or lower-coupling scenarios.

Thus, for very weak driving, the light is very strongly bunched and super-poissonian. At $\mathcal{E} = 0.32$, the $\left[g_{aa}^{(2)}(0)\right]_{ss}$ peak from fig. 5.5(a) begins splitting into two sub-peaks. By the time we get to (c) where $\mathcal{E} = 15$, the dip has descended below the value one and the light is antibunched. Plotting the correlation function and the incoherent spectra at the peak value of Δ gives (d) and (e). A slow oscillation in $\left[g_{aa}^{(2)}(\tau)\right]_{ss}$ has developed in accordance with the Mollow-like side-peaks that are seen partially separated from the central peak in the spectrum. Plots (f)–(h) depict the same effect pushed further with higher drive.

The Mollow-like structure found suggests a saturation effect is taking place and some dynamic Stark splitting must be present. Perhaps at first, we may be tempted to explain away this observation in an exactly analogous manner to the two-level system case, except with two-photon transitions. I will now present quite a compelling collection of results which will convince us that the situation is, in fact, *much* more complicated. I will describe physically and show mathematically how we can explain the simpler of the scenarios examined below in the next chapter, with a clear indication as to how the more complicated cases can be understood.

Firstly, once again, we notice that the spectra of fig. 5.5 are asymmetric. The same kind of asymmetry as described for the vacuum Rabi state is also seen here, most clearly in fig. 5.5(h). However, more interestingly, a different, stronger, more *imposing* in a way, type of asymmetry is present. Obviously, the left-hand sideband is suppressed (and/or the right-hand sideband is enhanced) for both the atomic and field spectra. In fact, this suppression of one of the sidebands is observed for *all* the MPT cases. Moreover, whenever we drive $|n-\rangle$, the LHS peak is suppressed and whenever we drive $|n+\rangle$, it is the RHS peak which is smaller.

This asymmetry is present quite obviously for relatively modest drive strengths. One is thus led to postulate that the cause of this asymmetry is somehow fundamental to the process that produces the Mollow triplet (unlike that seen in the vacuum Rabi peak case). We are unable to explain this effect until we get to the next chapter but nevertheless, some comments can be made. First of all, we must realize that the $|1-\rangle$ state will be much more important than $|1+\rangle$ for mediating all the two-photon transitions (confirmed by simulations) because it is much less detuned from the ideal "half-frequency". Therefore, at the minimum, one must have the states $|g, 0\rangle$, $|1-\rangle$, $|2-\rangle$ in the basis.

We observe that:

- The essential basis states only do produce an asymmetry, but the wrong peak is suppressed.

- Adding the state $|3-\rangle$ to the basis gives the spectrum its correct form. Thus, in this
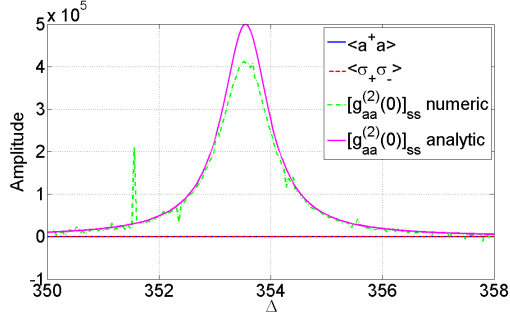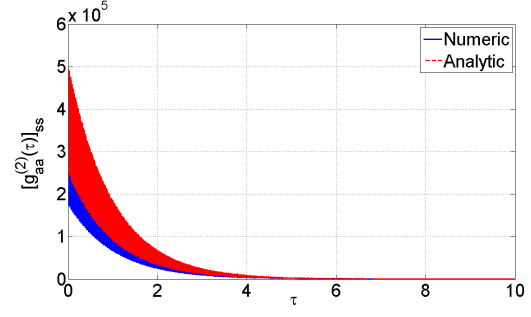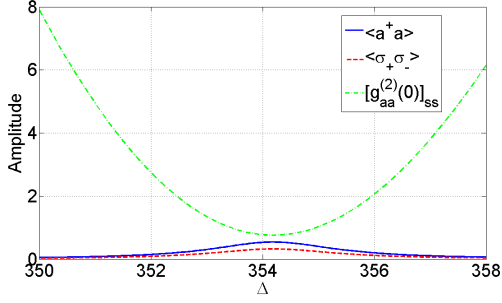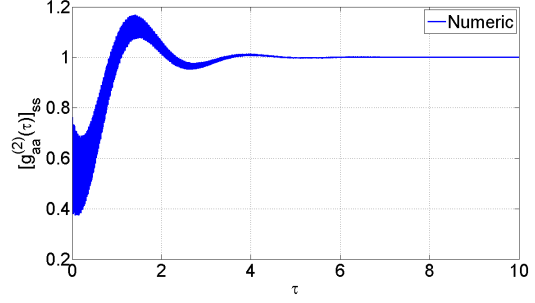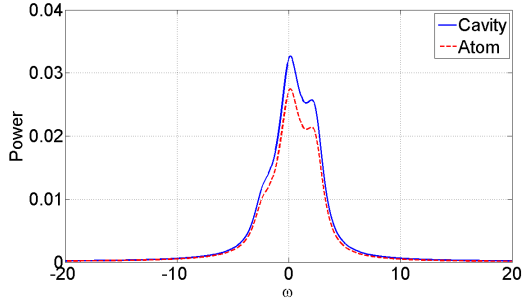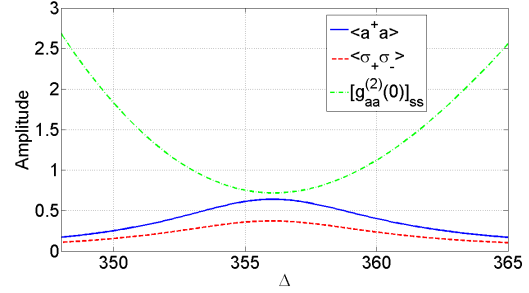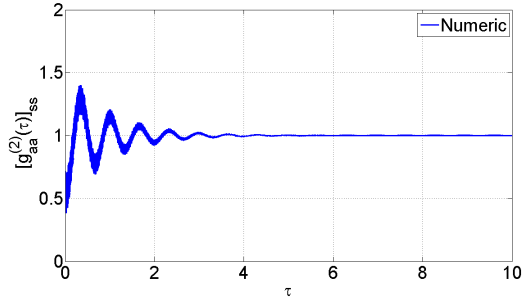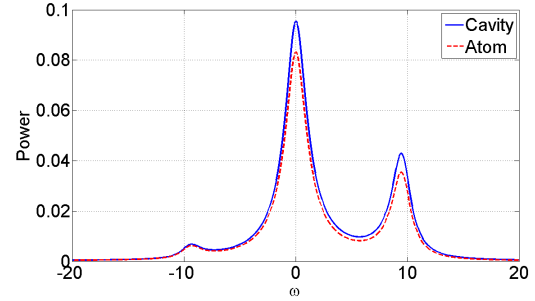
Figure 5.5: Peak 2, $g = 500$. (a), (c), (f) – Mean excitation and second-order intensity correlation function at zero delay vs. detuning; (b), (d), (g) – Second-order intensity correlation function; (e), (h) – Incoherent spectra.

case as well, the asymmetry appears mostly due to the next dressed state of the same polarity as the driven state. But then one must wonder what causes the (strong) asymmetry in the bullet point above!

- The asymmetry gets weaker with increasing drive, as quantified by the ratio of the height of the side-peaks.

This asymmetry in the Mollow triplet for MPT seems to be very characteristic and "regular" in the sense that we can make observations and generalize them readily to all the multi-photon cases. Therefore I believe there exists a simple physical explanation. A resolution to the mystery is proposed in the next chapter.

Another clue as to the actual mechanism responsible for the Mollow triplet observed can be obtained by considering the Homodyne spectrum. The Homodyne spectra for MPT are very surprising: a small amount of the light contributing to the sidebands actually oscillates in-phase with the central peak and vice versa! Even though I will not explain the mechanism of Homodyne detection (for example, see [3] §15.6.1 and §10.5.), we will presently see how it can be calculated, and then use the formula to illustrate the above statement.

Let us denote the covariance of operators ν and μ by

$$\left\langle \nu^\dagger(\tau), \mu(0) \right\rangle = \left\langle \nu^\dagger(\tau)\mu(0) \right\rangle - \left\langle \nu^\dagger \right\rangle \left\langle \mu \right\rangle.$$

The normalized Homodyne spectrum of the atom is the FT of the quantity

$$\left\{ e^{-2i\theta} \left\langle \sigma_-(\tau), \sigma_-(0) \right\rangle + e^{2i\theta} \left\langle \sigma_+(\tau), \sigma_+(0) \right\rangle + \left\langle \sigma_+(\tau), \sigma_-(0) \right\rangle + \left\langle \sigma_+(0), \sigma_-(\tau) \right\rangle \right\} / \left\langle (\sigma_+ + \sigma_-)^2 \right\rangle_{ss},$$

while that of the field is the FT of

$$\left\{ e^{-2i\theta} \left\langle a(\tau), a(0) \right\rangle + e^{2i\theta} \left\langle a^\dagger(\tau), a^\dagger(0) \right\rangle + \left\langle a^\dagger(\tau), a(0) \right\rangle + \left\langle a^\dagger(0), a(\tau) \right\rangle \right\} / \left\langle (a^\dagger + a)^2 \right\rangle_{ss},$$

with θ the phase of the local oscillator. Usually, for a classical Mollow triplet, when $\theta = 0$ only the central peak is present in the Homodyne spectrum. Conversely, when $\theta = \pi/2$, only the sidebands appear. That is, the phase allows one to choose which quadrature is to be "detected".

(a) $\theta = 0$ (b) $\theta = \pi/2$
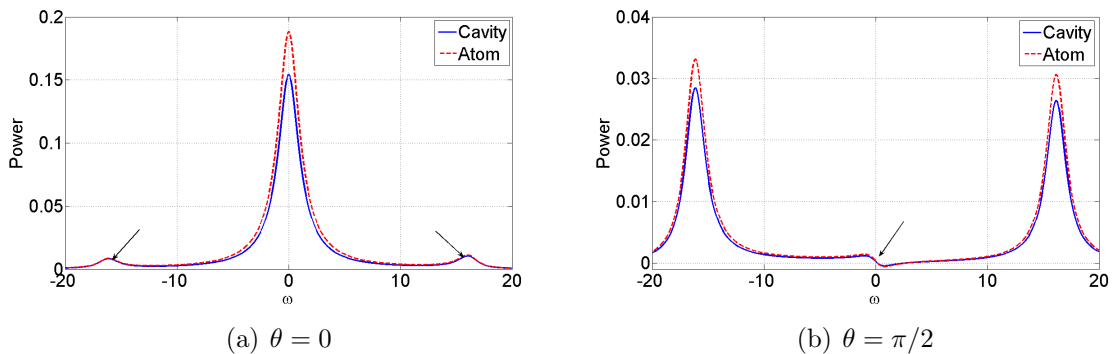
Figure 5.6: Peak 2, $\mathcal{E} = 40$, $\Delta = 358.09$. Homodyne spectra for the cavity and atom. Arrows indicate "abnormal" features that are not usually present.

Fig. 5.6 shows an example of the Homodyne spectra calculated when the system is driven strongly on the two-photon resonance to $|2-\rangle$. As we can see, there are small side-peaks in (a) and an indication of the central peak in (b). This cannot happen for a two-level system (and indeed does not when we drive $|1\pm\rangle$) but occurs for all the multi-photon Mollow spectra. This tells us that the periodic solutions (see discussion at the end of §4.4) are much more complicated and more than one transition contributes to each of the three peaks of the Mollow spectrum.

The final piece of the puzzle is contained in the higher frequencies seen in the optical spectra. Fig. 5.7(a) shows four peaks (apart from the one at the origin) at ±147.8 and ±853.4. These frequencies are just the frequencies of the intermediate states $|1\pm\rangle$ minus the drive frequency, i.e. $\pm g(\frac{1}{\sqrt{2}} \pm 1)$. Note that (a) is plotted before a Mollow triplet has developed and that these resonances are naturally expected to be present. Now, panel (b) is plotted when the Mollow triplet is fully developed, as one can see. Each of the resonances from (a) is split into a *doublet*, the splitting of which is equal to the sideband frequency in the Mollow triplet. Small peaks at $\pm 2g$ are also observed to be shifted by the sideband frequency.

(a) $\mathcal{E} = 10$, $\Delta = 353.82$ (b) $\mathcal{E} = 40$, $\Delta = 358.09$
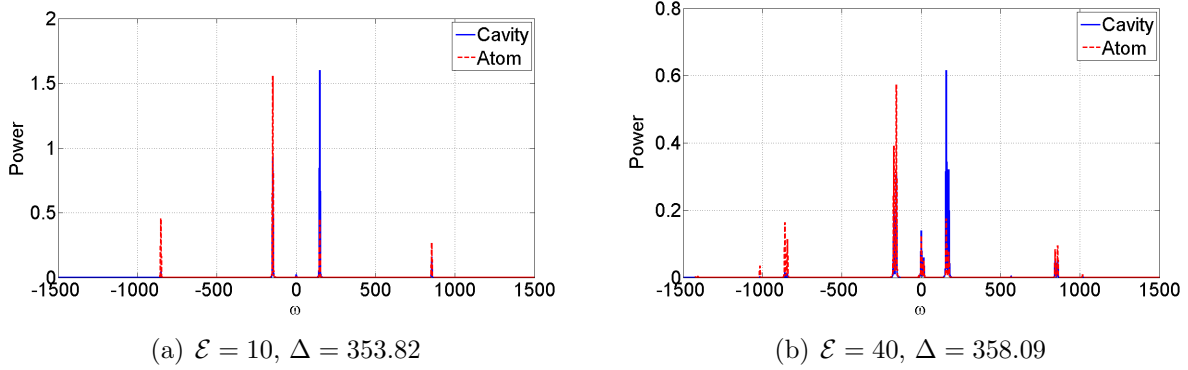
Figure 5.7: Peak 2, Optical spectra for the cavity and atom.

Any explanation we may come up with in the next chapter for the process of multi-photon saturation will have to account for these facts!

5.2.6.3   Three-photon peak

We now briefly present similar results for the third peak as we did for the second. In fig. 5.8 we see the incoherent spectra and the second-order intensity correlation function, both of which develop traits we have come to recognize as signs of Photon Blockade. Plots (g) and (h) are calculated with $\gamma = 0$, so that (as advertised earlier) $\left[g_{aa}^{(2)}(0)\right]_{ss}$ falls below one (more precisely, it is 0.9377). Note that the negative sideband in the spectrum is now practically completely suppressed, as it will be for the four-photon peak.

Now we proceed to inspect the spectra at higher frequencies. Fig. 5.9 shows the developing spectrum as a function of drive strength. As the reader can probably tell, the situation is getting a little too messy for comfort! However, at the moment, we do not strive to explain every single resonance peak but rather make a particular point. To start
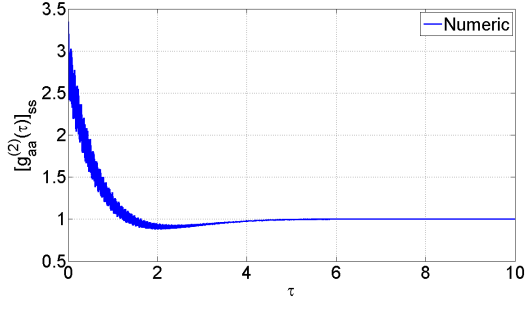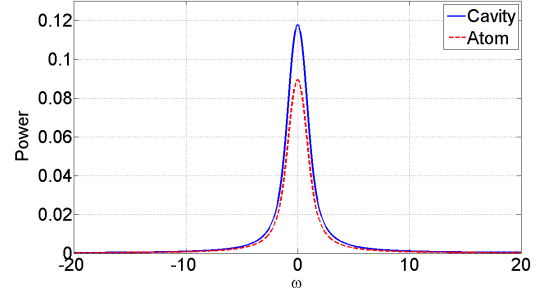
(a) $\mathcal{E} = 20$, $\Delta = 289.375$ (b) $\mathcal{E} = 20$, $\Delta = 289.375$
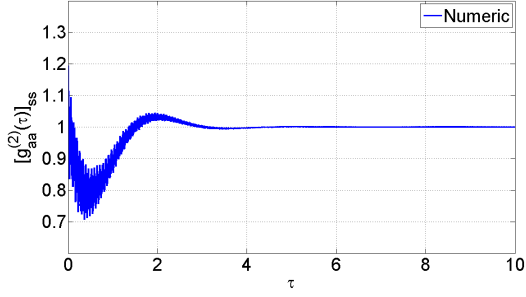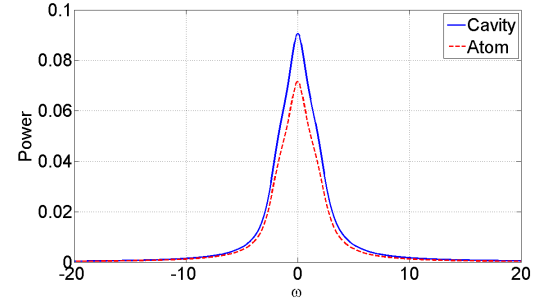
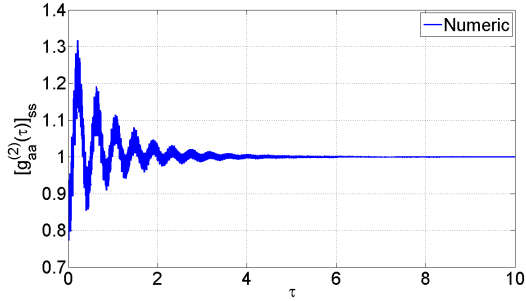(c) $\mathcal{E} = 30$, $\Delta = 290.26$ (d) $\mathcal{E} = 30$, $\Delta = 290.26$
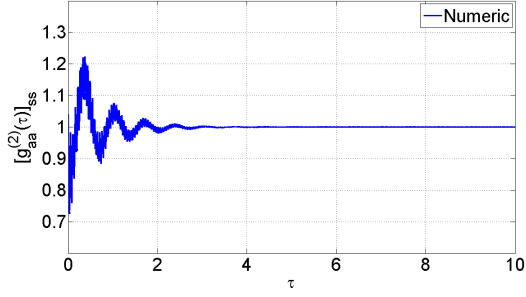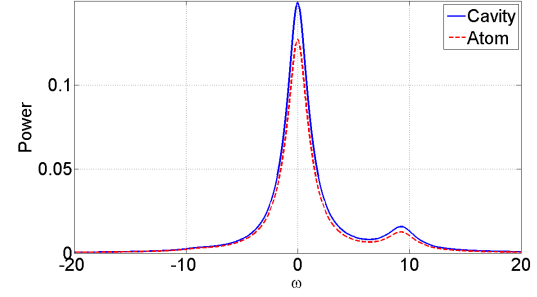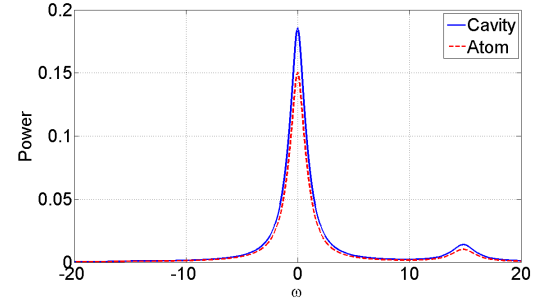
(e) $\mathcal{E} = 50$, $\Delta = 293.17$ (f) $\mathcal{E} = 50$, $\Delta = 293.17$

(g) $\gamma = 0$, $\mathcal{E} = 60$, $\Delta = 295.2$ (h) $\gamma = 0$, $\mathcal{E} = 60$, $\Delta = 295.2$

Figure 5.8: Peak 3. (a), (c), (e), (g) – Second-order intensity correlation function; (b), (d), (f), (h) – Incoherent spectra.

65

with, we shall work through the spectrum at the lowest drive case out of those shown, because it is the simplest. Referring to fig. 5.9(a), peaks are seen at the frequencies -1284, -919.2, -211.2, 82.4, 129.6, 496.8, 789.6. Note that if we had driven the $|3+\rangle$ state instead of the $|3-\rangle$ these numbers would be changed to their negatives. We would like to explain these peaks, which is quite readily achieved.

Consider the JC spectrum up to the $|3-\rangle$ dressed state. We have possible one-photon transitions between the states shown in table 5.3; remember also that one must subtract ω_L from all transition frequencies for consistency with our Interaction picture. As explained

Transition	Freq. (Int. Pic.)	Comment
$|3-\rangle \rightarrow |2+\rangle$	$g(1/\sqrt{3} - \sqrt{3} - \sqrt{2}) = -1284.45$	Observed.
$|3-\rangle \rightarrow |2-\rangle$	$g(1/\sqrt{3} - \sqrt{3} + \sqrt{2}) = 129.76$	Observed.
$|2+\rangle \rightarrow |1+\rangle$	$g(1/\sqrt{3} - 1 + \sqrt{2}) = 495.78$	Observed.
$|2+\rangle \rightarrow |1-\rangle$	$g(1/\sqrt{3} + 1 + \sqrt{2}) = 1495.78$	Not observed. Appears for stronger drive.
$|2-\rangle \rightarrow |1+\rangle$	$g(1/\sqrt{3} - 1 - \sqrt{2}) = -918.432$	Observed.
$|2-\rangle \rightarrow |1-\rangle$	$g(1/\sqrt{3} + 1 - \sqrt{2}) = 81.57$	Observed.
$|1+\rangle \rightarrow |g,0\rangle$	$g(1/\sqrt{3} + 1) = 788.675$	Observed.
$|1-\rangle \rightarrow |g,0\rangle$	$g(1/\sqrt{3} - 1) = -211.325$	Observed.

Table 5.3: System driven on a three-photon MPT to $|3-\rangle$. Possible 1-photon transitions and their frequencies (in the Dirac picture). Compare to frequencies of peaks shown in the power spectrum of fig. 5.9(a).

on page 56, the path of least detuning is the one that follows entirely along states of the same polarity as the state being driven. This is confirmed in our example: the detunings from the drive shown in table 5.3 are indeed least for transitions between "-"states. Moreover, fig. 5.9(a) supports the argument that the amplitude for this transition dominates, as these are three of the highest peaks in the power spectrum. Keep in mind that there is no preference for the decay pathway, but if all transitions are equally likely as decays and some are preferred as excitations, the least detuned transitions *will* have a bigger amplitude. Nonetheless, the transition matrix elements probably also come into play.

With increasing drive more peaks sprout up corresponding to either more detuned, more excited, or higher order transitions. Up to and including plot (d), the Mollow triplet has yet to develop. This occurs between panels (d) and (e). Correspondingly, some of the singlet resonances in (d) are split into doublets of peaks in (e)! This is similar to what was observed for the two-photon peak. Although this scenario is too complicated to be predicted fully from analytical considerations, we shall address this main feature in general in the next chapter.

5.2.6.4 Four-photon peak

Finally, very briefly, I present plots for the four-photon peak. These are shown in fig. 5.10. Note that for (g) and (h), I have used Fock state truncation $N = 15$. Once again, the last pair of plots is taking $\gamma = 0$ and demonstrates that antibunching for the four-photon transition is also possible ($\left[g^{(2)}_{aa}(0)\right]_{ss} = 0.9962$). The higher frequency optical spectra plots are not included because they are very dense and give us no new information. The most important
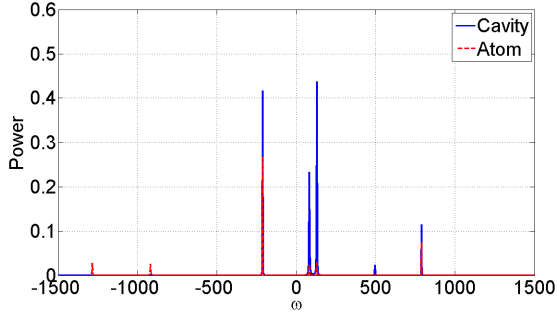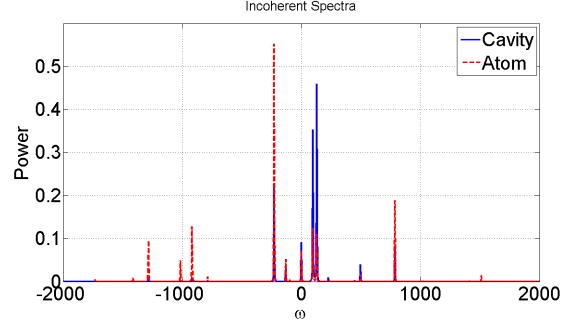
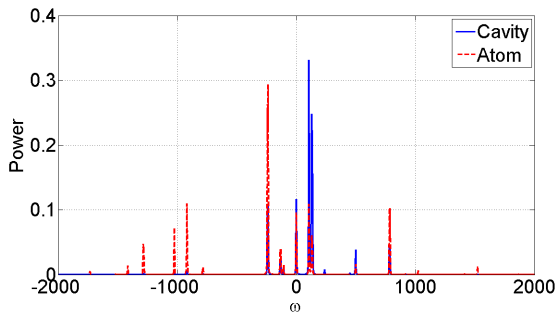(a) $\mathcal{E} = 5$, $\Delta = 288.72$
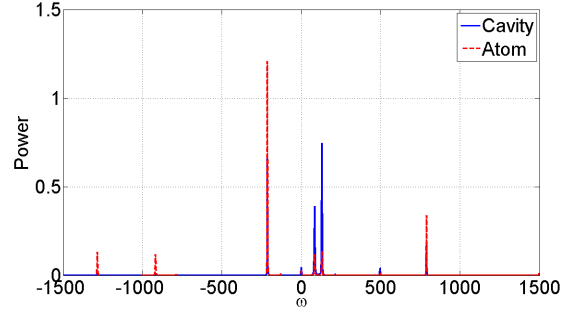
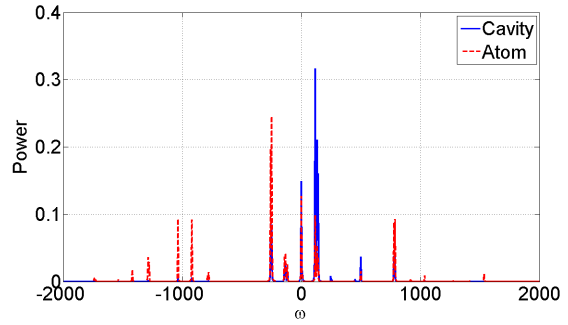(b) $\mathcal{E} = 10$, $\Delta = 288.85$
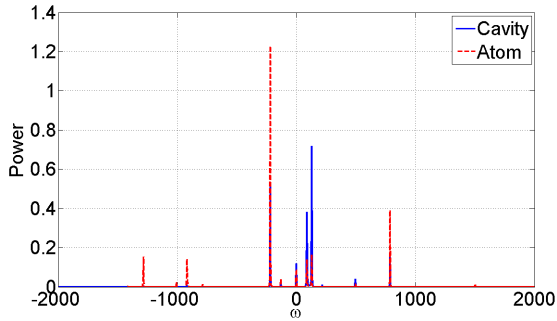
(c) $\mathcal{E} = 20$, $\Delta = 289.37$

(d) $\mathcal{E} = 30$, $\Delta = 290.25$

(e) $\mathcal{E} = 40$, $\Delta = 291.5$

(f) $\mathcal{E} = 50$, $\Delta = 293.16$

Figure 5.9: Peak 3, Optical spectra for the cavity and atom.

comment is that when the Mollow triplet develops, multiple splittings of the resonance peaks into doublets is seen.

5.2.6.5 Dynamic Stark Splitting

There is another result I would like to bring to the reader's attention, and that is the Stark splitting observed for the different peaks. In §4.4, for a one-photon process in a true two-level qubit, we have seen that the splitting was proportional to $\mathcal{E}$. In our case, one might guess that for an n-photon process (including $n = 1$!), the splitting would go as a polynomial of order n in $\mathcal{E}$. The reason we have generalized that guess from just "proportional to $\mathcal{E}^n$" is because we anticipate that in this much more complicated scenario, splitting will also depend on detunings, decay rates etc. In the next chapter, we will see that many different transitions are important in the process, whereby all order transitions up to n must be considered. Only perhaps in the very strong drive limit one might see the proportionality emerge as a good approximation.

Our guess is in fact confirmed, as shown in fig. 5.11. This is simply understood as follows: the original multi-photon transition which is responsible for causing saturation requires n photons at the least to take place. Now, the amplitude to have a photon available is proportional to $\mathcal{E}$, therefore the amplitude to have n photons available is proportional to $\mathcal{E}^n$, and the splitting is "proportional" (see discussion above) to the amplitude for the transition.

5.3   Overview

To summarize our results, we can safely claim that Multi-Photon Blockade *is* observed as characterized by the saturation of the driven MPT causing a dynamic Stark shift, as well as the eventual antibunching seen when we drive the system strongly.

However, we come out of this chapter with two main questions remaining:

1. The need to understand the behavior of $\left[g_{aa}^{(2)}(0)\right]_{ss}$ as a function of drive strength when our system is driven on a MPT. We can perhaps understand this process qualitatively: increasing the drive increases the excitation rate and therefore, also the population in the intermediate states (because decay rates remain unaltered). Any population in the states $|1\pm\rangle$ will contribute to the denominator but not the numerator of $\left\langle a^{\dagger 2} a^2 \right\rangle / \left\langle a^\dagger a \right\rangle^2$. For a two-level system this is precisely the reason we get antibunching. Here, in the multi-level case, this can decrease the value of $\left[g_{aa}^{(2)}(0)\right]_{ss}$ below one, but *not* all the way down to zero.

2. We need to apply the techniques of Floquet theory from §4.4 to the MPT saturation case and see if we can explain the spectra and other results presented above in connection. There is little doubt as to the physical cause for this saturation phenomenon. The reason is the same as for the two-level system (see page 42), except that our loop-like multiple coherent photon exchanges with the driving field are now a little different. For a simple qubit, a "loop" consists of one photon up and one photon down. For a MPT, a loop is n photons up and n down.
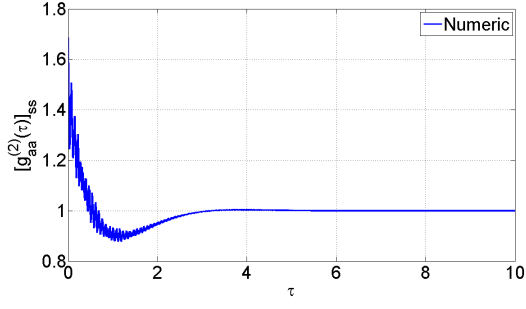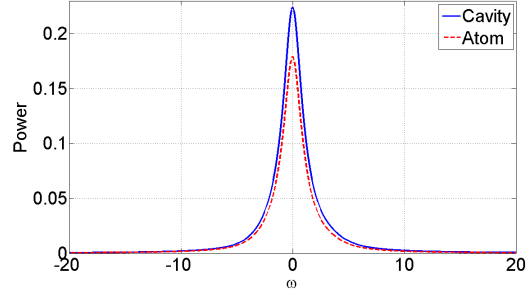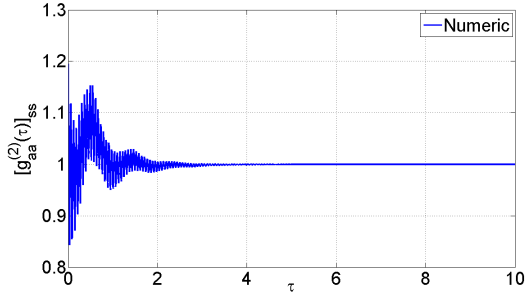
(a) $\mathcal{E} = 40$, $\Delta = 252.16$
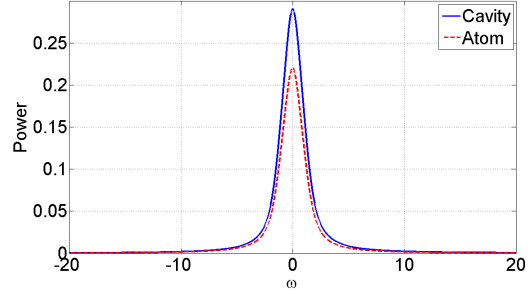
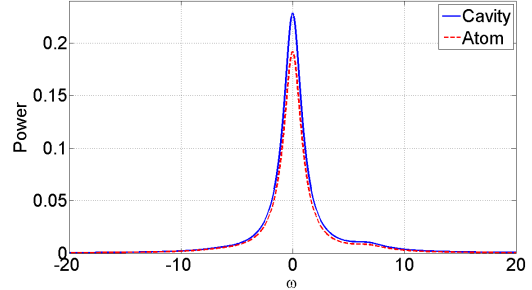(b) $\mathcal{E} = 40$, $\Delta = 252.16$
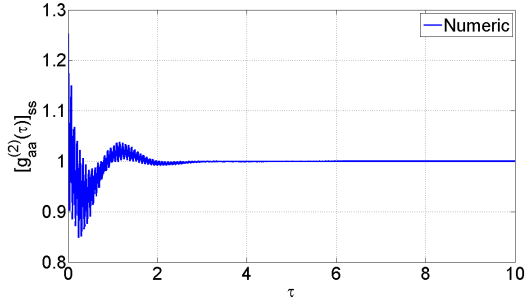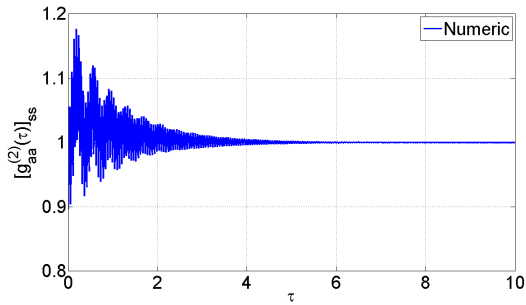
(c) $\mathcal{E} = 50$, $\Delta = 253.41$

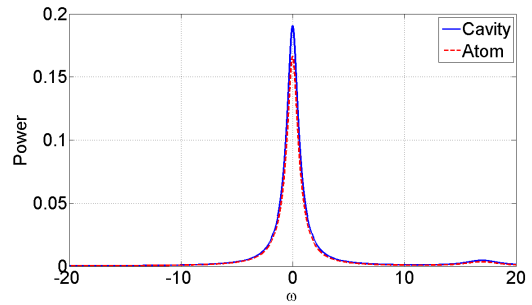(d) $\mathcal{E} = 50$, $\Delta = 253.41$

(e) $\mathcal{E} = 60$, $\Delta = 254.96$

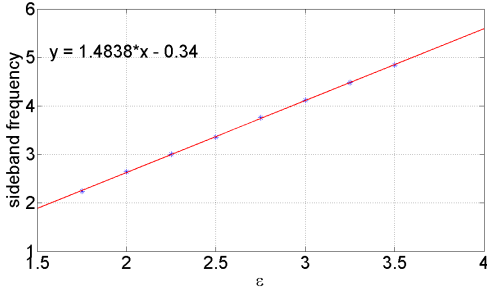(f) $\mathcal{E} = 60$, $\Delta = 254.96$

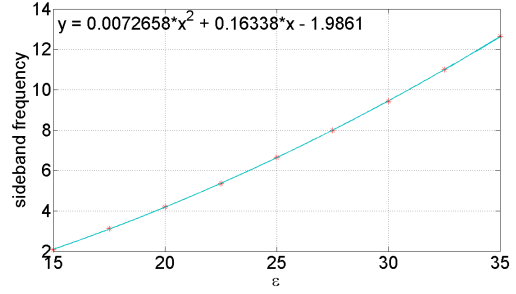(g) $\gamma = 0$, $\mathcal{E} = 80$, $\Delta = 258.965$

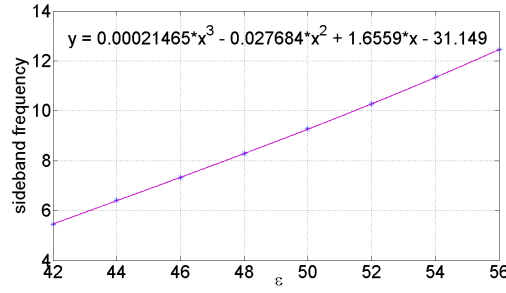(h) $\gamma = 0$, $\mathcal{E} = 80$, $\Delta = 258.965$

Figure 5.10: Peak 4. (a), (c), (e), (g) – Second-order intensity correlation function; (b), (d), (f), (h) – Incoherent spectra.

69

(a) Peak 1
(b) Peak 2
(c) Peak 3

Figure 5.11: Data obtained by tracking the peaks (i.e. shifts along the Δ axis due to high drive accounted for), plotting incoherent spectra and reading off side-peak frequencies. Least-squares fitting then gives equations for the curves. Notice that the gradient in (a) is 1.4838, not that far off from the predicted $\sqrt{2} = 1.414$.

Chapter 6

Interpretation of Results

6.1 Transition from Bunching to Antibunching

The first half of the chapter is dedicated to constructing a simple model to explain the transition from extreme bunching to antibunching encountered in the Results chapter. Ideally, one would like to be able to have a model which *quantitatively* predicts the behavior. Furthermore, it will turn out (as mentioned en passant before-hand) that the two-photon process is different to the higher order transitions as $\left[g_{aa}^{(2)}(0)\right]_{ss}$ starts off from the maximum value and just decreases with increasing drive. Hence one would hope to produce *two* models, one appropriate for the two-photon and the other for any higher order peak. What we hope to get out of this procedure is a *simple* analytic formula, one that gives insight into the functional form just by inspection.

Unfortunately, this will not be entirely possible. We will see that constructing a simple model which is analytically solvable is not so very difficult. It is the requirement that the *solution* be transparent that will limit our progress. I will first show how such a simple model can be written down, and we will apply the method to the two and three photon transitions. However, because of the complexity of the solutions, eventually we shall have to resort to a phenomenological model. The solution to that will be simple enough for the two-photon peak, but already too complicated for the three – we shall have to compromise yet again. Thus our success in this chapter will be somewhat limited. Nevertheless, we will have the satisfaction of identifying key ingredients for the effect to take place.

6.1.1 Two-photon transition

Consider driving the JC system on the two-photon resonance to $|2-\rangle$. To begin with, we need to choose a dressed-state basis truncation. In this case, we only need to keep $|g,0\rangle$, $|1-\rangle$ and $|2-\rangle$, because the $|1+\rangle$ state is much more detuned from the driving frequency and therefore will not contribute very much in terms of mediating the two-photon excitations. It is significant, though, when it comes to considering the decay of the system back to the ground state. On the other hand, we are wanting a model which is as simple as possible. Therefore, we will ignore $|1+\rangle$, getting a model which succeeds in qualitatively predicting the behavior but is quantitatively incorrect.

The next step is to express a and σ_- in this three-state basis. It is a simple procedure to calculate the matrix elements of these two operators because we know how they act on the bare states. In Appendix A.1, for reference, I present the general rules for the dressed state representation. Thus, in the basis $|g, 0\rangle$, $|1-\rangle$, $|2-\rangle$, we have

$$
a = \begin{pmatrix} 0 & 1/\sqrt{2} & 0 \\ 0 & 0 & \frac{1}{2}(\sqrt{2}+1) \\ 0 & 0 & 0 \end{pmatrix},
$$

$$
\sigma_- = \begin{pmatrix} 0 & -1/\sqrt{2} & 0 \\ 0 & 0 & -1/2 \\ 0 & 0 & 0 \end{pmatrix}. \tag{6.1.1}
$$

Finding H from eqn (5.1.2) with $\omega_L = \omega_o - g/\sqrt{2}$ leads to

$$
\frac{1}{\hbar}H = \begin{pmatrix} 0 & \mathcal{E}/\sqrt{2} & 0 \\ \mathcal{E}/\sqrt{2} & g(\frac{1}{\sqrt{2}}-1) & \frac{\mathcal{E}}{2}(\sqrt{2}+1) \\ 0 & \frac{\mathcal{E}}{2}(\sqrt{2}+1) & 0 \end{pmatrix}. \tag{6.1.2}
$$

We next need to find the Liouvillian. As explained on page 52, we need to write ρ – a 3×3 matrix – as a vector. We choose the convention that this is done by writing the columns of ρ one after the other in a column vector. We shall refer to this procedure as *flattening* ρ, denoting the result $\bar{\rho}$, and the inverse procedure as *reshaping* ρ. Then $\mathcal{L}$ is a 9×9 matrix, which we need to determine. This is most easily achieved if one does the following. We notice that the super-operator $\mathcal{L}$ (see eqn (5.1.3)) contains two basic operations: multiply ρ from the left or from the right by other operators.

We can represent each of the operations "multiply by A from the left" and "multiply by B from the right" by super-operators written as 9×9 matrices which would act on the flattened ρ. We will denote these as $spre(A)$ and $spost(B)$ (for *super* -pre and -post multiplication). The idea is that doing the 3×3 matrix multiplication $A\rho B$ and flattening the result should be equivalent to flattening ρ, and calculating $spre(A)spost(B)\bar{\rho}$. That is, the composite super-operator of both operations combined is $spre(A)spost(B)$. Thus, all super-operators act on $\bar{\rho}$ by multiplying from the left.

We now have the basic ideas required to deal with the Master equation. Numerically, one always does the calculations this way. Analytically, this is only feasible if the basis size is extremely small. In any case, in Appendix A.2, I present the general rules for constructing the super-operators $spre(A)$ and $spost(B)$ for arbitrary A and B, as the reader may verify.

Next, we shall denote $\mathcal{L}_H = \frac{1}{i\hbar}[H, \cdot]$ and $\mathcal{L}_j = \left(C_j \cdot C_j^\dagger - \frac{1}{2}C_j^\dagger C_j \cdot - \frac{1}{2} \cdot C_j^\dagger C_j\right)$ for $j = a, \sigma_-$. It is possible (and desirable!) to simplify $\mathcal{L}_j$, the damping terms in the Liouvillian, by making the so-called Secular approximation. The actual process is trivial since we are already working in the dressed-state basis.

Let E_i be the eigenvalue of the ith basis vector. Explicitly, the approximation amounts to the following. Consider the Master equation with $\mathcal{L}$ replaced by $\mathcal{L}_j$, i.e. $\dot{\rho} = \mathcal{L}_j\rho$. We can write this out as a set of coupled ODEs for the matrix elements of ρ. Under the Secular approximation, if the equation for $\dot{\rho}_{nm}$ contains a term proportional to ρ_{kl}, we keep this term

if $E_n - E_m = E_k - E_l$ and neglect it otherwise. When this is done, we can write out the new, effective damping Liouvillians and proceed to work with these.

Physically, we can justify this by considering a transformation of the entire Master equation to the Interaction picture with $H_o = H_{JC}$. Then, going back to the equation for $\dot{\rho}_{nm}$, all terms proportional to ρ_{kl} with $E_n - E_m = E_k - E_l$ are *constant*. However, if $E_n - E_m \neq E_k - E_l$, in the Dirac picture, the term is multiplied by an exponential of $\left\{ -\frac{i}{\hbar} \left[E_n - E_m - (E_k - E_l) \right] t \right\}$, and thus oscillates at the frequency difference. The Secular approximation assumes these frequencies are so large that when the Master equation is integrated over even a modest period on the time-scale of the evolution of ρ, the oscillating terms average to zero. Usually, this assumption is valid in the strong-coupling limit. Since our work is in the *extremely* strong-coupling limit, we can safely apply the approximation.

Now, one can easily use the above ideas to find the Liouvillian for the driven JC model, restricted to our three basis states. One could also find the nullspace of this $\mathcal{L}$, reshape ρ_{ss} and calculate $\langle a^{\dagger 2} a^2 \rangle / \langle a^\dagger a \rangle^2$, keeping the damping rates, drive strength and coupling parameters as variables. This *can* be done, but the end result is so complicated, it gives no insight. Therefore, instead, we will simplify the situation further by considering a phenomenological model very similar to the actual problem.

Imagine a three state system, driven on a two-photon resonance to the highest level. Let δ be the "energy"[1] of the intermediate state in the Interaction picture with the drive (so in this case, it is the equivalent of $g(\frac{1}{\sqrt{2}} - 1)$). We take

$$\frac{1}{\hbar} H = \begin{pmatrix} 0 & \mathcal{E} & 0 \\ \mathcal{E} & \delta & \mathcal{E} \\ 0 & \mathcal{E} & 0 \end{pmatrix},$$

$$D = \begin{pmatrix} 0 & 1 & 0 \\ 0 & 0 & 1 \\ 0 & 0 & 0 \end{pmatrix}, \tag{6.1.3}$$

where D is the single new equivalent of a and σ_-. We shall further denote the damping rate β, so we only have one collapse operator, $C_D = \sqrt{\beta} D$.

Finding the Liouvillian as a 9×9 matrix according to

$$\mathcal{L} = -\frac{i}{\hbar} \left\{ spre(H) - spost(H) \right\} + \left\{ spre(C_D) spost(C_D^\dagger) - \frac{1}{2} spre(C_D^\dagger C_D) - \frac{1}{2} spost(C_D^\dagger C_D) \right\},$$

gives the required matrix. We then find its nullspace, reshape ρ_{ss}, normalize the density matrix so that $tr\left[\rho_{ss} \right] = 1$ and calculate $tr\left[D^{\dagger 2} D^2 \rho_{ss} \right] / tr\left[D^\dagger D \rho_{ss} \right]^2$.
This gives

$$\left[g_{DD}^{(2)}(0) \right]_{ss} = \frac{48 \mathcal{E}^4 + 16 \beta^2 \mathcal{E}^2 + 4 \delta^2 \beta^2 + \beta^4}{(8 \mathcal{E}^2 + \beta^2)^2}. \tag{6.1.4}$$

This is illustrated in fig. 6.1(a) with chosen parameters approximating the real problem from the Results chapter. As we can see, the general treatment has produced exactly the trend

---

[1] In the Dirac picture, the Hamiltonian can no longer be interpreted as the energy...

we have found for the second peak in numerical simulations. Of course, the prediction is not expected to be quantitatively accurate, but the order of magnitude of all the numbers is very reasonable. Already at $\mathcal{E} = 10$ the curve has descended below one so antibunching *is* predicted to occur.
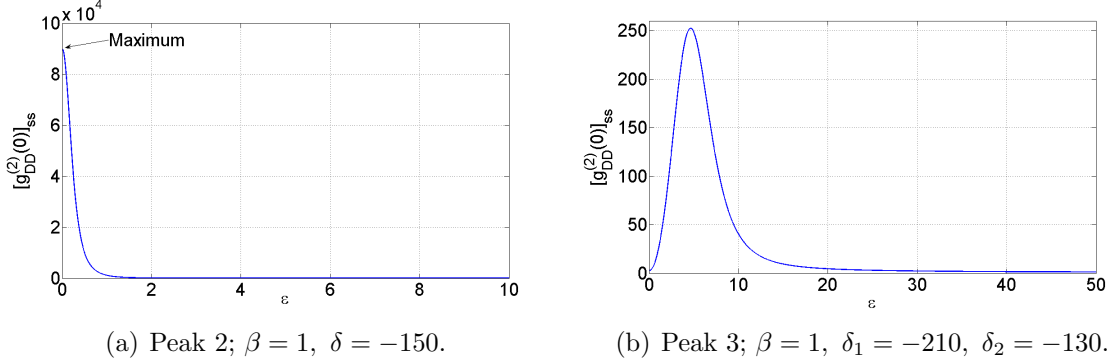

(a) Peak 2; $\beta = 1$, $\delta = -150$.   (b) Peak 3; $\beta = 1$, $\delta_1 = -210$, $\delta_2 = -130$.

Figure 6.1: Predictions from phenomenological models constructed to describe the two and three photon transitions in the driven JC model.

6.1.2   Three-photon transition

We can treat the next peak in much of the same way. Consider driving the $|3-\rangle$ dressed state on a three-photon resonance. Choose basis states to be $|g, 0\rangle$, $|1-\rangle$, $|2-\rangle$ and $|3-\rangle$. Again, we are ignoring intermediate states of the opposite polarity because they are much more detuned from the drive frequency. Writing down a typical model once more gives us

$$
\frac{1}{\hbar} H = \begin{pmatrix} 0 & \mathcal{E} & 0 & 0 \\ \mathcal{E} & \delta_1 & \mathcal{E} & 0 \\ 0 & \mathcal{E} & \delta_2 & \mathcal{E} \\ 0 & 0 & \mathcal{E} & 0 \end{pmatrix},
$$

$$
D = \begin{pmatrix} 0 & 1 & 0 & 0 \\ 0 & 0 & 1 & 0 \\ 0 & 0 & 0 & 1 \\ 0 & 0 & 0 & 0 \end{pmatrix}, \tag{6.1.5}
$$

with β as the damping rate as before and $\delta_{1,2}$ the "energies" of the intermediate states in the Interaction picture. Once again applying the Secular approximation as discussed above, we can write down the Liouvillian and find the steady-state density matrix. However, this is a very long and messy formula, so I will not present it here.

Instead, we plot the result in fig. 6.1(b) for typical parameter values. Once again, the form of $\left[g_{DD}^{(2)}(0)\right]_{ss}$ as a function of drive strength agrees with what we have seen in the previous chapter. Antibunching is predicted for drive strengths of about $\mathcal{E} = 100$ and higher. One can extrapolate this three-photon case to higher order transitions because the same behavior is found for all MPT. I have not attempted to do this analytically, but I have checked numerically that indeed a similar basis truncation for the other MPT reproduces the same trend.

6.2 Multi-Photon Saturation

The second half of the chapter is concerned with super-splitting calculations. We obviously will have to restrict the basis to the essential states only. Here, already, there is a problem. How do we define "essential" states? It is seen from numerical simulations with various basis truncations that in order to recover the full numerical results for most of the MPT spectra, a varying (and generally increasing) number of states must be retained.

It will not be possible to analytically solve the problem of MPT saturation for any but the second peak (much like in the last section). I will look at the two-photon transition in the smallest possible basis and then outline the general resulting situation for higher order MPT. A novel book-keeping method is introduced to simplify the analysis, but the approach is limited to certain special cases. We will comment on the asymmetry issue brought up in the Results chapter and propose a likely explanation.

6.2.1 Two-photon transition – minimal basis

We begin by solving the simplest model possible: the dynamic Stark splitting when the JCM is driven on a two-photon resonance to $|2-\rangle$. One might guess that as a first approximation, we could truncated the basis to $|g, 0\rangle$, $|1-\rangle$ and $|2-\rangle$, for the same reasons as in the previous section. This simple example is the only one I have been able to solve analytically. It will serve to remind us of the procedure, as well as give us some much needed intuition.

So, in this basis and in the normal Interaction picture with the drive, H is given by eqn (6.1.2). Following the same method as in §4.4, we should now find the eigenstates and eigenvalues of this matrix. Finding the eigenvalues gives:

$$0, \quad \frac{g}{2}\left(\frac{1}{\sqrt{2}} - 1\right) \pm \frac{1}{2}\sqrt{g^2\left(\frac{1}{\sqrt{2}} - 1\right)^2 + \mathcal{E}^2\left[2 + \left(\sqrt{2} + 1\right)^2\right]}.$$

With an appropriate application of the Binomial theorem (using the fact that $\mathcal{E} \ll g$), and introducing the Stark splitting parameter

$$S = \frac{\mathcal{E}^2\left[2 + \left(\sqrt{2} + 1\right)^2\right]}{4g\left(1 - \frac{1}{\sqrt{2}}\right)}, \tag{6.2.6}$$

we can write these in increasing order as

$$\begin{aligned}
\lambda_1 &= g\left(\frac{1}{\sqrt{2}} - 1\right) - S, \\
\lambda_2 &= 0, \\
\lambda_3 &= S. \tag{6.2.7}
\end{aligned}$$

Note that S really does depend on $\mathcal{E}$ quadratically, as observed in the previous chapter, but the coefficient of $\mathcal{E}^2$ from fig. 5.11(b) is not well approximated by eqn (6.2.6). This is to be expected – we shall see why in a moment.

Moreover, for convenience, let us denote $\omega_{2-} = 2\omega_o - \sqrt{2}g$ and $\delta_{1-} = g\left(\frac{1}{\sqrt{2}} - 1\right)$, the frequency of $|1-\rangle$ in the Interaction picture. Under the same Binomial approximation, the three respective eigenvectors are

$$\vec{\nu}_1 = \begin{pmatrix} \frac{\sqrt{2}}{\sqrt{2}+1} \\ \frac{2}{\sqrt{2}+1}\frac{\delta_{1-}-S}{\mathcal{E}} \\ 1 \end{pmatrix},$$

$$\vec{\nu}_2 = \begin{pmatrix} -(1+\frac{1}{\sqrt{2}}) \\ 0 \\ 1 \end{pmatrix},$$

$$\vec{\nu}_3 = \begin{pmatrix} \frac{\sqrt{2}}{\sqrt{2}+1} \\ \frac{2}{\sqrt{2}+1}\frac{S}{\mathcal{E}} \\ 1 \end{pmatrix}. \tag{6.2.8}$$

The next step is to convert these eigenvalues in the Dirac picture to quasi-frequencies in the Schrödinger picture. We know how to do this rigorously from our analysis of the vacuum Rabi peak saturation. We thus need the free evolution frequencies of the eigenkets of H_o, removed in the transition to the Interaction picture. Since we are using $H_o = \hbar\omega_L\left(\sigma_+\sigma_- + a^\dagger a\right)$ (see page 43) with $\omega_L = \omega_o - g/\sqrt{2}$, and we are only concerned with the three dressed states that constitute our truncated basis, it is easy to work these out.

It is trivial to write down the unitary time evolution operator generated by H_o and conclude that the free frequencies of the states $|g,0\rangle$, $|1-\rangle$ and $|2-\rangle$ are respectively 0, $\omega_{2-}/2$ and ω_{2-}.

If one only wishes to compute the quasi-frequencies of the system, following the method of §4.4 amounts to basically taking all possible combinations of the eigenvalues λ_i (allowed by the eigenvectors $\vec{\nu}_i$) and the free frequencies, and *adding* them. We introduce a convenient, methodical way of keeping track of these frequencies as well as possible transitions between them, in what is essentially a simple table with a couple of rules. I shall refer to these tables as *Floquet Tableaux* (FT).

		0	$\omega_{2-}/2$	ω_{2-}
$\delta_{1-} - S$	$\delta_{1-} - S$	$\omega_{2-}/2 + \delta_{1-} - S$	$\omega_{2-} + \delta_{1-} - S$
0	0		ω_{2-}
S	S	$\omega_{2-}/2 + S$	$\omega_{2-} + S$

Table 6.1: Floquet Tableau for the dynamically Stark-split quasi-frequencies of the system when driven on a two-photon resonance.

6.2.2 Multi-photon dynamic Stark splitting

Table 6.1 gives the FT for our problem. Each eigenvalue λ_i corresponds to a row while each free frequency is assigned a column. This is done in increasing order top to bottom and left to right. Then each element of the table is the sum of the corresponding row and column

headers. Each column in the FT corresponds to a group of closely spaced quasi-frequencies, roughly of the order of $(n-1)\omega_o$ where n is the column number. Note that the middle entry is indeed empty as $\vec{\nu}_2$ has no contribution from $|1-\rangle$. This is a rather special case and will generally not happen.

I should warn the reader that FT are only straight-forward to use if the chosen basis state truncation includes one out of each pair of JC dressed-state doublets from the ground up to some arbitrary level. Each pair $|n\pm\rangle$ of the JC ladder should be represented by one of its members. If this condition does not hold, the application of the FT is unclear.

Here are some general properties of the FT:

- Transitions contributing to the central peak in the Mollow triplet occur across rows. MPT (i.e. skipping columns) are also possible.

- Transitions contributing to the sidebands are all single-photon processes (so between adjacent columns) and occur between the two neighboring rows the eigenvalues of which do not include any δ's. Scanning right to left, a link to the higher row constitutes the positive sideband and a link to the lower the negative.

- The elements of any row the eigenvalue of which contains a δ are strongly connected by one-photon processes to elements of the adjacent columns in rows which do not contain δ's in their headers. These transitions are detuned from the drive by $\sim \delta$.

- All transitions from such a δ-row to the first of the non-δ rows contribute to $\pm$ one of the peaks in the relevant doublets in the spectrum (symmetrically arranged about zero). All transitions from the same δ-row to the second of the non-δ rows contribute to $\pm$ the other peak in the detuned doublets in question.

- All transitions, in principle, can happen in both directions – excitation and decay. However, unless a transition is driven (or nearly so), it is more likely to be seen as a decay. A transition right to left across the FT is a decay, while left to right is an excitation. Real (as opposed to *virtual*) transitions within the same column are impossible.

- All columns are strongly interconnected via transitions across single rows.

- As for crossed column *and* row connections, the dominant processes link directly neighboring columns.

A final general comment is this: in principle, if the dimensionality of H is N, the total number of quasi-energies is N^2, whereby each state is "split" into N components. Despite the fact that H is infinite dimensional, the solution does converge very nicely. For example, the same calculation of the Mollow triplet with Fock space truncation $N = 10$ and $N = 15$ produces identical results. This is because when H in the Dirac picture is diagonalized, considerably higher eigenvectors tend to be unaffected by the saturation occurring a few levels of excitation below. Their eigenvectors to a good approximation do not mix in the other basis states and as a result, the level is essentially unsplit.

We are now in a position to understand quite a few of the observations made in the Results chapter. Firstly, the *splitting* of detuned resonance peaks in the spectrum into doublets

can be explained by the third and fourth bullet-points above. The frequency difference between transitions from a δ-row to the two non-δ rows is exactly the sideband frequency, as we found the splitting to be numerically. For example, consider the two-photon transition depicted in fig. 5.7. The closest doublet to the origin is due to $|1-\rangle$ while the next doublet out is due to $|1+\rangle$. A similar interpretation for the splitting in the higher order MPT is a straight-forward generalization of our argument.

Notice that there can only ever be two rows in the FT which do not contain δ's, no matter the order of the MPT. This is because in the Interaction picture, the only two states that have zero "energy" are the ground and the driven state. Thus, according to our theory, we are to expect splitting of detuned resonance peaks into doublets but not triplets or any higher multiplets. This is indeed what we find.

We have commented earlier on the Homodyne spectrum and the fact that the Mollow sidebands and central peak are not completely at quadrature. Now we can understand this since so many different transitions contribute to each peak. The full periodic solutions of the system are *much* more complicated then the simple example we have solved – even for the two-photon transition. One cannot expect the phase relationship between *all* these transitions in the cycle to be the same (in fact, it is probably not possible).

As briefly mentioned in the introduction to this section, one should give some consideration to the essential states that determine the Mollow spectrum for each MPT. First of all, we can neglect dressed states of the opposite polarity, as discussed many times before. As it turns out, to roughly achieve agreement with full numerical results regarding the Mollow sideband frequency, for the two-photon transition, keeping $|g, 0\rangle$, $|1-\rangle$, $|2-\rangle$ is sufficient. However, if we drive $|3-\rangle$, then in addition we need to keep $|4-\rangle$ and $|5-\rangle$.

The sideband frequency can be directly linked to the two eigenvalues of H closest to zero. If H is truncated prematurely, these eigenvalues are considerably off their true values. Thus, although the next few higher states at first sight appear not to directly participate in the saturation process, their presence influences the results significantly.

6.2.3 MPT Mollow spectrum asymmetry

The final issue remaining to discuss is the asymmetry found in the Results chapter. I do not have a rigorous explanation but rather just a suggestion, an indication of the likely direction one should follow if the matter is to be satisfactorily resolved.

Recall the observations we are trying to explain: when one drives a MPT to $|n-\rangle$, the negative Mollow sideband is suppressed and vice versa for $|n+\rangle$. This asymmetry is evident as soon as the sidebands in the Mollow triplet become distinguishable. Moreover, the effect weakens with increasing drive. It is observed whether or not "extra" states are included in the basis, but depending on the truncation, the weighting of the asymmetry can change.

The key to the mystery are the two eigenvalues of H in the Dirac picture which are closest to zero (i.e. contain no δ's). With a little thought, we see that generally, the eigenvalues of H are *close* to its diagonal elements (the "energies" of the basis dressed states in the

Dirac picture) but shifted by some small splitting parameter(s). Moreover, the corresponding eigenvectors have a dominant contribution from that very same basis dressed state. The example we have solved was very special: there, one of these eigenvalues was actually *equal* to the corresponding diagonal element. In general, there will be two non-zero splitting parameters S_1 and S_2, being the shifts of the ground and driven state frequencies due to the interaction.

Now, the main idea is that the eigenvectors corresponding to S_1 and S_2 are very different: one has a dominant contribution from $|g, 0\rangle$ and the other from $|n\pm\rangle$. This is in contrast to the vacuum Rabi peak scenario where the eigenvectors mixed both basis states with equal weighting. Also, usually, S_1 and S_2 will have opposite signs but approximately equal absolute values.

To be slightly more concrete, consider for example the two-photon transition to either of $|2\pm\rangle$. We have pointed out that if one chooses basis truncation $|g, 0\rangle$, $|1\pm\rangle$, $|2\pm\rangle$ then the asymmetry is present but the wrong peak is suppressed. We have already solved this problem and seen that it is quite a special case. Therefore, let us include $|3\pm\rangle$ which produces the correct asymmetry and come back to the analytically solved case at the end to test the hypothesis.

By empirical observation, we can state the following facts:

1. Driving $|2-\rangle$ and working in the negative polarity basis, our two important eigenvalues are $S_1 < 0$ and $S_2 > 0$. The eigenvector of S_1, $\vec{\nu}_1$, has the biggest contribution from $|2-\rangle$, the driven state, while the eigenvector of S_2, $\vec{\nu}_2$, is dominated by $|g, 0\rangle$.

2. Driving $|2+\rangle$ and working in the positive polarity basis, the two key eigenvalues are now $-S_1$ and $-S_2$. Furthermore, their corresponding eigenvectors are $\vec{\nu}_1$ and $\vec{\nu}_2$ with a sign change for two of the elements in each. The signs do not matter though, it is the fact that the absolute values of the elements are unchanged that is important.

Figure 6.2: Partial FT: blue (red) arrows show transitions contributing to the positive (negative) Mollow sidebands. The dominant basis ket contributing to the eigenvector of the eigenvalues is added on the LHS.

For visualization, let us draw up partial Floquet Tableaux for the two cases. This is shown in fig. 6.2. The top table illustrates the case of driving $|2-\rangle$ where the "blue" transitions are strong while the "red" are weak. The bottom table is the case of driving $|2+\rangle$ and here, blue transitions are weak while red are strong.

In general, I have found that the asymmetry comes down to the following: depending on which eigenvalue – that with the eigenvector dominated by the ground or the driven state – is higher, the sideband represented in the FT by positive or negative gradient arrows is stronger (respectively). We can test this rule of thumb by applying it to our analytical solution of the minimal basis two-photon saturation. In this case, $\lambda_2 = 0$ has eigenvector $\vec{\nu}_2$ dominated by the ground state while $\lambda_3 = S > 0$ has eigenvector $\vec{\nu}_3$ dominated by the driven state. Applying our ansatz to table 6.1 implies that the *negative* sideband should be stronger, as it is.

Now, although there is little doubt that it is the uneven weighting of the ground and driven states in the two new, mixed eigenstates of H that is responsible for the asymmetry, I do not have a complete explanation at this point. Notice however that when the drive strength is increased, more of the other basis states are mixed into all the eigenvectors, including those corresponding to S_1 and S_2, so the state-weighting evens out a little. According to the above speculations, this should cause the asymmetry to weaken, as we know it does.

Chapter 7

Conclusion

In this thesis, we have looked at the problem of the strongly driven Jaynes-Cummings model for a qubit coupled to a mode of EM radiation in the extreme strong-coupling regime. The focus was on multi-photon transitions to higher excitation dressed states. This investigation is most relevant to possible future realizations in the setting of Circuit QED. First, we solved the Master equation numerically and calculated the incoherent spectra as well as the second-order intensity correlation function when the drive frequency is tuned to such a multi-photon resonance.

We have found two main results:

- For small drive, the light leaking out of the cavity is very strongly bunched. With increasing drive, the correlation function at zero delay decreases very rapidly and the light becomes antibunched.

- The incoherent spectrum of the qubit and field mode both develop a clear Mollow triplet as the drive is increased.

Then, we considered simplified models and solved them analytically, interpreting the behavior seen in the numerical simulations. We concluded that the transition from bunching to antibunching would be observed for any multi-level system driven on a MPT. Physically, this can be understood analogously to the two-state system antibunching. As we drive stronger, the population in the intermediate states rises. Excitations and decays occur so quickly that the vacuum Rabi states gain a considerable steady-state population, which decreases the value of the second-order intensity correlation function at zero delay.

As for the saturation phenomenon, we have seen that MPT dynamic Stark splitting can be understood in the context of periodic solutions and quasi-energies of the system. Multi-photon transitions from the ground to the driven state are saturated with increasing drive strength as loop-like coherent exchanges of excitation between the JC system and the driving field dominate over decay processes. This results in multiple splittings of *all* energy levels nearby. We have succeeded in explaining the simplest of our numerical results, but all more complicated cases can be understood by extending the same ideas.

Finally, we can safely claim that Multi-Photon Blockade in the strongly coupled, strongly driven JCM is predicted to occur, as indicated by both the saturation behavior and anti-

bunching of the output light. We hope and look forward to the possibility that in the very near future, these theoretical considerations will be put to the test in the laboratory.

7.1 Future Work

I would like to summarize all the interesting issues/questions mentioned in the course of the dissertation but that were either not considered at all or not fully resolved.

- The evolution of the peaks shown in fig. 5.1 (a) and (b) is not at all understood at the moment. What physical processes determine the widths and heights? Likewise, in panel (c) of the same figure, the peak structure at the smaller detuning range has been left completely unexplored.

- We have noticed that for certain parameter values, MPT peaks of order higher than two did not show antibunching due to what I have called "background", global processes in the system. But what are these processes, what parameter choices actually allow antibunching and why?

- What determines the characteristic points of the MPT peaks listed in table 5.2.4?

- We have only scarcely used Quantum Trajectories in this study, but knowing of their power in aiding the physical interpretation, it could be worth-while to re-solve some of the problems by using Trajectory theory. Perhaps additional insight can be gained. . .

- The issue of the anticorrelated asymmetry in the Mollow triplet observed for the vacuum Rabi case has been left open. One suggestion is that the anticorrelation is required by conservation of energy. We do know however that it is due to the presence of the second vacuum Rabi state and the next dressed state of the same polarity as the one being driven. Note that this was also observed for MPT – but in this case, the situation is so much more complicated, this asymmetry between the field and qubit is understandable.

- Of course, also, there remains the question of the more fundamental asymmetry present for MPT where one of the side-peaks is suppressed. Although we have outlined a possible direction for the resolution, this problem requires further investigation and clarification.

- I wonder if it is possible to deduce, at least approximately, the phase relationships (in the Glauber sense) between the different frequency components, all present simultaneously when a MPT is saturated. This also could be an interesting extension.

Appendix A

A.1 Dressed-State representation

Recall that H_{JC} has ground state $|g, 0\rangle$ with eigenvalue 0, and excited eigenkets $|n\pm\rangle = \frac{1}{\sqrt{2}} (|g\rangle |n\rangle \pm |e\rangle |n - 1\rangle)$ with corresponding eigenvalues $E_n^\pm = \hbar (n\omega_o \pm \sqrt{n}g)$. Let (for convenience) the ground state have index *zero*, the lower dressed states have odd natural indices and the upper – even, and choose the ordering of the states to be according to increasing energy eigenvalue. Below, where-ever α is not explicitly said to be equal to zero, it is implied that $\alpha, \beta \in \mathbb{N}$.

$$
\begin{aligned}
(\sigma_-)_{\alpha\beta} = \quad &\text{if } \alpha = 0,\ \beta = 1 \Rightarrow \frac{-1}{\sqrt{2}}, \\
&\text{if } \alpha = 0,\ \beta = 2 \Rightarrow \frac{1}{\sqrt{2}}, \\
&\text{if } \alpha,\ \beta \text{ are even and } \beta = \alpha + 2 \Rightarrow \frac{1}{2}, \\
&\text{if } \alpha,\ \beta \text{ are odd and } \beta = \alpha + 2 \Rightarrow -\frac{1}{2}, \\
&\text{if } \alpha \text{ is even, } \beta \text{ is odd, and } \beta = \alpha + 1 \Rightarrow -\frac{1}{2}, \\
&\text{if } \alpha \text{ is odd, } \beta \text{ is even, and } \beta = \alpha + 3 \Rightarrow \frac{1}{2}, \\
&\text{zero otherwise.} \quad\quad\quad\quad\quad\quad\quad\quad\quad\quad\quad (A.1.1)
\end{aligned}
$$

$$
\begin{aligned}
(a)_{\alpha\beta} = \quad &\text{if } \alpha = 0,\ \text{and } \beta = 1 \text{ or } 2 \Rightarrow \frac{1}{\sqrt{2}}, \\
&\text{if } \alpha,\ \beta \text{ are even and } \beta = \alpha + 2 \Rightarrow \frac{1}{2}\left\{ \sqrt{\frac{\beta}{2}} + \sqrt{\frac{\alpha}{2}} \right\}, \\
&\text{if } \alpha,\ \beta \text{ are odd and } \beta = \alpha + 2 \Rightarrow \frac{1}{2}\left\{ \sqrt{\frac{\beta + 1}{2}} + \sqrt{\frac{\alpha + 1}{2}} \right\}, \\
&\text{if } \alpha \text{ is even, } \beta \text{ is odd, and } \beta = \alpha + 1 \Rightarrow \frac{1}{2}\left\{ \sqrt{\frac{\beta + 1}{2}} - \sqrt{\frac{\alpha}{2}} \right\}, \\
&\text{if } \alpha \text{ is odd, } \beta \text{ is even, and } \beta = \alpha + 3 \Rightarrow \frac{1}{2}\left\{ \sqrt{\frac{\beta}{2}} - \sqrt{\frac{\alpha + 1}{2}} \right\}, \\
&\text{zero otherwise.} \quad\quad\quad\quad\quad\quad\quad\quad\quad\quad\quad (A.1.2)
\end{aligned}
$$

A.2 Super-Operator representation

Let A and B be two $N \times N$ matrices. Then for all $m, n = \{1, \ 2 \ldots N\}$ and $k = \{1, \ 2 \ldots (N-1)\}$,

$$
\begin{align}
[spre(A)]\,(m + kN, \ n + kN) &= A(m, n), & \text{(A.2.3)} \\
[spost(B)]\,(nN - k, \ mN - k) &= B(m, n), & \text{(A.2.4)}
\end{align}
$$

with all other matrix elements being zero.

Bibliography

[1] E.T. Jaynes and F.W. Cummings, *Comparison of quantum and semiclassical radiation theories with application to the beam maser*, Proceedings of the IEEE, **51**, 89 (1963).

[2] Matthias Kronenwett, *Photon Correlations in Two-Mode Cavity Quantum Electrodynamics*, Master's thesis, University of Auckland, 2007.

[3] D.F. Walls and G.J. Milburn, *Quantum Optics*, 2nd ed., Springer, 2006.

[4] J.J. Sakurai, *Modern Quantum Mechanics*, revised ed., Addison-Wesley, 1994.

[5] S. Kryszewski, *Density Operator*, unpublished lecture notes, downloadable at `http://iftia9.univ.gda.pl/~sjk/skok/ou02.pdf`

[6] M.G. Minty, *Some examples and concept-reinforcement*, unpublished lecture notes, downloadable at `http://minty.stanford.edu/Ph195/wednesday4.pdf`

[7] H.J. Carmichael, *Statistical Methods in Quantum Optics*, vol. 1, Springer, 1999.

[8] Simon James Whalen, *Photon correlation functions and photon blockade in two-mode cavity QED*, Honours thesis, University of Auckland, 2008.

[9] Simon James Whalen, *Derivation of the master equation in Lindblad form*, unpublished notes.

[10] L. Tian and H.J. Carmichael, *Quantum trajectory simulations of the two-state behavior of an optical cavity containing one atom*, Physical Review A, **46**, R6801 (1992).

[11] P. Alsing, D.S. Guo, H.J. Carmichael, *Dynamical Stark effect for the Jaynes-Cummings system*, Physical Review A, **45**, 7 (1992).

[12] Carmen Chicone, *Ordinary Differential Equations with Applications*, 2nd ed., Springer-Verlag, New York, 1999.

[13] Lev S. Bishop, J.M. Chow, Jens Koch, A.A. Houck, M.H. Devoret, E. Thuneberg, S.M. Girvin and R.J. Schoelkopf, *Nonlinear response of the vacuum Rabi resonance*, Nature Physics, **4**, 12 (2008).

[14] J.M. Fink, M. Goppl, M. Baur, R. Bianchetti, P.J. Leek, A. Blais and A. Wallraff, *Climbing the Jaynes-Cummings ladder and observing its $\sqrt{n}$ nonlinearity in a cavity QED system*, Nature, **454**, 315-318 (2008).

[15] Sze Meng Tan, *A Quantum Optics Toolbox for Matlab 5*, User's guide, downloadable at `http://www.qo.phy.auckland.ac.nz/qotoolbox.html`